

The role of expressed sequence *Aa467197* in macrophage responses to inflammation

Dissertation with the aim of achieving a doctoral degree (Dr. rer. nat.)
at the MIN Faculty of Mathematics, Informatics and Natural Sciences

Department of Biology

University of Hamburg

Submitted by Madeleine Hamley

Hamburg, 2021

Date of oral defence: 29.10.2021

Evaluation committee:

- PD Dr. Thomas Jacobs
- Prof. Dr. Christian Lohr
- Prof. Dr. Julia Kehr
- Prof. Dr. Tim Gilberger
- Prof. Dr. Minka Breloer

Eidesstattliche Versicherung

Hiermit erkläre ich an Eides statt, dass ich die vorliegende Dissertationsschrift selbst verfasst und keine anderen als die angegebenen Quellen und Hilfsmittel benutzt habe.

Hamburg, 15.05.2021

Ort, Datum

A handwritten signature in black ink, appearing to read 'Kollwitz', written over a horizontal line.

Unterschrift

Bestätigung der Korrektheit der englischen Sprache

Hiermit erkläre ich, Madeleine Hamley, geboren 02.10.1991 in London, dass die vorliegende Dissertation "The role of expressed sequence *Aa467197* in macrophage responses to inflammation" sprachlich korrekt ist.

Hamburg, 15.05.2021

Ort, Datum

A handwritten signature in black ink, appearing to read 'Madeleine Hamley', written over a horizontal line.

Unterschrift

Index

Eidesstattliche Versicherung	3
Bestätigung der Korrektheit der englischen Sprache	4
Index	5
List of figures	9
List of tables.....	10
Abbreviations	11
1. Abstract	15
2. Introduction.....	16
2.1 Brief overview of the immune response	16
2.2 The role of macrophages in immune system responses.....	17
2.2.1 Macrophage heterogeneity and development	17
2.2.2 Macrophage functions and polarisation during inflammation	18
2.3 Expressed sequence <i>Aa467197</i> and its potential role in anti-inflammatory macrophages...	20
2.4 Chronic inflammatory disease	21
2.4.1 Inflammatory bowel disease	23
2.4.2 Schistosomiasis	25
2.5 The aim of this study	28
3. Materials	30
3.1 Consumable plastic and glass materials	30
3.2 Human samples.....	31
3.3 Mouse lines.....	31
3.4 Cell lines	32
3.5 Parasites.....	32
3.6 Chemicals, enzymes, and cytokines	32
3.6.1 Chemicals	32
3.6.2 Enzymes	34
3.6.3 Cytokines	34
3.7 Buffers and media.....	35
3.8 Laboratory equipment.....	36
3.9 Commercial kits	37

3.10	DNA oligonucleotides	38
3.10.1	Genotyping primers	38
3.10.2	qPCR primers	38
3.11	Antibodies	39
3.11.1	FACS antibodies.....	39
3.11.2	Other antibodies	41
3.12	Software and Databases	41
4.	Methods.....	42
4.1	Human samples.....	42
4.1.1	Colon samples	42
4.1.2	Peripheral blood mononuclear cells (PBMCs).....	42
4.2	L929 cell culture.....	43
4.3	Mice	43
4.3.1	Genotyping	43
4.4	Isolation of cells from mouse organs	45
4.4.1	Bone marrow	45
4.4.2	Isolation of cells from the colon/lamina propria	45
4.4.3	Isolation of cells from the liver	46
4.4.4	Serum	46
4.4.5	Mesenteric lymph nodes.....	46
4.4.6	Thymus	46
4.5	Cell counting.....	46
4.6	<i>In vitro</i> stimulation assays	47
4.7	RNA isolation	47
4.7.1	QiaShredder Kit and RNeasy Mini Kit	47
4.7.2	Phenol-chloroform extraction with TRIzol™ reagent.....	47
4.8	cDNA synthesis	48
4.9	qPCR	48
4.10	Flow cytometry.....	49
4.10.1	Blocking	49
4.10.2	Extracellular staining.....	49
4.10.3	Cell fixation, permeabilisation, and intracellular staining.....	50

4.10.4	PrimeFlow™ assay	50
4.10.5	Compensation.....	51
4.10.6	LEGENDplex™ assay.....	51
4.10.7	Flow cytometric analysis.....	51
4.10.8	Cell sorting.....	51
4.11	Enzyme-linked immunosorbent assay (ELISA).....	52
4.12	Extracellular flux analysis	52
4.13	Phagocytosis assay.....	53
4.14	Bulk-RNA sequencing	53
4.15	Dextran sodium sulfate (DSS)-induced colitis	53
4.16	<i>Schistosoma mansoni</i>	54
4.16.1	Infection	54
4.16.2	Egg count in liver and colon	54
4.16.3	Measurement of alanine transaminase (ALT) levels	54
4.17	Statistics	54
5.	Results.....	55
5.1	Expression kinetics of <i>Aa467197</i> and markers of IL-4-activated macrophages in mouse BMDMs	55
5.2	Expression of genes associated with IL-4-activated macrophages in wildtype and <i>Nmes1^{-/-}</i> mice	57
5.3	<i>In vitro</i> functional analyses	59
5.3.1	Assessing mitochondrial function in mouse BMDMs with ablated <i>Aa467197</i>	59
5.3.2	Modulation of <i>Aa467197</i> expression during phagocytosis	61
5.4	Analysis of transcriptional profile of IL-4-stimulated cells with ablated <i>Aa467197</i>	62
5.5	Expression of <i>NMES1</i> in human cells and tissue.....	64
5.6	Analysis of <i>Aa467197</i> in a model of dextran sodium sulfate (DSS)-induced colitis	66
5.6.1	Expression of <i>Aa467197</i> during DSS colitis in wildtype mice	66
5.6.2	Phenotype of <i>Nmes1^{-/-}</i> mice during DSS colitis.....	67
5.7	Analysis of <i>Aa467197</i> in a model of infection with <i>Schistosoma mansoni</i>	70
5.7.1	Expression of <i>Aa467197</i> in colons of mice during <i>S. mansoni</i> infection.....	70
5.7.2	Phenotype of <i>Nmes1^{-/-}</i> mice at week 14 of infection with <i>S. mansoni</i>	71
5.7.3	Analysis of myeloid cell populations in <i>Nmes1^{-/-}</i> mice at week 14 of <i>S. mansoni</i> infection.....	74
5.8	Expression of <i>Aa467197</i> in <i>in vitro</i> -cultured neutrophils derived from bone marrow.....	80

6.	Discussion	82
6.1	The role of <i>Aa467197</i> in macrophage polarisation after stimulation with IL-4	82
6.2	Macrophage tissue remodelling functions may be influenced by <i>Aa467197</i>	85
6.2.1	<i>Aa467197</i> may play a role in regulating macrophage migration, chemotaxis of cells to sites of inflammation, and the response to microbial infection	85
6.2.2	<i>Aa467197</i> may act as a regulator of blood vessel development and angiogenesis	86
6.2.3	<i>Aa467197</i> expression may depend on macrophage cytoskeletal functions	87
6.3	The role of <i>Aa467197</i> in models of chronic disease	88
6.3.1	Expression of <i>Aa467197</i> may affect microbiota composition, which leads to stronger colitis induction by DSS	88
6.3.2	Expression of <i>Aa467197</i> may affect egg retention in the colon as well as parasite maturation during <i>S. mansoni</i> infection	90
6.3.3	<i>Aa467197</i> expression exacerbates fibrosis in the intestine through upregulation of pro-fibrotic pathways and recruitment of monocytes to the colon during schistosomiasis	91
6.3.4	<i>Aa467197</i> may contribute to fibrosis development in the liver by blocking expression of ARG1 in macrophages	92
6.3.5	<i>Aa467197</i> does not modulate neutrophil infiltration or function during infection with <i>S. mansoni</i>	93
6.4	<i>NMES1</i> may contribute to recovery from UC by promoting accumulation and wound healing functions of macrophages	94
7.	Conclusion and future perspectives	95
8.	References	98
9.	Acknowledgements	122

List of figures

Figure 1: <i>Aa467197</i> was expressed earlier than markers of IL-4-activated macrophages in BMDMs stimulated with IL-4.	56
Figure 2: <i>Aa467197</i> alters the gene expression of IL-4-induced macrophage tissue remodelling markers.....	57
Figure 3: <i>Aa467197</i> does not regulate expression of IL-4-induced tissue remodelling proteins in macrophages.....	58
Figure 4: <i>Aa467197</i> does not regulate oxygen consumption rates (OCRs) and ATP production in BMDMs.....	60
Figure 5: Ablation of <i>Aa467197</i> does not impact extracellular acidification rates (ECARs) of BMDMs.	61
Figure 6: Phagocytosis of apoptotic cells does not regulate <i>Aa467197</i> expression.	62
Figure 7: <i>Aa467197</i> expression affects the transcriptional profile of BMDMs untreated or treated with IL-4 for 6h and 24h.	63
Figure 8: <i>Aa467197</i> affects expression of IL-4-induced macrophage genes even in untreated BMDMs.	64
Figure 9: NMES1 expression is not induced in MDMs treated with IL-4, but is increased in colons of patients in remission from UC.	65
Figure 10: <i>Aa467197</i> is more highly expressed in mouse colons compared to other intestinal compartments, and expression is microbiota-independent.....	65
Figure 11: <i>Aa467197</i> expression in mouse colon macrophages increases during the recovery phase of DSS colitis.	67
Figure 12: <i>Aa467197</i> protects co-housed wildtype and <i>Nmes1^{-/-}</i> mice from DSS-induced colitis and influences expression of <i>Arg1</i> and <i>Chil3</i> in myeloid colon cells.	69
Figure 13: <i>Aa467197</i> expression is upregulated in mouse colon macrophages during infection with <i>S. mansoni</i>	71
Figure 14: <i>Aa467197</i> controls accumulation of <i>S. mansoni</i> eggs in the intestine and regulates fibrosis progression at w14 of <i>S. mansoni</i> infection.	72
Figure 15: <i>Aa467197</i> does not control accumulation of <i>S. mansoni</i> eggs in the liver at w14 of infection, and does not affect expression of fibrosis-associated markers in the liver.....	72
Figure 16: <i>Aa467197</i> does not affect liver damage caused by <i>S. mansoni</i> infection.	73
Figure 17: <i>Aa467197</i> regulates infiltration of neutrophils and monocytes into the colon at week 14 of infection with <i>S. mansoni</i>	75
Figure 18: <i>Aa467197</i> regulates the infiltration of CCR2 ⁺ colon monocytes during infection with <i>S. mansoni</i>	76
Figure 19: <i>Aa467197</i> does not modulate neutrophil activation in the colon at week 14 of <i>S. mansoni</i> infection.	77
Figure 20: <i>Aa467197</i> is expressed in liver neutrophils of mice during infection with <i>S. mansoni</i>	78
Figure 21: <i>Aa467197</i> does not modulate frequencies of resident or infiltrating myeloid cell populations in the liver at week 14 of infection with <i>S. mansoni</i>	78
Figure 22: <i>Aa467197</i> regulates the expression of ARG1 in blood-derived liver macrophages during infection with <i>S. mansoni</i>	79

Figure 23: *Aa467197* does not modulate neutrophil activation in the liver at week 14 of *S. mansoni* infection. 80

Figure 24: IL-4 does not induce *Aa467197* expression in neutrophils *in vitro*. 81

List of tables

Table 1: List of consumable plastic and glass materials 30

Table 2: List of human patient samples from sigmoid colon, anonymised..... 31

Table 3: List of mouse lines 31

Table 4: List of chemicals 32

Table 5: List of enzymes..... 34

Table 6: List of cytokines 34

Table 7: List of buffers and media 35

Table 8: List of laboratory equipment 36

Table 9: List of commercial kits 37

Table 10: List of primers used for mouse genotyping 38

Table 11: List of primers used for qPCR on mouse samples..... 38

Table 12: List of primers used for qPCR on human samples..... 39

Table 13: List of FACS antibodies used for extracellular staining 39

Table 14: List of FACS antibodies used for intracellular staining 40

Table 15: List of target probes used for PrimeFlow™ staining..... 41

Table 16: List of other antibodies 41

Table 17: List of software and databases..... 41

Abbreviations

AHR	Aryl hydrocarbon receptor
AIDS	Acquired immunodeficiency syndrome
ALT	Alanine transaminase
APC	Antigen-presenting cell
AQP	aquaporin
ARG1	Arginase 1
ART	Antiretroviral treatment
aT	Apoptotic thymocyte
BAI	Brain angiogenesis inhibitor
bFGF	Basic fibroblast growth factor
BMDM	Bone marrow-derived macrophage
BSA	Bovine serum albumine
C15orf48	Chromosome 15 open reading frame 48
CCL	C-C chemokine ligand
CCR	C-C chemokine receptor
CD	Cluster of differerentiation
cDNA	Complementary DNA
CrD	Crohn's disease
CSF	Colony stimulating factor
CSF1R	Colony stimulating factor 1 receptor
CX3CL	Chemokine (C-X3-C motif) ligand
CX3CR	Chemokine (C-X3-C motif) receptor
CytD	Cytochalasin D
DAMP	Damage-associated molecular pattern
DC	Dendritic cell
DMEM	Dulbecco's Modified Eagle Medium
DNA	Desoxyribonucleic acid
DSS	Dextran sodium sulfat
ECAR	Extracellular acidification rate
EDTA	Ethylenediaminetetracetic acid

Abbreviations

EGF	Endothelial growth factor
EGFR	Epidermal growth factor receptor
ELISA	Enzyme-linked immunosorbent assay
ET	Endothelin
FACS	Fluorescence-activated cell sorting
FCCP	Carbonyl cyanide-p-trifluoromethoxyphenylhydrazone
FCS	Fetal calf serum
GAS6	Growth arrest-specific 6
GATA3	GATA binding protein 3
GI	Gastrointestinal
GO	Gene ontology
GPR183	G-protein-coupled receptor 183
HBSS	Hank's Balanced Salt Solution
HCC	Hepatocellular carcinoma
HIF1 α	Hypoxia-induced factor 1 alpha
HIV	Human immunodeficiency virus
HOXC	Homeobox-containing gene
HSP	Hepatic stellate cell
IBD	Inflammatory bowel disease
IFN- γ	Interferon gamma
IKK	Inhibitor of κ kinase
IL	Interleukin
IL-13R α	IL-13 receptor alpha
IL-4R α	IL-4 receptor alpha
iNOS	Inducible nitric oxide synthase
JNK	c-jun N-terminal kinase
LPS	Lipopolysaccharide
LY6	Lymphocyte antigen 6
MACS	Magnetic-activated cell sorting
MDM	Monocyte-derived macrophage
MDP	Muramyl dipeptide

Abbreviations

MFI	Median fluorescence intensity
MHC	Major histocompatibility complex
miR	microRNA
MMP	Matrix metalloprotease
MPO	Myeloperoxidase
mRNA	Messenger RNA
<i>N.</i>	<i>Nippostrongylus</i>
NDUFA4	NDUFA4 mitochondrial complex associated
NF-κB	Nuclear factor kappa B
NMES1	Normal mucosa of esophagus-specific gene 1 protein
NO	Nitric oxide
OCR	Oxygen consumption rate
OXPPOS	Oxidative phosphorylation
PAMP	Pathogen-associated molecular pattern
PBS	Phosphate-buffered saline
PBMC	Peripheral blood mononuclear cell
PCR	Polymerase chain reaction
PDGF	Platelet-derived growth factor
PKR	Protein kinase R
PPARγ	Peroxisome proliferator-activated receptor gamma
PROS1	Protein S
PRR	Pattern recognition receptor
PtdSer	Phosphatidylserine
qPCR	Quantitative real-time polymerase chain reaction
RAP2B	Ras-related protein Rap-2b
RELM	Resistin-like molecule
RNA	Ribonucleic acid
RNAseq	RNA sequencing
RORγt	RAR-related orphan receptor gamma t
ROS	Reactive oxygen species
<i>S.</i>	<i>Schistosoma</i>

Abbreviations

s.c.	subcutaneous
SDH	Succinate dehydrogenase
SLPI	Secretory leukocyte protease inhibitor
STAT	Signal transducer and activator of transcription
<i>T.</i>	<i>Trypanosoma</i>
TAM	TYRO3, AXL, and MER
TGF	Transforming growth factor
Th cell	T helper cell
TIM	T cell immunoglobulin and mucin receptor
TIMP	Tissue inhibitors of metalloprotease
TLR	Toll-like receptor
TMB	Tetramethylbenzidine
TNF	Tumour necrosis factor
UBE2N	Ubiquitin-conjugating enzyme E2N
UC	Ulcerative colitis
VEGF	Vascular endothelial growth factor
VHL	von Hippel–Lindau
YM1	Chitinase-like protein 3
γc	IL-2 receptor gamma c

1. Abstract

Chronic inflammatory diseases are one of the greatest threats to human health in the modern world, contributing to a number of debilitating disease pathologies and deaths. One of the key cell types involved in the inflammatory response are macrophages, which contribute to the initiation of inflammation through secretion of pro-inflammatory mediators and inducing neutrophil migration to affected tissues. However, they are also crucial for the resolution of inflammation by initiating and regulating the tissue remodelling response. Failure to properly induce the anti-inflammatory, tissue healing response or inadequate regulation of the pro-inflammatory response by macrophages has been identified as a cause of pathology in a number of chronic diseases. Accordingly, understanding how macrophages are polarised towards an anti-inflammatory phenotype and which factors contribute to the exertion of tissue remodelling functions is essential to develop new treatments for chronic inflammatory diseases. In the last few years, the expressed sequence *Aa467197* has emerged as a candidate gene which may be involved in inducing or contributing to macrophage tissue remodelling functions, inducing a negative feedback loop in the LPS-induced inflammatory response and being one of the most highly expressed genes in macrophages which have acquired tissue remodelling functions through stimulation with IL-4. Accordingly, the aim of this thesis was to determine how *Aa467197* is expressed in tissue remodelling macrophages, how *Aa467197* can affect expression of tissue remodelling markers and genes related to macrophage tissue remodelling functions by using RNAseq, and how *Aa467197* affects disease outcome in mouse models of colitis and schistosomiasis. The findings presented in this thesis suggest that *Aa467197* may regulate macrophage polarisation early after sensing of anti-inflammatory cytokines, influencing the transcription of genes characteristic for tissue remodelling macrophages, such as *Chil3* and *Gata3*. In addition, *Aa467197* may contribute to the induction of macrophage tissue remodelling functions, including chemotaxis, blood vessel development, and angiogenesis, and may play a role in initiating pathways induced by cytoskeletal remodelling in macrophages. Finally, expression of *Aa467197* may contribute to the pathogenesis of colitis through alterations in the microbiota composition, while in schistosomiasis *Aa467197* contributes to monocyte infiltration and fibrosis development in the intestine as well as ARG1 expression in macrophages of infected livers. Overall, there is evidence that *Aa467197* contributes to the function of tissue remodelling macrophages during intestinal inflammation, and further investigations should be performed to assess whether it may present a good target for macrophage-related therapies for chronic diseases.

2. Introduction

2.1 Brief overview of the immune response

Living organisms are constantly subjected to pathogenic microbes and harmful substances that threaten to disrupt homeostasis and harm or kill the organism. Accordingly, living creatures require defence mechanisms to protect the body from invading pathogens. The mammalian immune response is one such defence mechanism. It is broadly split into two branches: the innate immune response, which is fast and unspecific, and the adaptive immune response, which takes longer to activate, but it more specific to the invading pathogen. The interplay of the innate and the adaptive immune system is critical for a successful immune response.

In general, after a pathogen breaches the initial protective barriers, such as skin or mucous membranes, the pathogen-associated molecular patterns (PAMPs) are recognised and bound by pattern recognition receptors (PRRs) on the surface of cells such as mast cells, macrophages, or dendritic cells (DCs)^{1,2}. This binding leads to a signalling cascade that induces production of inflammatory mediators by macrophages, such as interleukin (IL)-1, IL-6, and tumour necrosis factor (TNF), which regulate a number of functions during an inflammatory response, such as cell death, vascular endothelial permeability, and production of acute-phase proteins. Importantly, they also induce recruitment of further cells such as neutrophils, which become activated through contact with the pathogens or binding of inflammatory cytokines. This induces neutrophils to release toxic components, such as reactive oxygen species (ROS), myeloperoxidase (MPO), cathepsin G, and protease 3³, to eliminate the pathogens.

At the same time, specialised antigen-presenting cells (APCs), which include macrophages, DCs, and neutrophils uptake and digest the pathogens. Pathogen antigens are then exposed on the surface of the APCs via major histocompatibility complex (MHC) molecules and presented to naïve T cells. MHC class I receptors activate T cells which express cluster of differentiation 8 (CD8⁺ T cells), which mature into cytotoxic CD8⁺ T cells, while MHC class II receptors activate CD4⁺ T cells, which mature into T helper (Th) cells. Depending on additional factors in the tissue microenvironment and the type of pathogen, Th cells can mature into different subtypes, the best characterised of which are Th1, Th2, and Th17 cells^{4,5}. Th17 cells are characterised by expression of the transcription factor RAR-related orphan receptor gamma t (RORγt) and the production of IL-17 and IL-22, and are thought to play a role in protecting against extracellular pathogens and fungi⁶. They also contribute to the pathogenesis of a number of inflammatory diseases, including rheumatoid arthritis, multiple sclerosis, and inflammatory bowel disease⁷. Th1 cells are characterised by the expression of T-bet and the production of interferon-γ (IFN-γ), and generally contribute to cell-mediated responses against intracellular pathogens. Th1 immune responses are generally characterised as pro-inflammatory responses. Th2 responses often occur alongside Th1 responses, but Th2 cells are characterised by the expression of GATA binding protein 3 (GATA3), the production of anti-inflammatory cytokines IL-4, IL-5, and IL-13, and are associated with responses to extracellular pathogens, particularly helminth parasites^{5,8}. The Th2 response is also generally associated with a humoral-based response, in which T helper cells activate B cells via co-stimulatory CD40/CD40L sensing and binding of the MHC class II complex on B cells to the T cell receptor. This leads to the release of antibodies, which provide further support for the

clearance of pathogens. Th2 cells and granulocytes also play a crucial role in regulating the initial, pro-inflammatory response through the release of anti-inflammatory cytokines⁹. The release of IL-4 and IL-13 leads to inhibition of type 1 inflammation¹⁰, which limits the damage caused by the initial inflammatory response and dampens the response in order to mitigate damage to the surrounding tissue. Crucially, the release of anti-inflammatory cytokines shifts macrophages towards an anti-inflammatory, wound-healing phenotype, which is essential for the resolution of the inflammatory response.

Macrophages have been shown to be key players in a number of inflammatory diseases, including allergic asthma, chronic liver diseases such as non-alcoholic fatty liver disease or hepatitis infection, obesity, and several cancers^{11–15}. It is therefore essential to understand the development and functions of these cells, to better understand their role in the context of inflammatory disease.

2.2 The role of macrophages in immune system responses

2.2.1 Macrophage heterogeneity and development

Macrophages are a highly heterogeneous population of myeloid immune cells that play essential roles in the development of an organism, during homeostasis, and upon tissue damage. Mice with a knock-out for the colony-stimulating factor 1 receptor (*Csf1r*), in which macrophages are depleted due to the inability to respond to CSF1, a crucial myeloid cell differentiation growth factor, show reduced macrophage survival, chemotaxis, and proliferation¹⁶. These mice rarely survive until adulthood due to the development of severe osteopetrosis^{17,18}, reduced numbers of microglia, and disruption of brain morphology¹⁹.

Macrophages perform a variety of functions in homeostasis and during an immune response, and in many cases these functions are highly tissue-specific. For example, microglia, resident macrophages in the brain, play roles in the regulation of synaptic pruning²⁰ and modulate axon extension in the forebrain²¹, while intestinal macrophages, which reside in a microbe-rich environment, are hyporesponsive to Toll-like receptor stimulation²². Even within one organ, different macrophage populations can have distinct functions: splenic red pulp macrophages primarily clear apoptotic erythrocytes, while white pulp macrophages are specialised in clearing external antigens. Meanwhile, marginal zone macrophages play roles in immune surveillance, capturing blood borne antigens, and apoptotic cell phagocytosis²³.

This heterogeneity comes from a number of different sources. For one, mature tissue-resident macrophages derive from different progenitor cell populations^{24–26}, with microglia and Langerhans cells deriving directly from yolk sac progenitors and other tissue macrophages being seeded from fetal liver macrophages, as is the case for Kupffer cells in the liver, alveolar macrophages in the lung, and splenic red pulp macrophages. However, some populations of macrophages are derived from blood monocytes, such as intestinal macrophages²⁴ and small peritoneal macrophages²⁷. Another important source of heterogeneity is the tissue microenvironment, which has been shown to modulate the enhancer environment of tissue macrophages, causing upregulation of transcription factors specific to the tissue, such as *Runx3* in the intestine, *Clec4f* in the liver, or *Car4* in the lung²⁸. Interactions between macrophages and other factors in the tissue microenvironment, such as commensal microbiota in the

intestine^{29,30}, or interactions with hepatocytes, endothelial cells, and stellate cells in the liver³¹, have also been shown to influence macrophage heterogeneity.

In addition to tissue-resident macrophages, populations of monocyte-derived infiltrating macrophages can be found across tissues, to which they are recruited during an inflammatory response^{32,33}. Specifically, during inflammation, classical and non-classical monocytes (characterised in mice as CD11b⁺ LY6C⁺ CCR2^{hi} CX3CR1^{low} and CD11b⁺ LY6C⁻ CCR2^{low} CX3CR1^{hi}, respectively³³) are recruited to the affected tissue from the bone marrow through expression of C-C chemokine receptor 2 (CCR2) ligands, such as C-C chemokine ligand 2 (CCL2) or CCL7³⁴, or chemokine (C-X3-C motif) ligand 1 (CX3CL1), the ligand for chemokine (C-X3-C motif) receptor 1 (CX3CR1)³⁵. Upon tissue infiltration, the monocytes can develop into macrophages, as directed by tissue-specific signals and depending on the monocyte subset.

2.2.2 Macrophage functions and polarisation during inflammation

As an essential component of the innate immune system, macrophages are highly plastic and capable of responding to changing factors in the tissue environment. These factors subsequently influence the functions macrophages perform, and can even impact their physiology. Many attempts have been made to sort macrophages into distinct categories based on polarising factors and marker expression^{36,37}, with the most pervasive (and still commonly used) categories being M1 (“classically activated” by type 1 inflammatory cytokines and microbial products) and M2 (“alternatively activated”), with the latter being split into multiple categories (M2a activated by IL-4/IL-13, M2b by immune complexes in combination with TLR ligands or IL-1 β , M2c by IL-10 and glucocorticoids, and M2d by TLR antagonists^{38,39}). However, this paradigm has been subject to scrutiny with increased understanding of macrophage plasticity and the acknowledgement that the local milieu in which macrophages act involves a complex interplay of factors^{40,41}. However, macrophages can broadly be split into pro-inflammatory and anti-inflammatory phenotypes.

2.2.2.1 Pro-inflammatory macrophages

Macrophages generally acquire a pro-inflammatory phenotype through exposure to inflammatory cytokines, such as IFN- γ , bacterial or viral components, which induce signalling pathways through TLR4 and TLR3, respectively⁹. The sensing of these pro-inflammatory mediators triggers a number of signalling cascades within the macrophage, such as the MyD88-dependent and TRIF-dependent signalling pathways downstream of TLR4, which lead to activation of nuclear factor kappa B (NF- κ B)⁴², or activation of signal transducer and activator of transcription 1 (STAT1) and STAT3^{43,44}. This in turn leads to expression of CD80, CD86, inducible nitric oxide synthase (iNOS), and MHC class II, as well as secretion of pro-inflammatory cytokines such as IL-1, IL-6, IL-12, and TNF³⁸. In addition, activation of hypoxia-induced factor 1 alpha (HIF1 α) leads to metabolic changes within the macrophage, shifting its energy production towards the pentose-phosphate pathway and glycolysis and interrupting the Krebs cycle^{45,46}.

The primary role of pro-inflammatory macrophages during an immune response is to promote clearance of invading pathogens. This is accomplished directly through alteration of the arginine metabolism to promote the production and release of nitric oxide (NO)⁴⁷ and other ROS, and indirectly through the release of IL-1, IL-6, IL-12, and TNF, which lead to recruitment and activation of further cell subsets,

such as Th1 and Th17 cells⁹. Together, this leads to a potent antimicrobial response. However, the response is also unspecific and can cause extensive tissue damage to the host. Without proper regulation of the macrophage-mediated inflammatory response, this can lead to a so-called cytokine storm and, ultimately, sepsis^{48–50}.

Accordingly, anti-inflammatory mechanisms are required to regulate the acute inflammatory response and initiate tissue repair.

2.2.2.2 Anti-inflammatory macrophages

Macrophages acquire an anti-inflammatory, tissue remodelling phenotype through sensing of the anti-inflammatory Th2 cytokines IL-4 or IL-13 via the IL-4 receptor α chain (IL-4R α) complex⁵¹. Specifically, IL-4 sensing takes place through binding of IL-4 to the IL-4R α chain, which can then form a complex with IL-2 receptor γ c (γ c), known as the type I IL-4 receptor, or with the IL-13 receptor α 1 (IL-13R α 1), the type II IL-4 receptor. Sensing of IL-13 is induced by binding of IL-13 to IL-13R α 1 of the type II receptor. Signalling through the Type II receptor leads to activation of STAT6, which dimerises and induces transcription of genes such as CD23 or arginase 1 (ARG1), while signalling through the type I receptor additionally leads to induction of IRS2, which activates a number of pathways, including PI3K/Akt and PKB/mTOR, which induce Th2 differentiation and macrophage polarisation^{10,52}. Important transcription factors associated with anti-inflammatory macrophages are GATA3 and peroxisome proliferator-activated receptor gamma (PPAR γ)^{53–55}. Unlike in inflammatory macrophages, in anti-inflammatory macrophages the Krebs cycle remains intact, with cells showing enhanced oxidative phosphorylation (OXPHOS) and fatty acid oxidation^{45,46}.

Anti-inflammatory macrophages are characterised by increased expression of the mannose receptor (CD206), the MHC class II receptor, ARG1, resistin-like molecule α (RELMA), and chitinase-like protein 3 (YM1), as well as production of anti-inflammatory cytokines like IL-10, transforming growth factor (TGF)- β , and IL-1ra, as well as growth factors^{56–58}. Overall, these allow macrophages to perform a number of functions associated with tissue repair and resolution of inflammation. For instance, ARG1 is a urea cycle enzyme which competes with iNOS for the substrate L-arginine. While iNOS is induced by pro-inflammatory cytokines like IFN- γ and metabolises L-arginine to NO and citrulline, ARG1 hydrolyses L-arginine to ornithine and urea⁵⁹. Ornithine is subsequently converted into proline, an essential amino acid known to be involved in collagen production, by ornithine-aminotransferase, or used as a substrate for polyamine synthesis by ornithine-aminodecarboxylase, which promotes cell proliferation⁶⁰. In addition, induction of vascular endothelial growth factor (VEGF), endothelial growth factor (EGF), and platelet-derived growth factor (PDGF)^{61,62} by macrophages contribute to angiogenesis, and expression of anti-inflammatory cytokines and decoy receptors^{56,63} allow macrophages to regulate inflammatory responses. Tissue remodelling macrophages can also synthesise extracellular matrix components such as fibronectin and beta IG-H3⁶⁴, which in turn contribute to the recruitment of monocytes, keratinocytes, and fibroblasts^{65–67}. Another crucial function of anti-inflammatory macrophages is the clearance of apoptotic cells through phagocytosis. Macrophages express a number of receptors with which to recognise and bind phosphatidylserine (PtdSer), which is exposed on the surface of dying cells^{68,69}. These include receptors that can bind PtdSer directly, such as stabilin-2, T cell immunoglobulin and mucin receptor 4 (TIM4), and brain

angiogenesis inhibitor 1 (BAI1)⁷⁰, or indirectly, such as the TAM (TYRO3, AXL, and MER) receptor kinases, which require the bridging molecules growth arrest-specific 6 (GAS6) or protein S (PROS1) to bind to PtdSer^{71,72}. Importantly, sensing of apoptotic cells alongside anti-inflammatory cytokines such as IL-4 is crucial to induce the tissue remodelling response of macrophages, as evidenced by the downregulation of tissue remodelling-associated genes in macrophages with genetic ablation of AXL and MER, or in which sensing of PtdSer is blocked through application of annexin V⁷³.

In contrast, the functions of some markers which are highly specific for tissue remodelling macrophages are not as well characterised. RELMa is expressed in macrophages upon helminth infection and sensing of IL4/IL-13^{74,75} and plays a context-dependent role during inflammation, acting as a negative regulator of Th2 responses during helminth infection^{76,77}, but also contributing to intestinal inflammation^{78,79}. However, the exact mechanisms through which RELMa mediates these effects has not yet been elucidated. Similarly, the function of *Chil3* (or YM1) in macrophages and neutrophils has not yet been characterised in detail, but it is strongly induced in macrophages upon stimulation with Th2 cytokines^{74,80}. YM1 has been characterised as a neutrophil granule protein⁸¹ that binds heparin and heparan sulfate, and may contribute to lysis of glycosaminoglycans^{82,83}. Increased levels of YM1 in mouse lungs during infection with *Nippostrongylus braziliensis* have also been shown to increase numbers of neutrophils by changing expression of IL-17A in $\gamma\delta$ T cells⁸⁴.

Overall, anti-inflammatory macrophage functions are vital for the resolution of inflammation, though the contributing factors and exact mechanisms through which they mediate tissue remodelling inflammatory regulation still need to be examined in greater detail.

2.3 Expressed sequence Aa467197 and its potential role in anti-inflammatory macrophages

In 2013, Gundra et al. investigated whether alternatively activated macrophages have phenotypical and functional differences depending on their source, i.e. whether they were monocyte-derived, infiltrating macrophages or tissue-resident macrophages⁸⁵. Using microarray analysis, they examined differentially expressed genes in untreated macrophages, IL-4-treated resident macrophages, or IL-4 and thioglycollate-treated infiltrating macrophages. The analysis showed that the most highly upregulated gene in both monocyte-derived and tissue-resident macrophages activated by IL-4 was the expressed sequence *Aa467197*.

Expressed sequence *Aa467197*, also known as *Nmes1* or miR-147, is a hitherto uncharacterised gene located on mouse chromosome 2, 60.64 cM⁸⁶ with a human homologue in chromosome 15 open reading frame 48 (C15orf48)⁸⁷. In humans it is known to encode for normal mucosa of esophagus-specific gene 1 protein (NMES1), a nuclear protein which is known to be downregulated in human esophageal squamous cell carcinoma⁸⁸ and which shows sequence similarity to the electron complex I NDUFA4 subunit family⁸⁹. NMES1 has also been shown to be localised in the mitochondria⁸⁹. In addition, *Aa467197* encodes for the pre-miRNA sequence of the microRNA miR-147.

miR-147 has been described to play a protective role in a number of cancer models. In colorectal cancer tissues and cell lines, miR-147 is downregulated and functions as an inhibitor of cancer cell proliferation, cell cycle progression, and invasion by targeting Ras-related protein Rap-2b (RAP2B)⁹⁰ and the

cytochrome C oxidase subunit NDUFA4⁹¹. It has also been described to improve endothelial barrier integrity during LPS-induced challenge by targeting ADAM disintegrin and metalloproteinase 15⁹² and reverse resistance to epidermal growth factor receptor (EGFR) inhibitor anti-cancer drugs by repressing phosphorylation of protein kinase B (Akt)⁹³. Inhibition of Akt/mTOR pathway signalling by miR-147 has also been shown to repress cell proliferation, invasion, and migration when exogenously induced in an aggressive breast cancer cell line⁹⁴. However, the role of miR-147 in hepatocellular carcinoma (HCC) is more controversial, with one study reporting that miR-147 is downregulated in HCC cell lines and tissues, functioning as an inhibitor of cell proliferation and migration by targeting homeobox-containing gene 6 (HOXC6)⁹⁵, but another study describing that miR-147 is upregulated in HCC tissues and promotes tumour growth by targeting ubiquitin-conjugating enzyme E2N (UBE2N)⁹⁶. miR-147 is reportedly also upregulated in liver tissues of patients with chronic hepatitis C virus infection⁹⁷. In addition, in a lung adenocarcinoma cell line miR-147 mediated tolerance, rather than resistance, towards EGFR inhibitors by targeting the von Hippel–Lindau (VHL) protein and succinate dehydrogenase (SDH), which are part of the pseudohypoxia response and the tricarbalic acid cycle, respectively⁹⁸. Together, this indicates that more studies are needed to properly dissect the function of miR-147.

miR-147, and by extension *Aa467197*, has also been shown to contribute to macrophage function. In macrophages, *Aa467197* is highly upregulated in both pro- and anti-inflammatory bone marrow-derived macrophages³⁶, and miR-147 is induced by stimulation of TLR4, but also TLR2 and TLR3, and induces a negative feedback loop in the LPS-induced inflammatory response by downregulating the expression of IL-6 and TNF⁹⁹. In addition, *Aa467197*-expressing macrophages derived from CX3CR1⁺ monocyte precursors were found to induce expression of genes related to the cell cycle and proliferation¹⁰⁰, some of which are also involved in macrophage tissue remodelling functions, such as chemokine (C-X-C motif) ligand 16 (*Cxcl16*)^{101,102}, the copper chaperone Antioxidant-1 (*Atox1*)^{103–105}, or Galectin-3 (*Lgals3*)^{106–108}.

The strongly increased expression of *Aa467197* in macrophages associated with tissue remodelling and wound healing functions^{85,100}, and the role of miR-147 in the suppression of macrophage inflammatory responses⁹⁹ suggests that this gene may be involved in the regulation of the tissue remodelling response. This is further supported by the finding that mice with impaired sensing of apoptotic cells through genetic ablation of the AXL and MER tyrosine receptor kinases have strongly decreased levels of *Aa467197* in a model of infection with *N. braziliensis*⁷³. Accordingly, *Aa467197* may contribute to macrophage tissue remodelling functions, though the exact nature of the response and functions have yet to be explored.

2.4 Chronic inflammatory disease

Inflammation is an essential defence mechanism for organisms to eliminate invading pathogens. However, the unspecific nature and toxicity of the acute inflammatory response also damages the host tissue and requires mechanisms to mitigate and repair the damage caused. Failure to induce this anti-inflammatory immune response, or prolonged acute inflammation, can lead to the development of chronic inflammatory disease.

Chronic inflammatory diseases encompass a variety of conditions all characterised by pathological, chronic inflammation, such as ischemic heart disease, stroke, cancer, diabetes mellitus, chronic kidney

disease, and non-alcoholic fatty liver disease. Systemic chronic inflammation has also been described to contribute to increased risk of metabolic syndrome, type 2 diabetes¹⁰⁹, cardiovascular disease¹¹⁰, neurodegenerative and autoimmune diseases^{111,112}, and depression^{113,114}. Combined, chronic inflammatory diseases pose one of the greatest threats to human health in the modern world, with approximately 50% of deaths in 2017 being attributable to non-communicable inflammatory conditions^{115,116}.

Incidences of chronic inflammatory disease have been increasing over time, with many causes of chronic inflammation linked to modern lifestyle changes. Particular focus has been placed on low-key, chronic inflammation as a systemic response to obesity, in which excess consumption of nutrients over an extended period of time can lead to activation of PRRs and cytokine release pathways. The resulting activation of inhibitor of κ kinase (IKK), c-jun N-terminal kinase (JNK), and protein kinase R (PKR) drives insulin resistance and activates pro-inflammatory pathways, leading to increased release of TNF, IL-1 β , IL-6, and CCR2, which drive immune cell recruitment and differentiation^{117,118}. Of particular note is the obesity-induced increase in pro-inflammatory adipose tissue macrophages, which contribute to the maintenance of the pro-inflammatory tissue environment and drive insulin resistance¹². In addition, exposure to xenobiotics, disruption of the circadian rhythm, and social isolation as a result of a highly urbanised lifestyle have also been identified as risk factors for inflammatory disorders¹¹⁵.

Infections with bacteria and pathogens have also been described to provoke pro-inflammatory immune responses which can develop into chronic disease, as is the case for infection with *Yersinia enterocolitica*, which leads to microbiome alterations and development of chronic gastrointestinal (GI) tract inflammation in the absence of TLR1¹¹⁹. Viral infections are a common cause of chronic disease, with up to 40% of individuals chronically infected with hepatitis B or C developing cirrhosis, liver failure, or hepatocellular carcinoma^{120,121}. Interestingly, while antiretroviral treatment (ART) has strongly increased life expectancy and mitigated complications associated with acquired immunodeficiency syndrome (AIDS), human immunodeficiency virus (HIV) infection and the toxicity of ART have still been described to cause persistent inflammation and associated morbidities, such as lymphoid fibrosis, metabolic syndrome, liver and kidney dysfunction, and cancer¹²². Finally, parasitic infections can also lead to the development of chronic inflammatory disease, though the exact nature of the disease varies strongly depending on the infiltrating parasite. Chronic infection with the protozoan parasite *Trypanosoma cruzi* leads to chronic cardiomyopathy in 30-40% of patients, with contributing factors being establishment of an inflammatory tissue environment and virulence of the *T. cruzi* strain¹²³, but also regulatory mechanisms, such as control of the parasite load through cytotoxic CD8⁺ T cells¹²⁴. In contrast, chronic infection with helminth parasites, such as *Strongyloides stercoralis* or *Schistosoma mansoni*, is associated with a Th2-induced, anti-inflammatory response^{125,126}, which in *S. mansoni* infection is even required to prevent the host's death¹²⁷. However, in *S. mansoni* infection, these responses also allow parasite persistence in the host and can lead to development of hepatic fibrosis and chronic morbidity¹²⁸.

With inflammation being such an integral mechanism behind so many pathological conditions, it is crucial to understand the exact mechanisms involved the inflammatory process, in particular the triggers and cellular and molecular determinants involved in the resolution of inflammation. In this thesis, the

main focus will be on investigating the role of *Aa467197* in shaping macrophage tissue remodelling functions, specifically in the context of intestinal inflammation using models for inflammatory bowel disease (IBD) and schistosomiasis.

2.4.1 Inflammatory bowel disease

2.4.1.1 Introduction to inflammatory bowel disease

IBD refers to two conditions that are characterised by chronic inflammation of the GI tract. IBD describes both Crohn's disease (CrD), which can affect the entire GI tract, though is most prevalent in the small intestine, and ulcerative colitis (UC), which only occurs in the colon and rectum¹²⁹. Common symptoms of IBD are persistent diarrhea, abdominal pain, rectal bleeding and bloody stool, weight loss, and fatigue.

Many of the risk factors associated with the development of other inflammatory diseases have also been linked to increased risk of IBD. In particular, genetic risk factors¹³⁰, increased consumption of Western-type diets (characterised by high amounts of refined sugars, animal fats and proteins, and salt, as well as low dietary fibre¹³¹), microbiota composition^{132,133}, and obesity are considered particularly important in IBD development. In addition, IBD patients are at higher risk of developing additional diseases such as intestinal cancer¹³⁴ and extra-intestinal co-morbidities such as hepatobiliary diseases^{135–137} and autoimmune diseases^{138,139}, though the latter remains controversial¹⁴⁰, with IBD potentially mediating a milder disease course in multiple sclerosis patients¹⁴¹.

The prevalence of IBD has increased substantially in many regions over time, with approx. 6,9 million people affected worldwide in 2017 and the number of prevalent cases increasing. IBD has generally been considered a disease of high-income nations, with a rapid increase in cases in newly industrialised countries, such as South America, eastern Europe, Asia, and Africa¹⁴². The costs of treating IBD, as well as the indirect costs of IBD through additional sick leave, loss of productivity and leisure time, and early retirement¹⁴³, are a major burden for IBD patients and their families¹⁴⁴. These have also been projected to present an economic challenge to developing countries¹⁴⁵.

2.4.1.2 The pathogenesis of IBD

Clinical manifestations of IBD differ slightly depending on the subtype. UC is characterised by diffuse, continuous mucosal inflammation extending proximally from the rectum and gradually decreasing in severity¹⁴⁶. Neutrophils infiltrate the crypt epithelium and lumina, causing characteristic crypt abscesses and driving inflammation. Goblet cell depletion is also common in UC^{147,148}. In CrD, the terminal ileum is most commonly affected, with diseased bowel segments frequently separated by normal areas ("skip lesions")^{146,147}. Typical features of CrD are small aphthous ulcers over Peyer's patches and formation of granuloma through aggregation of macrophages, epithelioid cells, and giant cells^{146,148}.

A number of interconnected factors contribute to the pathogenesis of IBD, the best characterised of which are genetic risk factors, environmental factors, GI microbiota composition, and immune dysregulation. One of the first genetic risk factors identified for IBD was NOD2 (also known as CARD15 or IBD1)^{149,150}, a microbial sensor expressed on myeloid cells¹⁵¹ that recognises muramyl dipeptide (MDP) and lipopolysaccharide (LPS) and leads to the induction of pro-inflammatory pathways, such as the NF- κ B pathway^{151,152}. NOD2 variants found in CrD are hypothesised to contribute to increased inflammation through impaired epithelial defence, IL-12 dysregulation, and enhanced IL-1 β

processing¹⁵³. Toll-like receptor (TLR) signalling has also been shown to play a role in alleviation or development of colitis^{154,155}, with altered expression of TLR2, TLR3, TLR4, and TLR5 found in pouch mucosal biopsies from UC patients¹⁵⁶. Impaired TLR4 signalling through Asp299gly polymorphism has also been associated with both UC and CrD^{157,158}. Together with NOD2, this indicates that proper pattern recognition is essential to prevent intestinal disease development. In addition to pattern recognition receptors, autophagy genes have been identified as susceptibility loci for CrD, while regulatory pathway genes (including IL-10, genetic ablation of which causes spontaneous colitis in mice in a MyD88-dependent manner¹⁵⁹) and intestinal epithelial cell function genes are loci specific to UC¹³⁰. In addition to genetic susceptibility, tissue environmental factors have been described as a primary risk factor in IBD development. One of the main environmental drivers of IBD is dysbiosis of the commensal microbiota. In different areas of the GI tract and in human faecal samples, the most abundant microbial phyla have been identified as Bacteroidetes and Firmicutes, though the exact composition of the microbiota varies between individuals^{160,161}. IBD patients, on the other hand, have higher proportions of Actinobacteria and Proteobacteria, with a decrease in Bacteroidetes¹⁶¹, and lower microbial diversity overall¹⁶². These changes can affect the host immune system by altering metabolite production and differentiation of cells, but also disrupting mucosal barrier integrity through degradation of mucus and alteration of mucosal permeability¹⁶³. Microbiota composition has also been shown to influence the function of CX3CR1⁺ APCs in the lamina propria, with a disrupted microbiome or depletion of CX3CR1⁺ mononuclear phagocytes leading to an accumulation of Th1 and Th17 cells and increased pathology upon *Salmonella* or *Helicobacter* infection¹⁶⁴. Finally, a key factor in development of IBD is dysregulation of the innate and adaptive immune response. In addition to altered pattern recognition, as described above, reduced mucin expression^{165,166} and defects in the epithelial barrier function¹⁶⁷ have been described in both CrD and UC. Another crucial factor in IBD development is the altered expression of cytokines¹⁶⁸ and the resulting effects on immune cell functions. Cytokines play key roles in regulating immune responses in inflammatory diseases, and many have been shown to play roles in regulating or exacerbating IBD. Mice with genetic ablation of regulatory cytokines, such as IL-2 or IL-10, develop spontaneous colitis^{169,170}, while patients with CrD have been shown to have larger amounts of Th1 and Th17 cells due to increased levels of IL-12 and IL-23^{171,172}, which drive production of the pro-inflammatory cytokines IL-6, IL-17, and TNF, among others, thereby exacerbating colitis. Accordingly, TNF blockers has been found to be an effective treatment for CrD¹⁷³. Interestingly, UC is associated with a more Th2-like response, with increased levels of IL-5 and IL-13, though not IL-4^{174,175}. In this case, the pathogenesis of UC can be linked to IL-13 and its effect on epithelial tight junction alterations, apoptosis, and epithelial restitution arrest¹⁷⁵.

With pattern recognition and cytokine production being some of the most important factors in IBD development, it is unsurprising that pro-inflammatory macrophages have been identified as one of the most important contributors to disease progression. While resident intestinal macrophages are strongly anergic to inflammatory mediators, lacking LPS receptor components such as CD14 and downregulating inflammatory cytokine production¹⁷⁶, high amounts of monocyte-derived CD14⁺ macrophages have been found to accumulate in inflamed tissue in IBD. In CrD and UC, CD14⁺ CD163^{low} myeloid cells have been shown to induce the development of Th17 cells and release high levels of IL-6, IL-23, and TNF, thereby contributing to disease pathology¹⁷⁷. This accumulation of CD14⁺ cells has been shown to be

mediated by increased production of monocyte-attracting chemokines¹⁷⁸. For instance, expression of CCL2, a potent macrophage and monocyte chemoattractant¹⁷⁹, is increased in inflamed mucosa biopsies of IBD patients¹⁸⁰, and blocking production or sensing of CCL2 reduced colitis severity and colitis-associated carcinogenesis in experimental mouse models^{181,182}. At the site of inflammation, production of inflammatory cytokines by macrophages has been shown to be essential for IBD pathogenesis. Local depletion of macrophages has been shown to prevent development of chronic colitis in IL-10-deficient mice¹⁸³, which they otherwise exacerbate through increased production of IL-12 and IL-23¹⁸⁴. Production of TNF- α , IL-1, IL-6, and IL-12 by *Stat3*-deficient macrophages leads to the development of chronic enterocolitis in mice¹⁸⁵ and macrophage-produced IL-1, IL-6, TNF- α , IL-23, IFN- γ , and ROS^{186–188} has been shown to disrupt the epithelial barrier¹⁸⁹. In addition, expression of *Ccl7*, *Ccl8*, and *Cxcl1* was found to be increased in monocytes and macrophages during dextran sodium sulfate (DSS)-induced colitis¹⁹⁰, leading to additional recruitment of monocytes and neutrophils and further exacerbating inflammation. Lastly, phagocytosis of apoptotic cells in the intestine has been shown to confer an immune-suppressive signature to macrophages¹⁹¹, with inhibited sensing of apoptotic cells through ablation of TAM receptor tyrosine kinases AXL and MERTK leading to increased susceptibility to DSS colitis and increased production of pro-inflammatory cytokines IL-6, IL-12, IL-17, and TNF in lamina propria macrophages¹⁹².

In summary, the recruitment of inflammatory monocytes and macrophages, and the subsequent production of inflammatory mediators by these macrophages, have been shown to be one of the main drivers of IBD pathogenesis.

2.4.2 Schistosomiasis

2.4.2.1 Introduction to schistosomiasis

Schistosomiasis, also referred to as bilharzia, is a disease caused by infection with parasitic flatworms of the genus *Schistosoma*. It is considered a neglected tropical disease endemic to tropical and subtropical areas and affects an estimated 240 million people worldwide, generally poor communities with little access to safe drinking water and sanitation.^{193,194} Around 89% of cases are located in Africa, with communities in the Eastern Mediterranean (8,7%), the Western Pacific (1,3%), the Americas, and South-East Asia (1% combined) also affected by the disease¹⁹⁵.

Schistosomiasis can take two major forms: urogenital schistosomiasis, caused by infection with *S. haematobium*, and intestinal schistosomiasis, caused by infection with *S. mansoni*, *S. japonicum*, *S. mekongi*, *S. guineensis*, or *S. intercalatum*. As the name suggests, urogenital schistosomiasis affects the urogenital system, with typical symptoms being blood in urine, fibrosis of the bladder and ureter, and even kidney damage or bladder cancer in severe cases. The disease can also lead to infertility. Common symptoms of intestinal schistosomiasis are abdominal pain, diarrhoea, and blood in the stool, with more severe cases also leading to enlargement of the liver and spleen, fluid accumulation in the peritoneal cavity, and pulmonary hypertension¹⁹³.

Chronic schistosomiasis causes devastating health, social, and financial burdens to individual households and governments alike. In many cases infection with *Schistosoma* leads to malnourishment and disability, affecting job performance and increasing the risk of acquiring a secondary illness¹⁹⁶.

Children with schistosomiasis have been reported to show stunted growth and reduced academic performance^{196,197}. Together, these factors are considered key causes for sustained poverty. In addition, the costs of preventative treatment and treatment of existing schistosomiasis places a high financial burden on the countries, many of which cannot afford the required medicine or are not invested in providing other preventative measures, such as providing clean water supplies¹⁹⁸.

Currently, the main strategy for combating schistosomiasis is preventative chemotherapy through mass application of praziquantel¹⁹³, selected due to its low cost, high efficacy against mature parasites, and few or mild side-effects. However, praziquantel is less effective against juvenile forms of the parasite, making re-infection common and leading to repeated application of the drug. This increases the risk of drug resistance, and has already been shown to lead to reduced efficacy of praziquantel in African communities¹⁹⁹. Accordingly, new strategies for combating and preventing schistosomiasis are urgently needed, for which understanding the mechanisms by which *Schistosoma* parasites affect the host immune response could be of importance.

2.4.2.2 The life cycle of *S. mansoni*

The life cycle of *S. mansoni* takes place across two hosts, with asexual reproduction occurring in freshwater snails of the genus *Biomphalaria* and sexual reproduction occurring in one of several mammalian host species, including humans²⁰⁰.

The cycle begins when *S. mansoni* eggs are released into freshwater alongside faeces or urine from the mammalian host. In the water, the eggs hatch into miracidia, which can infect the intermediate host, the freshwater snail. In the snail, the miracidium develops into a sporocyst, which can asexually reproduce to generate more sporocysts (sporocystogenous sporocysts) or cercariae (cercariogenous sporocysts). The snails then shed the free-swimming cercariae back into the water, with 200 to 650 cercariae being shed per day²⁰¹. The cercariae can then infect the mammalian host by penetrating the skin and develop into schistosomula, which migrate to the host's lung via the bloodstream. There, the parasites develop into schistosomes before re-entering the vascular system to reach the hepatportal circulation, where the parasite develops into the adult worm. Adult *S. mansoni* settle in the mesenteric vessels of the large and/or small intestine, where they can live for extended periods (up to 10 years) and produce and lay up to 300 eggs per day²⁰². The eggs are released into the capillary walls and distributed via the bloodstream. To complete the life cycle, the eggs are released into freshwater alongside faeces or urine.

However, eggs can also be swept to other organs, such as the liver, and induce the formation of granuloma due to the high antigenicity of the egg^{203,204}, which in turn can lead to the formation of fibrotic tissue.

2.4.2.3 The immune response during *S. mansoni* infection

During infection with *S. mansoni*, the immune response is characterised by an acute stage, which takes place while the schistosomes are migrating through the host body, and a chronic stage, which begins when the adult worms have settled in the vascular systems of the intestine and liver and produce eggs. During the acute stage, the migrating schistosomes cause a type I allergic reaction in the host, with increased eosinophil counts and respiratory distress symptoms^{205,206}. In addition, serum levels of pro-

inflammatory cytokines, such as TNF- α , IL-6, and IL-1 are increased in patients with acute schistosomiasis²⁰⁶, which points towards a Th1-mediated immune response. Critically, induction of a Th2-mediated immune response through IL-4 is essential for the survival of the host, as demonstrated in *Il-4^{-/-}* mice, which succumb to TNF- α -mediated cachexia during acute schistosomiasis¹²⁷. The transition towards a Th2-mediated immune response takes place 5 to 6 weeks post infection, when the schistosomes have settled in the intestine and liver and begun laying eggs. The released eggs excrete IPSE/alpha-1, which leads to release of IL-4 by basophils^{203,204,207} and an associated Th2-mediated response, with decreased levels of IFN- γ and increased IL-5, IL-4, IL-10, and IL-13. The intensity of this egg-mediated Th2 response peaks at about week 8 of infection, before stabilising to a more muted, but chronic response after approximately week 12²⁰⁸. The completion of the *S. mansoni* life cycle requires the excretion of the eggs via the gastrointestinal system. This requires eggs to be extravasated from the bloodstream through the endothelial border, reach the intestinal tissue environment, become encapsulated in a granuloma and transported to the intestinal lumen, passing through the intestinal epithelium in the process^{209,210}. However, the eggs themselves appear to have no methods of propulsion, and many eggs are swept to other organs, such as spleen, the stomach, the pancreas, and the gall bladder²¹¹, through the bloodstream. A large proportion of eggs end up in the liver, causing strong granulomatous inflammation and hepatic fibrosis. This is the primary cause of the morbidities associated with chronic schistosomiasis¹²⁶.

Granuloma are formed around *Schistosoma* eggs through accumulation of cells and collagen. This has been best characterised in hepatic granuloma, in which neutrophils and eosinophils are first recruited to the egg, forming a neutrophilic microabscess²¹². This matures into a granuloma with the additional recruitment of epithelial cells and macrophages, which begin to replace the neutrophil-eosinophil layer. Over time, hepatic stellate cells (HSPs) in the Disse space of the liver become activated through the release of damage-associated molecular patterns (DAMPs) by damaged hepatocytes and develop into myofibroblasts, producing collagen around the granuloma^{213,214}. In addition, T cells and B cells begin to infiltrate the granuloma. As the egg degenerates and eventually calcifies, myofibroblasts and collagen fibre become the predominant structures and the granuloma begins to shrink in the 8 to 20 weeks post infection, but remains stable for at least another 32 weeks^{210,212}.

In contrast to hepatic granuloma, which become fibrotic over time since the eggs cannot be shed, the induction of intestinal granuloma formation by the *S. mansoni* eggs serves a number of purposes for both the host and the parasite. Granuloma formation is required to transport the egg into the intestinal lumen, and the granuloma protects the surrounding host tissues from toxins secreted by the egg, as well as from exaggerated immune responses caused by toxin secretion²¹⁵. Ultimately, this prolongs the survival of the host, which also benefits the parasite. The composition of intestinal granuloma is slightly different from hepatic granuloma, with fewer eosinophils, T cells, and B cells, but more macrophages²¹⁶. However, if eggs become trapped in the intestinal tissue, they undergo similar processes to the hepatic granuloma, recruiting fibroblasts to the periphery, which leads to collagen deposition²¹⁰.

While an imbalance in the ratio of matrix metalloproteases (MMPs) to tissue inhibitors of metalloproteases (TIMPs) mediated by fibroblasts has been described as a contributing factor for fibrosis development in the liver and colon^{217,218}, the key driver of granuloma formation and fibrosis in

schistosomiasis *mansoni* is the accumulation of CD4⁺ Th2 cells^{215,219} and the subsequent production of IL-13. In mouse models in which IL-13 has been knocked out (*Il-13*^{-/-} mice)²²⁰, IL-13 signalling has been blocked through genetic ablation of IL-4R α (*Il-4r α* ^{-/-} mice)²²¹, and in mice treated with IL-13 receptor α chain 2 (IL-13R α 2), which acts as an IL-13 blocker through high-affinity competitive binding of IL-13²²², mice develop smaller granuloma and do not develop hepatic fibrosis.

At first, considering macrophages polarised towards an anti-inflammatory phenotype by sensing of IL-4/IL-13 as mediators of IL-13-induced fibrosis would appear to make sense, since polarisation of macrophages with IL-13 leads to the activation of pathways associated with fibrosis development^{223,224}. In a model of IL-13-induced airway and parenchymal tissue fibrosis, activation of TGF- β was found to mediate the fibrogenic effects of IL-13²²⁵, and granuloma pathology is partially mediated by increased expression of ARG1. As described above (chapter 2.2.2.2), ARG1 hydrolyses L-arginine to ornithine and urea⁵⁹. Ornithine-aminotransferase subsequently converts ornithine into proline, which is an essential amino acid known to be involved in collagen production^{60,126}. This, in turn, may contribute to fibrosis development. In addition, depletion of CD11b⁺ F4/80⁺ LY6C⁺ macrophages led to decreased inflammation, fibrosis, and type 2 gene expression in the lungs of mice infected with *S. mansoni*²²⁶.

However, there is increasing evidence that anti-inflammatory macrophages play protective roles during schistosomiasis, in addition to being essential for survival of schistosomiasis through downregulation of Th1-mediated inflammatory responses²²⁷. *S. mansoni*-infected mice treated with bone marrow-derived monocytes had fewer, smaller liver granuloma and less fibrosis compared to wildtype mice, as well as lower expression of both pro-inflammatory (TNF- α , IL-1 β , IL-6) and pro-fibrogenic mediators (TGF- β , IL-4). In addition, expression of MMP-9 was increased, while levels of TIMP-1 and markers for pro-inflammatory macrophages (CCL5, IL-12 β , CCR2) were reduced in the livers of these mice²²⁸. Different populations of tissue remodelling macrophages have been shown to regulate fibrosis development and development of granulomatous inflammation in *S. mansoni* infection, with more immature *Lyz2*^{low} macrophages protecting against fibrosis development, and more mature *Lyz2*^{hi} macrophages controlling inflammation²²⁹. Notably, this is shown to be mediated through expression of ARG1, which suppresses Th2-dependent fibrosis development by inhibiting CD4⁺ T cell effector functions²³⁰. Together with the finding that macrophage-derived RELM α plays a protective role in *S. mansoni* infection, as demonstrated by increased granulomatous inflammation in the lungs and livers of *Retnla*^{-/-} mice^{77,231}, this suggests that anti-inflammatory macrophages play a protective role during both the acute and chronic stages of *S. mansoni* infection.

2.5 The aim of this study

With macrophages playing such a crucial role in the pathogenesis, but also the resolution of inflammation, understanding the mechanisms through which macrophages acquire and exert tissue remodelling functions could be essential to develop new treatment strategies for chronic inflammation. Previous research suggests that expressed sequence *Aa467197* may be involved in regulating macrophage tissue remodelling functions, but this has not been studied up to now. Accordingly, the aim of this thesis was to investigate the contribution of *Aa467197* to macrophage tissue remodelling functions. To this end, *in vitro* approaches were used to study the expression of *Aa467197* in polarised macrophages and the activation status of macrophages in which *Aa467197* had been genetically

ablated, including transcriptional profile analysis through RNA sequencing. In addition, the contribution of *Aa467197* to the development of IBD was studied via the *in vivo* mouse model of DSS-induced colitis. Similarly, the role of *Aa467197* in schistosomiasis was studied through infection of mice with *S. mansoni*. Together, the results of this thesis provide further evidence that *Aa467197* plays a role in macrophage tissue remodelling and give insight into potential mechanisms through which *Aa467197* may mediate the response.

3. Materials

3.1 Consumable plastic and glass materials

Table 1: List of consumable plastic and glass materials

Name	Company
Cannula, Sterican, 2G, 14G , 21G	B. Braun Melsungen AG, Melsungen, Germany
Cell culture flasks (T25, T75, T175)	Sarstedt, Nürmbrecht, Germany
Cell culture plate (6/24/96 U/R bottom)	Greiner bio-one, Frickenhausen, Germany
Cell Strainer (100, 70, 40µm)	Pluriselect, Leipzig, Germany
Cryo tubes	Nunc, Wiesbaden, Germany
ELISA plate (microplate high binding)	Greiner bio-one, Frickenhausen, Germany
FACS tubes	Sarstedt, Nürmbrecht, Germany
Falcons (15, 50mL)	Sarstedt, Nürmbrecht, Germany
Glass pipettes (2, 5, 10, 20mL)	Brand GmbH, Wertheim, Germany
Glass bottles (50, 100, 200, 500, 1000mL)	Schott AG, Mainz, Germany
Magnetic-activated cell sorting (MACS) columns (LS, MS)	Miltenyi Biotech, Bergisch Gladbach, Germany
Neubauer Chamber (0,1 x 0,0025mm ²)	Hecht-Assistent, Sondheim, Germany
Omnican 500/1000µL	B Braun Melsungen AG, Melsungen, Germany
Pasteur pipettes, glass	Fisher Scientific GmbH, Schwerte, Germany
Petri dish 15cm	Sarstedt, Nürmbrecht, Germany
Pipette tips (10, 20, 200,1000µL)	Sarstedt, Nürmbrecht, Germany
Plastic pipettes (5, 10, 25mL)	Sarstedt, Nürmbrecht, Germany
Reflotron® GPT/ALAT strips	Roche Diagnostics AG, Rotkreuz, Switzerland
Syringes (5 mL, 10 mL, 20 mL)	B Braun Melsungen AG, Melsungen, Germany
Seahorse assay culture plates	Aglient, Santa Clara, California, USA
Seahorse assay sensor cartridges	Aglient, Santa Clara, California, USA
Tubes (0,5mL, 1,5mL, 2mL)	Sarstedt, Nürmbrecht, Germany
Venofix A 21G butterfly	B.Braun Melsungen AG, Melsungen, Germany

3.2 Human samples

Table 2: List of human patient samples from sigmoid colon, anonymised

Treatment group	Patient ID
Healthy control	5307
	5289
	5281
	5276
	5364
Acute UC	5200
	5197
	5121
	5315
	5381
In remission from UC	5394
	5271
	5238
	5207
	5297

3.3 Mouse lines

Table 3: List of mouse lines

Name	Information	Origin
C57Bl/6J	Wildtype	Bred in-house, BNITM, Hamburg, Germany
<i>Nmes1</i> ^{+/+}	Wildtype	Bred in-house, BNITM, Hamburg, Germany
<i>Nmes1</i> ^{-/-}	Total knockout for gene expressed sequence <i>Aa467197</i> (<i>Nmes1</i>)	Breeding pair provided by the laboratory of Henao-Mejia, University of Pennsylvania, PA, USA, then bred in-house, BNITM, Hamburg, Germany

<i>Axl^{fl/fl}Mertk^{fl/fl}-Csf1r-Cre⁻</i>	Mice with loxP-flanked <i>Axl</i> and <i>Mertk</i> lacking expression of Cre recombinase	Breeding pair provided by the laboratory of Rothlin, Yale, USA, then bred in-house, BNITM, Hamburg, Germany
<i>Axl^{fl/fl}Mertk^{fl/fl}-Csf1r-Cre⁺</i>	Mice with loxP-flanked <i>Axl</i> and <i>Mertk</i> and expression of Cre recombinase at <i>Csf1r</i> promotor	Breeding pair provided by the laboratory of Rothlin, Yale, USA, then bred in-house, BNITM, Hamburg, Germany

In addition, RNA from intestinal tissues of C57Bl/6J mice raised germ-free was kindly provided by the group of Nicola Gagliani at the UKE.

3.4 Cell lines

Aliquots of the mouse fibroblast cell line L929 were kindly provided by the group of Thomas Jacobs at the Bernhard-Nocht-Institute for Tropical Medicine (BNITM) in Hamburg. Aliquots were frozen in liquid nitrogen at a concentration of 3×10^6 cells/mL.

3.5 Parasites

Schistosoma mansoni cercariae were generated, isolated, and purchased from Helmut Haas (Forschungszentrum Borstel).

3.6 Chemicals, enzymes, and cytokines

3.6.1 Chemicals

Table 4: List of chemicals

Name	Company
Agarose	Biomol, Hamburg, Germany
Ampuwa, water	Fresenius, Graz, Austria
Aqua bidestilled (aqua bidest)	Distilled in-house, BNITM, Hamburg, Germany
Bovine serum albumine (BSA)	Sigma Aldrich/Merck, Darmstadt, Germany
Calcium chloride (CaCl ₂)	Sigma Aldrich/Merck, Darmstadt, Germany or Carl Roth, Karlsruhe, Germany
Click's Medium	Merck, Darmstadt, Germany
Cytochalasin D	Thermo Fisher Scientific, Waltham, USA
Dextran sodium sulfate (DSS)	MP Biomedicals, Solon, Ohio, USA
Disinfection spray/Incidin liquid	Ecolab, Düsseldorf, Germany
Dulbecco's Modified Eagle Medium (DMEM)	PAA Laboratories GmbH, Pasching, Austria

Materials

Phosphate-buffered saline (PBS) 10 x	Capricorn, Ebsdorfergrund, Germany
Ethylenediaminetetraacetic acid (EDTA)	Thermo Fisher Scientific, Waltham, USA
FACSFlow™ sheath fluid	BD Biosciences, Heidelberg, Germany
FACSFlow™ cleaning solution	BD Biosciences, Heidelberg, Germany
Fetal calf serum (FCS)	Capricorn, Ebsdorfergrund, Germany
Generuler 100 bp DNA Ladder	Thermo Fisher Scientific, Waltham, USA
Gentamicin	Capricorn, Ebsdorfergrund, Germany
Heparin	Ratiopharm, Ulm, Germany
Hydrogen Peroxide (H ₂ O ₂)	Sigma Aldrich/Merck, Darmstadt, Germany or Carl Roth, Karlsruhe, Germany
L-Glutamine	Capricorn, Ebsdorfergrund, Germany
Glucose	Carl Roth, Karlsruhe, Germany
Isopropanol	Carl Roth, Karlsruhe, Germany
Lugol solution	Carl Roth, Karlsruhe, Germany
Magnesium chloride (MgCl ₂)	Sigma Aldrich/Merck, Darmstadt, Germany or Carl Roth, Karlsruhe, Germany
Percoll	Sigma Aldrich, Darmstadt, Germany
Phenol red	Sigma Aldrich/Merck, Darmstadt, Germany or Carl Roth, Karlsruhe, Germany
Potassium chloride (KCl)	Sigma Aldrich/Merck, Darmstadt, Germany or Carl Roth, Karlsruhe, Germany
Potassium phosphate (KH ₂ PO ₄)	Sigma Aldrich/Merck, Darmstadt, Germany or Carl Roth, Karlsruhe, Germany
RNAProtect Tissue Reagent	Qiagen, Hilden, Germany
RPMI 1640 without L-glutamine	PAA Laboratories GmbH, Pasching, Austria
Seahorse XF hydration solution	Aglient, Santa Clara, California, USA
Sodium bicarbonate (NaHCO ₃)	Sigma Aldrich/Merck, Darmstadt, Germany or Carl Roth, Karlsruhe, Germany
Sodium chloride (NaCl)	Sigma Aldrich/Merck, Darmstadt, Germany or Carl Roth, Karlsruhe, Germany
Sodium phosphate dihydrate (Na ₂ HPO ₄ • 2H ₂ O)	Sigma Aldrich/Merck, Darmstadt, Germany or Carl Roth, Karlsruhe, Germany

Sulfuric acid (H ₂ SO ₄)	Sigma Aldrich/Merck, Darmstadt, Germany or Carl Roth, Karlsruhe, Germany
Tetramethylbenzidine (TMB) substrate solution	Thermo Fisher Scientific, Waltham, USA
TRizoI™ reagent	Thermo Fisher Scientific, Waltham, USA
Trypan blue solution 0.4%	Invitrogen, Gibco, Auckland, New Zealand
Trypsin-EDTA (1x)	PAA Laboratories GmbH, Pasching, Austria
Tween® 20	Sigma Aldrich/Merck, Darmstadt, Germany
UltraPure™ TBE Buffer, 10x	Thermo Fisher Scientific, Waltham, USA
X-VIVO™ 10	Lonza, Verviers, Belgium
β-Mercapthoethanol	Invitrogen, Gibco, Auckland, New Zealand

3.6.2 Enzymes

Table 5: List of enzymes

Name	Company
Collagenase IV	STEMCELL Technologies, Cologne, Germany
Collagenase VIII	Worthington Biochemical Corporation, Lakewood, New Jersey, USA
DNase I	Roche AG, Basel, Austria or Qiagen, Hilden, Germany
Proteinase K	Qiagen, Hilden, Germany

3.6.3 Cytokines

Table 6: List of cytokines

Name	Company
Interleukin 4 (IL-4), murine	BD Biosciences, Heidelberg, Germany or Miltenyi Biotech, Bergisch Gladbach, Germany
Interleukin 4 (IL-4), human	R&D Systems, Abingdon, UK

3.7 Buffers and media

Table 7: List of buffers and media

Name	Composition
1x PBS	1:10 10x PBS in aqua bidest
Click's medium (complete)	Click's medium with 10% (v/v) FCS, 2,5% (v/v) L-glutamine, and 0,5% (v/v) gentamicin
Colon digestion buffer I	Per sample: 20mL HBSS-- with 200µL 0,5M EDTA
Colon digestion buffer II	Per sample: 5mL HBSS-- with 2% FCS, 3µL DNase I (20KU/mL), 5mg collagenase VIII
ELISA blocking buffer	1x PBS with 1% (w/v) BSA
ELISA substrate buffer	0,1M NaH ₂ PO ₄ solution with 0,016% (v/v) TMB solution and 10% (v/v) H ₂ O ₂ (30% solution)
FACS blocking buffer	1x PBS with 1:10000 α-mouse CD16/CD32
FACS measurement buffer	1x PBS with 2% (v/v) FCS
Hank's Balanced Salt Solution (HBSS)--	Aqua bidest (BNITM) with 0,8% (w/v) NaCl, 0,04% (w/v) KCl, 0,006% (w/v) Na ₂ HPO ₄ • 2H ₂ O, 0,006% (w/v) KH ₂ PO ₄ , 0,1% (w/v) glucose, 0,035% (w/v) NaHCO ₃ , 0,001% phenol red, and 1% (v/v) gentamicin, pH 7,5
L929 culture medium	RPMI1640 with 20% (v/v) FCS, 1% (v/v) 200mM L-glutamine, and 0,5% (v/v) gentamicin
Liver digestion buffer	Per sample: 10mL DMEM with 10mg collagenase IV, 100µL 0,2M MgCl ₂ solution, 40µL 0,5M CaCl ₂ solution, and 50uL DNase I (150 U/mL)
Macrophage culture medium	RPMI1640 with 20% (v/v) FCS, 1% (v/v) 200mM L-glutamine, 0,5% (v/v) gentamicin, and 20-30% (v/v) L929 supernatant (see chapter 4.2)
MACS buffer	1x PBS with 0,5% (w/v) BSA and 2mM EDTA
Neutrophil culture medium	RPMI1640 with 20% (v/v) FCS, 1% (v/v) 200mM L-glutamine, and 0,5% (v/v) gentamicin
PBMC culture medium	RPMI1640 with 10% (v/v) FCS, 1% (v/v) 200mM L-glutamine, and 0,5% (v/v) penicillin/streptomycin
PBS/Tween	1x PBS with 0,05% (v/v) Tween

Proteinase K digestion buffer	0,1M Tris Cl (pH 8) with 0,005M EDTA, 0,2M NaCl, and 0,2% (v/v) SDS
Seahorse assay medium	Seahorse XF DMEM with 1mM pyruvate and 2mM L-glutamine
TBE buffer	1:10 UltraPure™ TBE Buffer in aqua bidest

3.8 Laboratory equipment

Table 8: List of laboratory equipment

Name	Company
Agarose gel electrophoresis chamber	BioRAD, Munich, Germany
Analytical scale	Sartorius AG, Göttingen, Germany
Benchtop centrifuge	Eppendorf, Hamburg, Germany
Cell sorter FACSaria III	BD Biosciences, Heidelberg, Germany
Centrifuge	Eppendorf, Hamburg, Germany
ChemiDoc™ Touch Imaging System	BioRAD, Munich, Germany
Corbett RotorGene 6000	Qiagen, Hilden, Germany
Dissection instruments (forceps & scissors)	Neolab, Heidelberg, Germany
ELISA Photometer	MRX-II Dynex Technologies, Berlin, Germany
Flow cytometer Accuri C6a	BD Biosciences, Heidelberg, Germany
Flow cytometer LSR II	BD Biosciences, Heidelberg, Germany
Freezer -20°C /-70°C	Liebherr, Biberach an der Riss, Germany
Fridge Comfort	Liebherr, Biberach an der Riss, Germany
Incubator	Heraeus instruments, Hanau, Germany
Laminar flow FlowSafeB-(MacPro) ³ -130	Brener, Elmshorn, Germany
MACS Magnet	Miltenyi Biotech, Bergisch Gladbach, Germany
Multichannel pipettes	Eppendorf, Hamburg, Germany
NanoDrop 2000C	Thermo Fisher Scientific, Waltham, USA
PCR cycler (Peqstar 96x Universal Gradient)	Peqlab, Erlangen, Germany
Pipettes 10 µL, 20 µL, 100 µL, 200 µL, 1000 µL	Eppendorf Hamburg Germany / Gilson, Middleton, Wisconsin, USA
Pipettboy Acujet pro	Brand, Wertheim Germany

Pipettes (10 µL, 20 µL, 200 µL, 1000 µL)	Gilson, Middleton, Wisconsin, USA
Power supply	BioRAD, Munich, Germany
Reflotron®	Roche Diagnostics AG, Rotkreuz, Switzerland
Seahorse XF Extracellular Flux Analyser	Aglient, Santa Clara, California, USA
Thermomixer MM	B Braun, Melsungen, Germany
Vortexer Genie 2	Bender & Hobein AG, Zürich, Switzerland
Water bath	Haake, Karlsruhe, Germany

3.9 Commercial kits

Table 9: List of commercial kits

Name	Company
10x Perm/Wash™ Buffer	BD Biosciences, Heidelberg, Germany
CD14 ⁺ MACS cell isolation kit	Miltenyi Biotech, Bergisch Gladbach, Germany
DreamTaq Green PCR Master Mix (2X)	Thermo Fisher Scientific, Waltham, USA
FITC Annexin V Apoptosis Detection Kit with PI	BioLegend, San Diego, USA
Intracellular Fixation/Permeabilisation Buffer Set Fxp3	Thermo Fisher Scientific, Waltham, USA
iScript™ cDNA synthesis Kit	BioRAD, Munich, Germany
LEGENDplex™ mouse 8-Plex Th1/Th2	Biolegend, Fell, Germany
Maxima SYBR Green qPCR Master Mix with separate ROX vials	Thermo Fisher Scientific, Waltham, USA
Mouse DuoSet ELISA Kits (IL-5, IL-13)	R&D Systems, Abingdon, UK
Neutrophil MACS cell isolation kit	Miltenyi Biotech, Bergisch Gladbach, Germany
PrimeFlow™ RNA Assay	Thermo Fisher Scientific, Waltham, USA
QiaShredder	Qiagen, Hilden, Germany,
RNeasy Mini Kit	Qiagen, Hilden, Germany
Seahorse XF Cell Mito Stress Test Kit	Aglient, Santa Clara, California, USA

3.10 DNA oligonucleotides

All oligonucleotides were synthesised and purchased from Eurofins Genomics Germany GmbH, Ebersberg, Germany.

3.10.1 Genotyping primers

Table 10: List of primers used for mouse genotyping

Name	Sequence (5' to 3')
<i>Nmes1</i> WT fwd	TCTATCGCTGCCTGTTTGTG
<i>Nmes1</i> WT rev	CAAACCCGGAAGAGCTACTG
<i>Nmes1</i> KO fwd	GCTTTCTGCGACTGTTGGAC
<i>Nmes1</i> KO rev	ATGCAGGATCCAAAGAATGC

3.10.2 qPCR primers

3.10.2.1 Mouse primers

Table 11: List of primers used for qPCR on mouse samples

Name	Sequence (5' to 3')
<i>Aa467197</i> fwd	GGAGCCACATCTTTCGCTTTG
<i>Aa467197</i> rev	CTCCTCAACGGGCTTCCATTG
<i>Ahr</i> fwd	GGCTTTCAGCAGTCTGATGTC
<i>Ahr</i> rev	CATGAAAGAAGCGTTCTCTGG
<i>Arg1</i> fwd	CATTGGCTTGCGAGACGTAGAC
<i>Arg1</i> rev	GCTGAAGGTCTCTTCCATCACC
<i>Chil3</i> fwd	CTGGAATTGGTGCCCCTACA
<i>Chil3</i> rev	CAAGCATGGTGGTTTTACAGGA
<i>Fzd4</i> fwd	TGCCAGAACCTCGGCTACA
<i>Fzd4</i> rev	ATGAGCGGCGTGAAAGTTGT
<i>Gapdh</i> fwd	TCCCACTCTTCCACCTTCGA
<i>Gapdh</i> rev	AGTTGGGATAGGGCCTCTCTT
<i>Gata3</i> fwd	GCTGGATGGCGGCAAAG
<i>Gata3</i> rev	GTGGGCGGGAAGGTGAA
<i>Il-1β</i> fwd	GAAGAAGTGCCCATCCTCTG

Materials

<i>Il-1β</i> rev	AGCTCATATGGGTCCGACAG
<i>Mmp13</i> fwd	GTTTACCTTCGCCTCACTAG
<i>Mmp13</i> rev	TCTCTCCTTCCCAGGGCAAGCAT
<i>Retnla</i> fwd	CCAATCCAGCTAACTATCCCTCC
<i>Retnla</i> rev	CCAGTCAACGAGTAAGCACAG
<i>Socs5</i> fwd	GACGGCTTAGTATCGAAGAA
<i>Socs5</i> rev	GCTTATACAATGGGTTGACC
<i>Timp1</i> fwd	GCGGTTCTGGGACTTGTGGGC
<i>Timp1</i> rev	GCATCTCTGGCATCTGGCATC

3.10.2.2 Human primers

Table 12: List of primers used for qPCR on human samples

Name	Sequence (5' to 3')
<i>GAPDH</i> fwd	GCGAGATCCCTCCAAAATCAA
<i>GAPDH</i> rev	GTTACACCCATGACGAACAT
<i>NMES1</i> fwd	AGCTCATTCCCTTGGTGGTG
<i>NMES1</i> rev	CAAAGGTGCTAAGGTTTGGGC

3.11 Antibodies

3.11.1 FACS antibodies

All FACS antibodies were used to stain mouse cell samples. Unless otherwise noted, antibodies were sourced from BioLegend, San Diego, USA.

3.11.1.1 Extracellular antibodies

Table 13: List of FACS antibodies used for extracellular staining

Epitope	Fluorochrome	Clone	Dilution	Company
CCR2	BV510	SA203G11	1:300	
CD11b	APC/Cy7	M1/70	1:400	
	BV510	M1/70	1:200	
	FITC	M1/70	1:500	
CD44	PerCP-Cy5.5	IM7	1:300	

Materials

CD45	BV510	30-F11	1:500	
	PE/Cy7	30-F11	1:1300	
CD80	PE-Texas Red	16-10A1	1:300	
CX3CR1	AF700	SA011F11	1:300	
	PE/Cy7	SA011F11	1:500	
F4/80	APC/Cy7	BM8	1:400	
	AF700	BM8	1:400	
	FITC	BM8	1:300	
LY6C	BV510	HK1.4	1:300	
	PerCP-Cy5.5	HK1.4	1:300	
LY6G	APC/Cy7	IA8	1:300	
	BV421	IA8	1:300	
	PerCP-Cy5.5	IA8	1:300	
MHCII	PerCP	M5/114.15.2	1:2000	

3.11.1.2 Intracellular antibodies

Table 14: List of FACS antibodies used for intracellular staining

Epitope	Fluorochrome	Clone	Dilution	Company
a-goat IgG	FITC	Poly4606	1:300	Invitrogen, Gibco, Auckland, New Zealand
a-rabbit IgG	BV421	Poly4064	1:300	
	BV510	Poly4064	1:300	
ARG1	APC	A1exF5	1:500	Invitrogen, Gibco, Auckland, New Zealand
	PE	A1exF5	1:500	Invitrogen, Gibco, Auckland, New Zealand
CD68	BV421	FA-11	1:500	

Histone 3 (citrullinated)	Purified	Polyclonal rabbit IgG	1:200	Abcam plc., Cambridge, United Kingdom
MPO	FITC	2D4	1:200	Abcam plc., Cambridge, United Kingdom
RELMa	Purified	Polyclonal rabbit IgG	1:200	PreproTech GmbH, Hamburg, Germany
YM1	Purified	Polyclonal goat IgG	1:200	R&D Systems, Abingdon, UK

3.11.1.3 PrimeFlow™ target probes

Table 15: List of target probes used for PrimeFlow™ staining

Construct name	Colour type	Assay ID	Company
<i>Aa467197</i>	Type 1 (AF647)	VB1-6001250	Thermo Fisher Scientific, Waltham, USA
<i>B2m control</i>	Type 6 (AF750)	VB6-12836-PF	Thermo Fisher Scientific, Waltham, USA

3.11.2 Other antibodies

Table 16: List of other antibodies

Name	Company
anti-CD3ε (for T cell activation)	BioLegend, San Diego, USA

3.12 Software and Databases

Table 17: List of software and databases

Software	Purpose
Adobe Reader DC	Reading PDF files
BD FACS DIVA 6.2	Acquiring FlowJo data
ClustVis	Heatmap generation

David v6.8	GO term analysis
Flow Jo Version 10.01	Analysis of flow cytometry data
Graphpad Prism 8 for Windows	Statistical analysis and graphics processing
LEGENDplex v8.0	Analysis of LEGENDplex data
Image Lab v5.2.1	Analysis of agarose gel images
Mendeley Desktop 1.16.3	Citations
Microsoft Office 2013	Word and graphics processing
Rotor-Gene Q Series Software 2.3.1	Analysis of qPCR data
Seahorse Wave Desktop V2.6	Extracellular flux analysis

4. Methods

4.1 Human samples

4.1.1 Colon samples

RNA from total sigmoid colons of IBD patients was kindly provided by the group of Samuel Huber at the University Clinic Hamburg-Eppendorf (UKE) in Hamburg. For these samples, endoscopic biopsy specimens were obtained from the colon (sigma/rectum) from patients with IBD or suspicion of intestinal disease. An additional biopsy was taken from the largest foci of macroscopic inflammation. Human studies were approved by the local ethical committee (Ethik-Kommission der Ärztekammer Hamburg PV4444) ²³².

4.1.2 Peripheral blood mononuclear cells (PBMCs)

PBMCs were kindly provided by the group of Thomas Jacobs at the Bernhard-Nocht-Institute for Tropical Medicine (BNITM) in Hamburg. All PBMC samples were provided frozen, originally sourced from buffy coats from healthy donors provided by the UKE to the BNITM.

4.1.2.1 Preparation of PBMCs for downstream applications

To prepare frozen PBMCs for *in vitro* experiments, PBMCs were removed from storage in liquid nitrogen and thawed at hand temperature. 1mL X-VIVO™ 10 medium, pre-warmed to 37°C, was added to the thawed PBMC suspension drop by drop and carefully mixed in before being transferred to an additional 8mL pre-warmed X-VIVO™ 10 and carefully mixed. The suspension was then centrifuged at 300 x g for 10 minutes at 4°C. The supernatant was discarded and the cell pellet was carefully washed in 9mL pre-warmed PBMC culture medium (see Table 7) and centrifuged again at 300 x g for 10 minutes at 4°C. The supernatant was discarded and the cell pellet was resuspended in an appropriate volume of PBMC culture medium for counting (see chapter 4.5). After counting, PBMCs were plated at $0,33 \times 10^6$ cells/well in 24-well plates and used for further applications.

4.1.2.2 Differentiation of PBMCs into monocyte-derived macrophages (MDMs)

Isolated PBMCs were differentiated into MDMs by first isolating the CD14⁺ monocyte population, then differentiating the isolated monocytes into macrophages through incubation with recombinant M-CSF. CD14⁺ monocytes were isolated from total PBMCs via magnetic-activated cell sorting (MACS). Briefly, PBMCs were washed with MACS buffer (see Table 7), then transferred to a FACS tube and incubated with 50µL CD14 beads per 10⁷ cells at room temperature for 30 minutes. After 30 minutes, 1mL MACS buffer was added and the tube was placed inside a MACS magnet for 8-10 minutes at room temperature. The suspension of unbound beads was carefully removed by pipetting, and the bound cells remaining in the tube were washed twice with MACS buffer, with incubation steps in the magnet for another 8-10 minutes. Cells were then resuspended in PBMC medium, counted, and plated at 0,33x10⁶ cells/well in a 24-well plate. M-CSF was added at a final concentration of 30ng/mL. After 3 days, media were changed completely, including addition of fresh M-CSF. After 6-7 days, cells were used for further applications.

4.2 L929 cell culture

To obtain mature bone marrow macrophages, supernatant from the L929 mouse fibroblast cell line was used as a source of M-CSF. To generate M-CSF-containing L929 supernatant, L929 cells were seeded into T175 cell culture flasks and cultivated in L929 culture media (see Table 7) at 37°C/5% CO₂. The cells were monitored for growth and confluence using a light microscope. Once the cells were confluent, the cells were detached by scraping and split, with one flask being split into 3 flasks, each containing 100mL of fresh L929 culture media. The cells were then incubated at 37°C/5%CO₂. After two weeks (encompassing about 5 passages), all supernatant was harvested, filtered, and tested by monitoring the differentiation of isolated bone marrow cells into macrophages (see chapter 4.4.1.1.). L929 supernatant was stored in 50mL aliquots at -20°C.

4.3 Mice

All mouse experiments were approved by the office for consumer protection of the city of Hamburg (experiment protocols 66/17 and N042/2019, organ removal protocol O 055/2018). Mice were bred and maintained in a specific pathogen-free (SPF) facility at the BNITM.

4.3.1 Genotyping

In order to obtain wildtype *Nmes1*^{+/+} and knockout *Nmes1*^{-/-} littermates, *Nmes1*-het mice from previous C57Bl/6J x *Nmes1*^{-/-} pairings were paired for breeding. To determine the genotypes of mice from *Nmes1*-het x *Nmes1*-het pairings, DNA was isolated from mouse tissue samples (earmarks taken by employees of the animal facility at the BNITM). *Nmes1* wildtype (~250bp) and knockout (~150bp) segments were amplified by PCR, and the size of the PCR product was assessed using agarose gel electrophoresis.

4.3.1.1 DNA isolation

To isolate DNA from the provided tissue samples, the samples were first digested using proteinase K. To this end, each sample was incubated in 10µL proteinase K (Qiagen) and 90µL proteinase K digest buffer (see Table 7) at 37°C overnight. The next morning, 300µL Ampuwa was added to each sample to stop the proteinase K digest. The samples were vortexed rigorously to disrupt the tissue, then incubated at 100°C in a heating block for 10 minutes to fully deactivate the proteinase K. After

incubation, the samples were vortexed again to further disrupt the tissue before being centrifuged in a tabletop centrifuge at maximum speed (16000 x g) for 2 minutes to pellet remaining tissue components. The DNA remained in the supernatant.

4.3.1.2 PCR amplification

To amplify DNA segments, the DreamTaq Green PCR MasterMix was used (see Table 9). Briefly, the following components were mixed together for each sample:

DreamTaq reaction mix	
DreamTaq Green PCR MasterMix	12,5µL
Primers	0,1µL per primer
DNA template (supernatant)	2µL
Ampuwa	To 25µL total volume

The PCR reaction was performed in a PeqStar PCR cycler, using the following programme:

Genotyping PCR cycles		
Initial denaturation	94°C for 3 minutes	
Denaturation	94°C for 15 seconds	Repeat x35
Annealing	60°C for 30 seconds	
Extension	72°C for 60 seconds	
Final extension	72°C for 15 minutes	

4.3.1.3 Agarose gel electrophoresis

Upon completion of the PCR, the samples containing the amplified fragments were applied to an agarose gel and separated by electrophoresis to assess their size. To this end, an agarose gel was produced by combining 1,5g agarose and 100mL TBE buffer (see Table 7) (1,5% agarose gel) and heating the mixture in a microwave until the agarose had melted. 6µL ethidium bromide were added to the mixture, which was then poured into a gel chamber mould with electrophoresis combs and left to harden. After hardening, the gel was transferred to an electrophoresis chamber, the combs were removed, and 7µL of each PCR sample was added to the pockets left by the comb. To assess the size of the fragments, 5µL of a DNA ladder (see Table 4) ran alongside the samples. The electrophoresis was run in 1x TBE buffer at 80-100V for approximately 75 minutes. The DNA bands were then visualised using a ChemiDoc™ Touch and analysed using Image Lab v5.2.1.

4.4 Isolation of cells from mouse organs

4.4.1 Bone marrow

To isolate bone marrow from mice, femurs and tibias were removed and cleaned of muscle tissue, then rinsed briefly in 70% ethanol. Under sterile conditions, the bones were cut at one epiphysis and placed cut side down in a punctured 0,5mL tube placed within a 1,5mL tube, then centrifuged at maximum speed (16000 x g) for 2 minutes in a tabletop centrifuge. As a result, the bone marrow was collected in the bottom of the 1,5mL tube, while the bones were retained in the 0,5mL tubes. The bones and smaller tubes were discarded and the bone marrow was resuspended in 150µL RPMI 1640 containing 10% FCS. The bone marrow suspension was then filtered through a 40µm cell strainer before use for further applications.

4.4.1.1 Culture of bone marrow-derived macrophages

For differentiation into macrophages, the filtered bone marrow suspension was plated in 10mL macrophage culture medium (see Table 7) in a 10cm petri dish at 37°C/5%CO₂ for 7 days in total. On day 3, half the media was replaced with fresh media. On day 5, the cells were detached from the petri dish by placing the dish on ice and carefully pipetting ice-cold, sterile PBS over the surface of the plate until the cells were detached. The cell suspension was centrifuged down and split across two petri dishes, each containing 10mL culture media, and incubated at 37°C/5%CO₂ for the remaining 2 days. On day 7, the cells were detached and washed as on day 5, then counted (see chapter 4.5) and used for further applications.

4.4.1.2 Isolation of neutrophils from bone marrow

To isolate neutrophils from bone marrow, the MACS Neutrophil isolation kit by Miltenyi (see Table 9) was used according to the manufacturer's instructions. Briefly, the cells in the filtered bone marrow suspension were counted (see chapter 4.5), washed with MACS buffer (see Table 7), and incubated with the provided antibody cocktail for 10 minutes. The cells were then washed and incubated with the provided bead solution for 15 minutes. The cells were washed again and transferred to prepared MS or LS columns in Miltenyi MACS magnets. The flow-through containing the neutrophils was collected. The columns were washed three times, collecting the flow-through in the same tube, and the tube was then centrifuged at 300 x g for 5 minutes at 4°C. The isolated neutrophils were then resuspended in neutrophil culture medium (see Table 7), counted (see chapter 4.5), and used for further applications.

4.4.2 Isolation of cells from the colon/lamina propria

To isolate lamina propria cells, colons were removed from mice, cut open longitudinally, and washed in PBS to remove faeces. The washed colons were cut into 4 to 5 smaller pieces, then incubated in 20mL colon digestion buffer I (see Table 7) per sample at 37°C in a shaker for 20 minutes to detach epithelial cells. After this first digest, the colon pieces were washed in PBS 3-5 times to remove the epithelial cells. The remaining pieces were then minced to disrupt the tissue and digested in 5mL colon digestion buffer II (see Table 7) per sample for 45 minutes at 37°C on a shaker. After digestion, the suspension was mashed through a 100µm cell strainer, then filtered again through a 40µm cell strainer. The filtered suspension was centrifuged at 300 x g for 5 minutes at 4°C to pellet the cells, which were then used for further applications.

4.4.3 Isolation of cells from the liver

To isolate liver cells, livers were removed from mice and minced to disrupt the tissue. The minced tissue was incubated in 10mL liver digestion media (see Table 7) for 45 minutes at 37°C on a shaker, then mashed through a 70µm cell strainer to isolate the cells. The cell suspension was centrifuged at 300 x g for 5 minutes and the supernatant was carefully removed using a glass pipette. The cell pellet was washed using 10mL RPMI 1640 and centrifuged at 300 x g for 5 minutes. This step was repeated until the supernatant was clear. The cells were then resuspended in 10mL RPMI 1640 and centrifuged at 50 x g for 3 minutes to pellet the hepatocytes, leaving the non-parenchymal cells (NPCs) in the supernatant. The supernatant was transferred to a fresh 50mL tube and centrifuged at 300 x g for 5 minutes to pellet the NPCs. At this stage, samples could be used for further applications, such as FACS staining and analysis.

For sorting after *Schistosoma mansoni* experiments, the cells were further split using Percoll density centrifugation. To this end, the cells were resuspended in 6mL 37 % Percoll per liver and centrifuged for 10 minutes at 400 x g (with the break set to 1).

Before any further applications, red blood cells were removed through lysis by incubating the isolated cell suspension in 3 mL ery-lyse (see Table 7) for 5 minutes. After 5 minutes, 15 mL PBS were added to stop the reaction and the mixture was centrifuged 300 x g for 5 minutes at 4°C to isolate the cells. The isolated cells were then used for further applications.

4.4.4 Serum

To isolate serum from mouse blood, mice were sacrificed and whole blood was extracted via the inferior vena cava using a syringe rinsed in 20µL heparin to prevent coagulation. The heparinised whole blood was centrifuged at maximum speed (16000 x g) in a tabletop centrifuge for 15 minutes to separate the blood cell components from the serum. The serum was carefully transferred to fresh 1,5mL tubes and stored at -20°C before use for further applications.

4.4.5 Mesenteric lymph nodes

The mesenteric lymph nodes were removed from the mice, cleaned, and mashed through a 100µm cell strainer before being centrifuged at 300 x g for 5 minutes at 4°C. The cells were resuspended in complete Click's media (see Table 7), counted (see chapter 4.5), and seeded in 96-well plates at a concentration of 6×10^6 cells/well in duplicates. Half of the cells were stimulated with 1µg/mL of anti-CD3ε for 48h. After 48h, the supernatants were harvested, centrifuged, and stored at -20°C until further use.

4.4.6 Thymus

The thymuses were removed from the mice and mashed through a 40µm cell strainer before being centrifuges at 300 x g for 5 minutes at 4°C. The cells were then used for further applications.

4.5 Cell counting

For all experiments, cell counting was performed using a Neubauer chamber. The following formula was used to calculate the concentration of cells in a given suspension:

$$\frac{\text{cell count}}{\text{big squares}} \cdot \text{dilution factor} \cdot 10^4 = \text{cells/mL}$$

4.6 *In vitro* stimulation assays

All *in vitro* assays were performed under sterile conditions. Unless otherwise stated, cells were counted and seeded into wells of a 24-well plate at a concentration of $0,33 \times 10^6$ cells/well in 500 μ L of appropriate medium (see Table 7). Cytokines (see Table 6) were added to wells in the concentrations indicated in the individual experiments and the cells were incubated at 37°C/5%CO₂ for the indicated lengths of time before being processed for further analyses. Unless otherwise stated, recombinant IL-4 (murine and human) was added at a final concentration of 10ng/mL.

4.7 RNA isolation

Two methods were used for ribonucleic acid (RNA) isolation, depending on the application. For RNA samples sent for bulk RNA sequencing, samples were first lysed using the QiaShredder Kit, and RNA was isolated using the RNeasy Mini Kit (see Table 9). For all other applications, RNA was isolated from samples using phenol-chloroform extraction. All centrifugation steps were performed using a tabletop centrifuge.

4.7.1 QiaShredder Kit and RNeasy Mini Kit

To isolate RNA, samples were first lysed using the QiaShredder Kit. 350 μ L of the provided Buffer RLT, supplemented with 1% (v/v) β -mercaptoethanol, were added to the sample, which was then applied to the provided QiaShredder column. The column was centrifuged at maximum speed (16000 x g) for 15 seconds to elute the lysate. Lysates could be stored at -20°C and thawed for processing, or processed immediately.

To continue the RNA isolation, the RNeasy Mini Kit was used. 350 μ L 70% ethanol were added to the lysates, mixed by pipetting, and transferred to the provided RNeasy columns. The columns were centrifuged at maximum speed (16000 x g) for 15 seconds. In this step, the RNA in the sample was bound to the column membrane. The flow-through was discarded and the sample was washed with 350 μ L buffer RW1. A DNA digestion step was performed by applying 70 μ L DNase to the column membrane and incubating at room temperature for 15 minutes. To stop the DNase reaction, 350 μ L buffer RW1 were added to the membrane and the columns were centrifuged at maximum speed (16000 x g) for 15 seconds. The column was then washed twice using 500 μ L buffer RPE and centrifugation at maximum speed (16000 x g) for 2 minutes. The membranes were then dried by transferring the column to fresh, empty tubes and centrifuging at maximum speed (16000 x g) for 60 seconds. To elute the RNA, the columns were transferred to fresh 1,5mL tubes and an appropriate volume of Ampuwa, generally 25-32 μ L, was added to the membrane and incubated at room temperature for 5 minutes. The tubes containing the columns were then centrifuged at maximum speed (16000 x g) for 1 minute to elute the RNA. The RNA concentration was measured using a NanoDrop 2000C. RNA was then used for further applications or stored at -80°C.

4.7.2 Phenol-chloroform extraction with TRIzol™ reagent

For phenol-chloroform extraction, samples were mixed with 350 μ L TRIzol™ reagent (TRIzol) and incubated for 2-3 minutes at room temperature. If RNA was extracted from tissue samples, samples

were disrupted in TRIzol using a tissue homogeniser for 1-2 minutes. For longer term storage, samples were stored in TRIzol at -20°C and thawed prior to continuing.

To continue, 1/5 of the TRIzol volume (here: 70µL) chloroform were added to the sample, mixed by inverting for approximately 30 seconds, and incubated at room temperature for 2-3 minutes. The mixture was then centrifuged at 12000 x g for 15 minutes at 4°C. The upper aqueous phase was transferred to a fresh tube and isopropanol was added in a 1:1 volume. The mixture was carefully mixed by inverting for 30 seconds and incubated at room temperature for 10 minutes, then centrifuged at 12000 x g for 10 minutes at 4°C. The supernatant was discarded and the RNA pellet was washed with 500µL 80% ethanol, briefly vortexed to mix, and centrifuged at 7500 x g for 5 minutes at 4°C. The supernatant was removed and the pellet was air-dried for 30 minutes before being resuspended in an appropriate volume of Ampuwa (25-30µL for cell samples, 50µL for tissue samples). The RNA concentration was measured using a NanoDrop 2000C. RNA was then used for further applications or stored at -80°C.

4.8 cDNA synthesis

For quantitative real-time PCR (qPCR), RNA had to be retrotranscribed into complementary DNA (cDNA). This was performed using the iScript cDNA Kit (see Table 9). The following components were combined to form a reaction mix:

iScript cDNA reaction mix	
iScript Reverse Transcriptase	1µL
5x iScript Reaction Mix	4µL
RNA Template	Up to 1000ng, maximum 15µL
Ampuwa	To 20µL total volume

Once combined, the mix was mixed and spun down before the retrotranscription was performed in PeqStar PCR cycler, using the following programme:

cDNA PCR cycles	
Priming	25°C for 5 minutes
Reverse transcription	46°C for 20 minutes
Inactivation	95°C for 1 minute

cDNA was then diluted to 30ng/µL and used for qPCR or stored at -20°C.

4.9 qPCR

For qPCR, the Maxima SYBR™ Green qPCR Master Mix (see Table 9) was used. For each gene of interest, including housekeeping genes, a master mix was created containing the following components per 12µL reaction:

SYBR™ Green qPCR reaction mix	
SYBR Green 2x Master Mix	6µL
Primers	0,1µL per primer
cDNA Template	1µL
Ampuwa/Nuclease-Free water	To 12µL total volume

Gapdh was used as a housekeeping gene for all qPCR runs. The primers used are listed in chapter 3.10.2.

The qPCR reaction was performed using a Corbett RotorGene 6000, with analyses performed using the RotorGene software.

q PCR cycles		
Initial denaturation	95°C for 10 minutes	
Denaturation	95°C for 15 seconds	Repeat x40
Annealing	60°C for 30 seconds	
Extension	72°C for 30 seconds	
Melt	62°C to 95°C, increase by 1°C every 90 seconds	

Relative expression of genes was calculated using the $2^{-\Delta Ct}$ method²³³. To calculate the $2^{-\Delta Ct}$ for each gene of interest in each sample, ΔCt was calculated as follows:

$$\Delta Ct = Ct(\text{gene of interest}) - Ct(\text{reference gene})$$

4.10 Flow cytometry

Flow cytometry was used to analyse the expression of cell surface markers, intracellular markers, and mRNA on isolated cells and *in vitro*-stimulated cells. In addition, bead-based immunoassays were performed to measure cytokine expression in mouse serum samples. To this end, the following methods were used to stain the cells.

4.10.1 Blocking

Many cells, including monocytes, macrophages, dendritic cells, and B cells, express Fc receptors on their cell surface. These can lead to unspecific binding of antibodies. Accordingly, to prevent unspecific binding, all cell solutions were incubated with 50µl FACS blocking buffer (see Table 7) for 15 minutes at 4°C prior to extracellular staining.

4.10.2 Extracellular staining

Extracellular staining was used to label markers on the surface of cells for further analysis. To this end, fluorochrome-conjugated antibodies were bound to the specific markers of interest. Cells were incubated

in 25µL of blocking buffer containing a mixture of antibodies specific to the cell subtypes and markers to be analysed. The antibodies used are listed in Table 13. Extracellular staining was performed for 30 minutes at 4°C in darkness. After staining, cells were washed with 50µL FACS measurement buffer (see Table 7) and either analysed at the LSR II cytometer (see chapter 4.10.7), sorted using the FACS Aria (see chapter 4.10.8), or fixed and permeabilised for intracellular staining and/or PrimeFlow™ staining.

4.10.3 Cell fixation, permeabilisation, and intracellular staining

To perform intracellular staining and/or PrimeFlow™ staining, cells had to be fixed and permeabilised. Three different methods were used, depending on the specific application or type of sample:

For all samples to be stained using the PrimeFlow™ method, cells were fixed and permeabilised using the provided fixation and permeabilisation buffers in the PrimeFlow™ Kit (see Table 9). Briefly, cells were incubated in fixation buffer 1 for 30 minutes at 4°C and washed once in perm buffer. Intracellular staining was performed in perm buffer for 40 minutes. Antibodies used for intracellular staining are listed in Table 14. For staining involving non-conjugated antibodies, primary and secondary staining was performed sequentially in the same manner. After staining, cells were washed once in perm buffer, then incubated in fixation buffer 2 for 60 minutes at room temperature, or stored at 4°C overnight before continuing the PrimeFlow™ protocol.

For liver samples that were not stained using the PrimeFlow™ method, cells were fixed and permeabilised using the FoxP3 intracellular staining/permeabilisation kit (see Table 9). Briefly, cells were incubated in 100µL of the provided fixation solution (diluted according to manufacturer's instructions) for 30 minutes on ice in darkness. Cells were then washed in 100µL of the provided perm buffer (diluted 1:10 with distilled water) and incubated in perm buffer overnight at 4°C before intracellular staining in perm buffer for 40 minutes. Antibodies used for intracellular staining are listed in Table 14. For staining involving non-conjugated antibodies, primary and secondary staining was performed sequentially in the same manner. After staining, cells were washed and resuspended in FACS measurement buffer (see Table 7) for analysis at the LSR II cytometer.

For all other samples, cells were fixed through incubation in 1% paraformaldehyde (PFA) for 30 minutes on ice or overnight at 4°C. Cell samples could also be stored in 1% PFA for up to a week before measurement. To continue, cells were washed twice in Perm/Wash™ buffer (diluted 1:10 with distilled water) before intracellular staining in Perm/Wash™ buffer for 40 minutes. Antibodies used for intracellular staining are listed in Table 14. For staining involving non-conjugated antibodies, primary and secondary staining was performed sequentially in the same manner. After staining, cells were washed and resuspended in FACS measurement buffer (see Table 7) for analysis at the LSR II cytometer.

4.10.4 PrimeFlow™ assay

The PrimeFlow™ RNA assay is an *in situ* hybridisation assay that was used to analyse the expression of *Aa467197* mRNA at flow cytometry level. The assay was performed in 96-well-plates according to the manufacturer's instructions. All wash steps were performed twice with PrimeFlow™ wash buffer (wash buffer) and centrifugation at 1000 x g for 4 minutes at room temperature. Target probes (see

Table 15) were diluted 1:20 in the provided target probe diluent, and provided label probes were diluted 1:100 in the provided label probe diluent. After extracellular staining, fixation, permeabilisation, and intracellular staining (see chapter 4.10.3), cells were washed and incubated with 100µL wash buffer and 100µL diluted target probe for 2 hours at 40°C in an incubator. Afterwards, cells were washed and incubated with 100µL wash buffer and 100µL of the provided PreAmp mixture for 1,5 hours at 40°C. After washing, this step was repeated using 100µL wash buffer and 100µL of the provided Amp mixture. After washing, cells were incubated with 100µL wash buffer and 100µL diluted label probe for 1 hour at 40°C. Finally, cells were washed and resuspended in FACS buffer for acquisition at the LSR II flow cytometer.

4.10.5 Compensation

Compensation was performed using UltraComp eBeads™ or OneComp eBeads™ stained with a single antibody for each detection channel used for 15 minutes at 4°C in darkness. Stained beads were washed 2x with FACS measurement buffer (see Table 7), then resuspended in 200µL of FACS measurement buffer for acquisition. The compensation calculation function of the BD FACS Diva software at the LSR II and FACS Aria cytometers was used to calculate the compensations for each experiment.

4.10.6 LEGENDplex™ assay

To measure cytokine expression in mouse serum samples, the bead-based LEGENDplex™ assay was performed according to the manufacturer's instructions, with volumes of reagents and samples reduced by 2/3. The LEGENDplex™ assay allows simultaneous measurement of multiple cytokines by using beads that differ in size and fluorochrome intensity for each cytokine of interest.

Briefly, a bead mixture (equal parts of each bead for the cytokines of interest), matrix B (required for the standard when analysing serum samples), wash buffer, and serially diluted standard were prepared before applying the samples to be analysed and the diluted standard to wells of a 96-well plate. The bead mixture and provided detection antibody were added and the plate was incubated overnight at 4°C in darkness on a plate shaker. The next day, SA-PE was added to each well and incubated for 30 minutes at room temperature in darkness before washing the plate once with wash buffer and acquiring the samples at the Accuri C6. The results were analysed using the LEGENDplex™ software v8.0.

4.10.7 Flow cytometric analysis

All cell-based analyses were performed using the LSR II cytometer (BD). Cells were analysed based on forward and sideward scatter properties, indicating size and granularity respectively, as well as the expression of markers bound to fluorochrome-conjugated antibodies. The antibodies used are listed in Table 13, Table 14, and Table 15.

4.10.8 Cell sorting

To sort specific cell populations from a cell mixture, fluorescence-activated cell sorting (FACS) was used. Using FACS, individual cells can be sorted into separate populations by encasing them in liquid droplets, applying an electric charge to the droplet, and passing the cells through an electric field. The cells are then sorted into different populations according to the charge applied to the droplet.

For FACS, cells were labelled through extracellular staining with the antibodies of choice and sorted by the core facility of the BNITM using a BD FACSAria cell sorter. Prior to sorting, cells were filtered through a 30µm cell strainer. Sorting of cells was performed using a 70µm nozzle. Sorted cells were collected in cold FACS measurement buffer.

4.11 Enzyme-linked immunosorbent assay (ELISA)

To quantify cytokine levels in supernatants of stimulated and unstimulated mesenteric lymph node cells (see chapter 4.4.5), sandwich enzyme-linked immunosorbent assays (ELISA) were performed using Mouse DuoSet ELISA Kits (see Table 9) according to the manufacturer's protocol, with volumes of reagents and samples reduced by 1/2. Kits for IL-5 and IL-13 were used.

Briefly, ELISA 96-well plates were coated with a specific capture antibody for the cytokine of interest overnight at 4°C on a plate shaker. The next day, the plate was washed 2x with PBS/Tween and blocked with ELISA blocking buffer for 2 hours at room temperature before applying the samples to be analysed, along with the appropriate serially diluted standard for the cytokine of interest. The plates were incubated overnight at 4°C on a plate shaker. The next day, the plate was washed 5x with PBS/Tween before applying the detection antibody for the cytokine of interest for 2h at room temperature. After washing 5x with PBS/Tween, the plate was incubated with streptavidin/horseradish peroxidase (HRP) for 20 minutes at room temperature before washing and applying ELISA substrate buffer to begin developing the assay. To stop the enzyme reaction, 2M H₂SO₄ was added and the intensity of the colour reaction was measured at 450nm using an ELISA reader. The serially diluted standard was used to perform quantitative analysis of the measured optical densities.

4.12 Extracellular flux analysis

Extracellular flux analyses (Seahorse assays) were performed using Seahorse XF Cell Mito Stress Test Kits (see Table 9) according to the manufacturer's instructions on a Seahorse XF Extracellular Flux Analyser at the UKE.

Briefly, cells were seeded at 1x10⁵ cells/well in 96-well Seahorse assay plates 24 hours prior to analysis and incubated in an incubator at 37°C/5%CO₂. Cytokines were added at the appropriate concentrations for the indicated lengths of time. In addition, a 96-well sensor cartridge was hydrated overnight in hydration solution at 37°C in a non-CO₂ incubator. One hour prior to analysis, cell culture medium was replaced with Seahorse assay medium and cells were incubated at 37°C in a non-CO₂ incubator. During incubation, Cell Mito Stress Test kit compounds were loaded into the ports of the hydrated sensor cartridge. Final concentrations of reagents added during measurement were glucose 25mM, oligomycin 1,5µM, carbonyl cyanide-p-trifluoromethoxyphenylhydrazone (FCCP) 1 µM, rotenone/antimycin A 0,5 µM. The cartridge was then loaded into the Extracellular Flux Analyser for calibration. Upon completion of calibration, the cell plate was inserted into the analyser to initiate the assay. Oxygen consumption rates (OCRs) and extracellular acidification rates (ECARs) were measured three times before addition of components, as well as after adding each component respectively, as indicated in the images. The assay results were analysed using the Seahorse Wave Desktop software, V2.6.

4.13 Phagocytosis assay

For the phagocytosis assay, BMDMs were generated from mice as described in chapter 4.4.1.1. On day 6 of BMDM differentiation, isolated thymus cells (see chapter 4.4.6) were plated in RPMI1640 with 10% FCS and incubated for 24 hours to age the cells and induce apoptosis. After 24 hours, apoptosis was checked using the FITC Annexin V/PI kit (see Table 9). BMDMs were plated as described for in vitro stimulation assays (see chapter 4.6) and apoptotic thymocytes (aTs) were added at $1,65 \times 10^6$ cells/well for 1 hour. If indicated, cells were incubated on ice (0°C), at room temperature, or with the addition of 10µg/mL cytochalasin D (CytD) during this step. After 1 hour, cells were washed 5 times with ice-cold PBS to remove aTs that had not been uptaken or bound, and cells were incubated in macrophage culture medium supplemented with 10ng/mL IL-4 for 6 hours. Cells were then lysed for RNA isolation (see chapter 4.7)

4.14 Bulk-RNA sequencing

To investigate differentially expressed genes between BMDMs from wildtype and *Nmes1^{-/-}* mice in the context of IL-4 exposure, RNA sequencing was performed by BGI (Shenzhen, China). RNA was isolated from BMDMs from wildtype and *Nmes1^{-/-}* mice that had been left untreated or treated with 10ng/mL murine recombinant IL-4 for 6 hours or 24 hours using the RNeasy Mini Kit (see chapter 4.7.1). Isolated RNA was pooled and sent to BGI. Library preparation and transcriptome sequencing was performed using 100 base/paired-end reads on BGI's DNBSEQ™ Technology Platform.

Initial analysis of raw data was performed by Christian Casar of the bioinformatics facility at the UKE. For analysis, genes that were at least 1,5-fold increased after incubation with IL-4 at 6h or 24h compared to the untreated cells were selected and the fold change of the counts per million (CPM) was calculated and logarithmised (log2). Of these genes, those shared between wildtype and *Nmes1^{-/-}* cells were compared. The log2(CPM) of the 50 genes with the strongest difference in upregulation between wildtype and *Nmes1^{-/-}* cells at 6h and 24h of incubation with IL-4, respectively, were displayed in a heat map. Heat maps were generated using ClustVis ²³⁴.

Gene ontology (GO) term analysis was performed using David v6.8 ^{235,236}. Genes that were at least 1,25 more highly expressed in the wildtype compared to the *Nmes1^{-/-}* cells at 6 hours and 24 hours of incubation with IL-4, respectively, were chosen for GO term analysis. Plots show the logarithmised modified Fisher exact score (-log10(EASE)), with a dotted line indicating an EASE score/p-value of 0,05.

4.15 Dextran sodium sulfate (DSS)-induced colitis

Colitis was induced in mice by providing a 1,5% solution of dextran sodium sulfate (DSS) in place of drinking water for 5-7 days, followed by regular drinking water for 7-9 days. The maximum length of one experiment was 14 days. Mice were weighed and scored daily throughout each experiment. Mice were sacrificed at different time points during one experiment. Colons were removed and measured before isolation of lamina propria cells (see chapter 4.4.2) for analysis using flow cytometry (see chapter 4.10.7) or for sorting (see chapter 4.10.8).

4.16 *Schistosoma mansoni*

4.16.1 Infection

For infection with *Schistosoma mansoni*, mice were subcutaneously (s.c.) injected with 20-35 cercariae diluted in 200µL distilled water. The cercariae were obtained in cooperation with Helmut Haas (see chapter 3.5). To count the cercariae, 10µL cercariae-solution was diluted in 100µL distilled water in a 48-well plate with a grid. The cercariae were immobilised using 1mL Lugol solution and counted under a light microscope. Mice were sacrificed at 8 weeks and 14 weeks post infection. Colons, livers, blood, and mesenteric lymph nodes were collected and processed as described in the respective chapters (see chapter 4.4). In addition, tissue samples of lungs, livers, and colons were taken and stored in RNAProtect to analyse total RNA.

4.16.2 Egg count in liver and colon

A piece of the left loop of the liver and a piece of the colon were harvested, weighed and stored in 4% KOH solution for 8 hours or 16 hours, respectively, at 37°C in a 24-well plate with a grid. The tissue was further disrupted by resuspending with a 1mL pipette and the eggs were counted using a light microscope at 4x magnification. The eggs per gram liver/colon were calculated.

4.16.3 Measurement of alanine transaminase (ALT) levels

ALT levels in mouse sera (see chapter 4.4.4) were measured using a Reflotron®. 32µL of serum were applied to Reflotron® GPT/ALAT strips and inserted into the Reflotron®. Measurements were performed at 22°C.

4.17 Statistics

Statistical analyses of data were performed using the GraphPad Prism v8 software. Before applying statistical tests, all data were checked for Gaussian distribution (normal distribution) and outliers. Since none of the data were normally distributed, non-parametric statistical tests were used. If only two datasets were compared (such as wildtype and *Nmes1^{-/-}* for a single time point), the Mann-Whitney U test was applied. If more than two datasets were compared, the Kruskal-Wallis test was applied, with multiple comparisons performed using Dunn's test to determine exact p-values between samples. The exact statistical tests used are indicated in the respective graph descriptions. If no p-value is given, the difference between the datasets was non-significant ($p \geq 0.05$). Weight loss data are shown as mean \pm SD to indicate spread of data points, with numbers of mice indicated in the figure legend. All other data are shown as mean \pm SEM as a measure of precision of the estimated population mean, with each data point representing one sample/mouse. Numbers of samples are indicated in the figure legends.

5. Results

Multiple approaches were taken to analyse the function of *Aa467197* in IL-4-activated macrophages. Initially, *in vitro* primary cell cultures of mouse BMDMs were used to analyse the induction of *Aa467197* expression after exposure to IL-4 and the impact of *Aa467197* on the expression of other genes. In addition, *in vitro* functional assays and RNAseq were performed to investigate the functional impact of *Aa467197* in IL-4-activated macrophages. In parallel, expression of the human homolog of *Aa467197*, *NMES1*, was analysed in human cells. Finally, two *in vivo* mouse models – induction of colitis via DSS and schistosomiasis through infection with *S. mansoni* – were used to investigate the role of *Aa467197* in disease models in which the tissue remodelling response of macrophages is crucial to re-establish homeostasis.

5.1 Expression kinetics of *Aa467197* and markers of IL-4-activated macrophages in mouse BMDMs

Since very little is known about the function of *Aa467197* in IL-4-activated macrophages, the first approach was to investigate the expression of *Aa467197* and its effects on the expression of genes associated with the IL-4-activated macrophage phenotype *in vitro*. To this end, bone marrow was isolated from wildtype mice and the hematopoietic pluripotent stem cells within were differentiated into BMDMs. After differentiation, BMDMs were incubated with recombinant murine IL-4 for different lengths of time (1h, 6h, 12h, 24h, 36h, 48h, and 72h). Subsequently, RNA was isolated and expression of *Aa467197* and genes associated with the macrophage tissue remodelling phenotype, which are typically induced by sensing of IL-4 (*Arg1*, *Retnla*, and *Chil3*), was analysed.

Compared to untreated BMDMs, *Aa467197* expression was induced after addition of 10ng/mL IL-4, with the highest peak of expression at 6h post addition (approximately 10-fold increase) before decreasing at later time points. In contrast, expression of markers associated with macrophage tissue remodelling functions was increased at later time points, with significantly higher expression beginning at 24h post IL-4 treatment, and expression remaining elevated until 72h post addition (Figure 1).

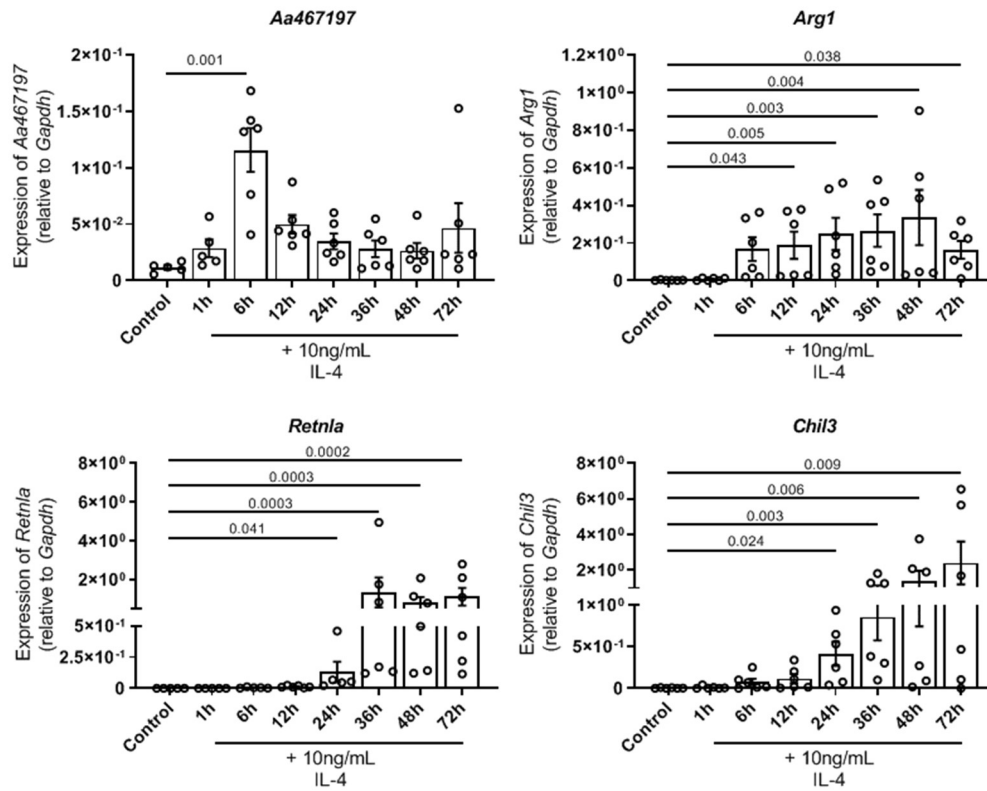


Figure 1: *Aa467197* was expressed earlier than markers of IL-4-activated macrophages in BMDMs stimulated with IL-4. Expression of *Aa467197*, *Arg1*, *Retnla*, and *Chil3* in BMDMs stimulated with 10ng/mL IL-4 for the indicated lengths of time. Control indicates untreated BMDMs. Each data point represents one sample/mouse; n=6. Expression relative to a housekeeping gene (*Gapdh*) is shown. Bars indicate mean \pm SEM. Indicated p-values were calculated using Kruskal-Wallis test, with Dunn's test for multiple comparisons; all treated samples were compared to the untreated control. Missing p-value bars indicate non-significance ($p > 0.05$).

5.2 Expression of genes associated with IL-4-activated macrophages in wildtype and *Nmes1*^{-/-} mice

To examine whether *Aa467197* can regulate the IL-4-induced tissue remodelling phenotype in macrophages, the expression of *Arg1*, *Retnla*, and *Chil3* was analysed at mRNA and protein level in BMDMs from wildtype and *Nmes1*^{-/-} mice, in which the gene for *Aa467197* has been ablated completely, after treatment with IL-4 for 24h or 48h.

At mRNA level, expression of all three genes was induced by the addition of IL-4, and *Chil3* expression was strongly reduced in the *Nmes1*^{-/-} BMDMs at 24h, with a tendency for it to still be reduced at 48h. In contrast, *Arg1* and *Retnla* was not significantly different between wildtype and *Nmes1*^{-/-} BMDMs 24h or 48h after treatment with IL-4 (Figure 2).

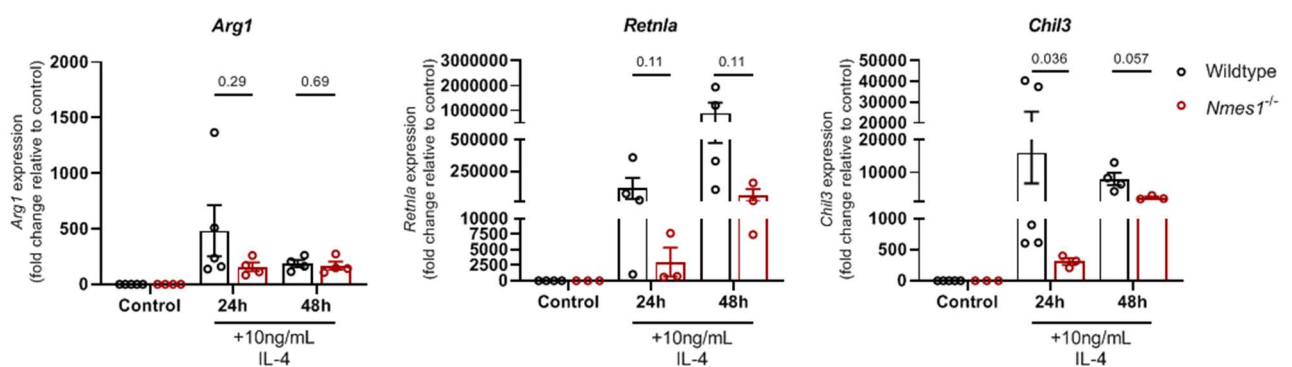


Figure 2: *Aa467197* alters the gene expression of IL-4-induced macrophage tissue remodelling markers. Expression of *Arg1*, *Retnla*, and *Chil3* in BMDMs isolated from wildtype and *Nmes1*^{-/-} mice treated with 10ng/mL IL-4 for 24h and 48h. Control indicates untreated BMDMs. Each data point represents one sample/mouse; n=3-5. Fold change relative to control is shown. Bars indicate mean \pm SEM. Indicated p-values were calculated using Mann-Whitney U test, comparing only the wildtype and *Nmes1*^{-/-} datasets at the indicated time point.

At protein level, while ARG1, RELMa, and YM1 expression was induced in macrophages treated with IL-4, no difference could be detected in their expression levels, neither in terms of percentage of positive cells nor median fluorescence intensity (MFI), between wildtype and *Nmes1*^{-/-} mice at either time point (Figure 3).

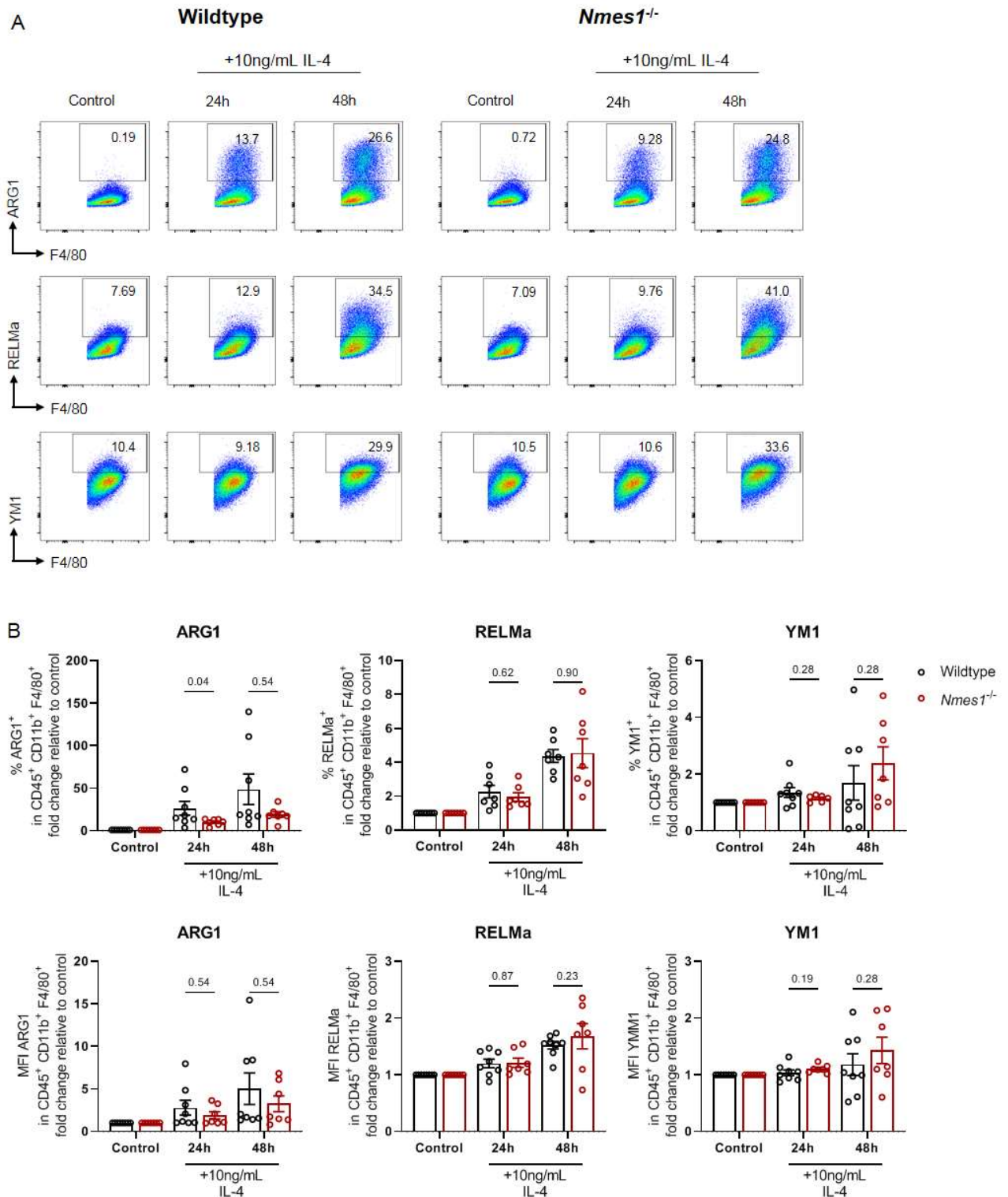


Figure 3: Aa467197 does not regulate expression of IL-4-induced tissue remodelling proteins in macrophages. (A) Representative dot plots of BMDMs from wildtype and *Nmes1*^{-/-} mice treated with 10ng/mL IL-4 for 24h or 48h. Control indicates untreated BMDMs. Cells are pre-gated on CD45⁺ Ly6G⁻ CD11b⁺ F4/80⁺ cells. Gates and frequencies indicate cells considered positive for the respective marker, based on FMOs (not shown). (B) Population frequencies and MFIs of ARG1, RELMa, and YM1 in BMDMs from wildtype and *Nmes1*^{-/-} mice 24h and 48h after treatment with 10ng/mL IL-4. Control indicates untreated BMDMs. Each data point represents one sample/mouse; n=7-8. Fold change relative to control is shown. Bars indicate mean \pm SEM. Indicated p-values were calculated using Mann-Whitney U test, comparing only the wildtype and *Nmes1*^{-/-} datasets at the indicated time point.

5.3 *In vitro* functional analyses

Since genetic ablation of *Aa467197* only affected IL-4-induced macrophage polarisation at mRNA level, further *in vitro* assays were performed to investigate whether *Aa467197* impacts additional functions in macrophages stimulated with IL-4. In particular, since *Aa467197* is known to be expressed in the mitochondria^{87,89}, mitochondrial function of *Nmes1^{-/-}* BMDMs in comparison to wildtype cells was investigated using extracellular flux assays. In addition, since *Aa467197* had been described to be strongly downregulated in macrophages with impaired phagocytic capacity due to genetic ablation of *Axl* and *MerTK* in a model of *N. braziliensis* infection⁷³, experiments were performed to assess the expression of *Aa467197* in BMDMs during phagocytosis of apoptotic cells and in BMDMs with impaired phagocytosis capacity.

5.3.1 Assessing mitochondrial function in mouse BMDMs with ablated *Aa467197*

To assess whether *Aa467197* plays a role in regulating mitochondrial function, extracellular flux analyses were performed on BMDMs generated from wildtype and *Nmes1^{-/-}* mice left untreated or treated with IL-4. Macrophages were differentiated from hematopoietic pluripotent stem cells in bone marrow and incubated with 10ng/mL IL-4 for 6h and 24h prior to analyses. OCRs and ECARs were measured as described in chapter 4.12. Different components were added during the assay to stimulate or inhibit components of the mitochondrial respiration complex. Oligomycin inhibits mitochondrial complex V, the ATP synthase, lowering the OCR and allowing calculation of adenosine triphosphate (ATP)-linked respiration rates. FCCP is an OXPHOS uncoupler which disrupts ATP synthesis by transporting electrons across the mitochondrial inner membrane. This leads to an OCR spike, which can be used to measure rates of maximal respiration and spare respiratory capacity. Rotenone and antimycin A inhibit complexes I and III, respectively, completely inhibiting mitochondrial respiration. The remaining rate of non-mitochondrial respiration remains is subtracted from the initial, untreated OCR measurements to reveal the basal respiration rate. To measure glycolysis rates, glucose was added, which raises ECARs due to the glycolytic conversion of glucose to lactate via pyruvate. Differences in the OCR and ECAR curves, as well as the calculated rates of ATP respiration, maximal respiration, and glycolysis, may give insight into how *Aa467197* may impact mitochondrial respiration.

In general, the OCRs of the samples treated with IL-4 for 24h increased in both the wildtype and the *Nmes1^{-/-}* cells compared to those of untreated cells, but not after treatment with IL-4 for 6h. The OCR levels of the untreated and 6h-treated *Nmes1^{-/-}* cells were slightly higher than the equivalent OCRs of the wildtype cells, though this increase was not statistically significant. There was no difference in ATP-linked respiration or maximal respiration between the wildtype and *Nmes1^{-/-}* cells at either time point (Figure 4).

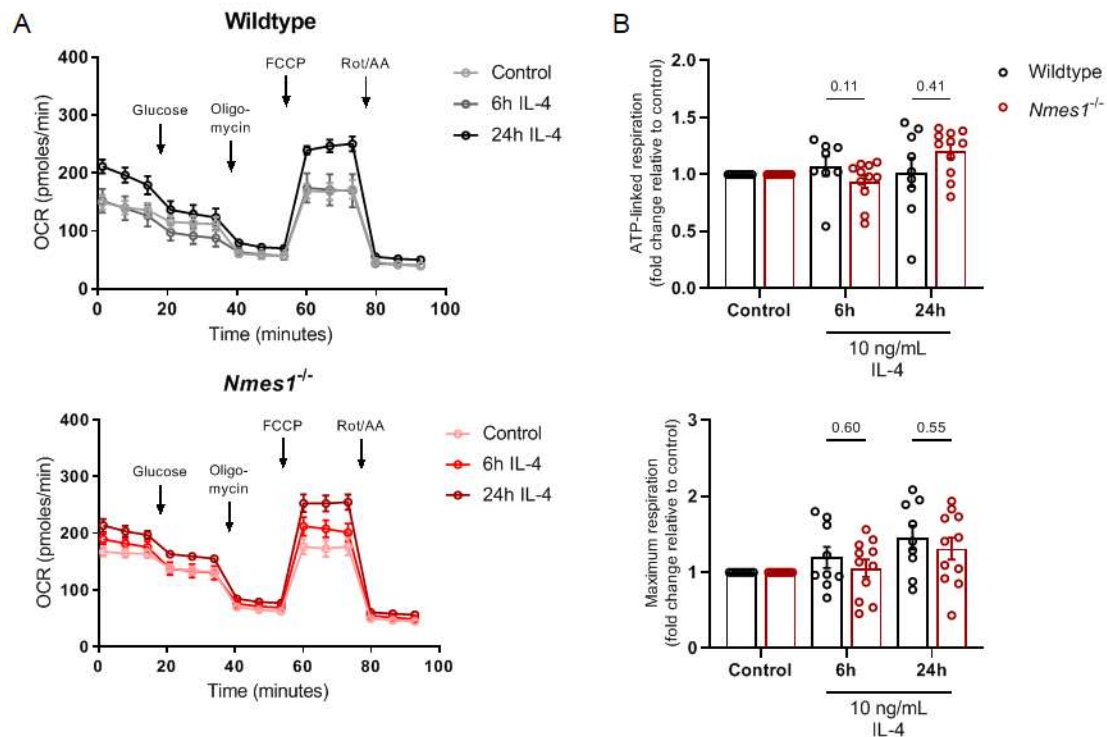


Figure 4: *Aa467197* does not regulate oxygen consumption rates (OCRs) and ATP production in BMDMs. (A) OCR curves of wildtype and *Nmes1^{-/-}* mice treated with 10ng/mL IL-4 for 6h or 24h. Control indicates untreated cells. Points indicate mean \pm SEM, each point represents $n=11$ samples/mice. (B) ATP-linked respiration and maximal respiration rates of BMDMs from wildtype and *Nmes1^{-/-}* mice 6h and 24h after treatment with 10ng/mL IL-4. Each data point represents one sample/mouse; $n=11$. Fold change relative to control is shown. Bars indicate mean \pm SEM. Indicated p-values were calculated using Mann-Whitney U test, comparing only the wildtype and *Nmes1^{-/-}* datasets at the indicated time point.

Similar to the OCRs, the ECARs of the samples incubated with IL-4 for 24h increased in both wildtype and *Nmes1^{-/-}* BMDMs, but only increased in the *Nmes1^{-/-}* cells at 6h. However, the basal ECARs of wildtype and *Nmes1^{-/-}* cells were at similar levels. There were no differences in glycolysis rate or maximal glycolysis rate between the wildtype and *Nmes1^{-/-}* BMDMs for any treatment (Figure 5).

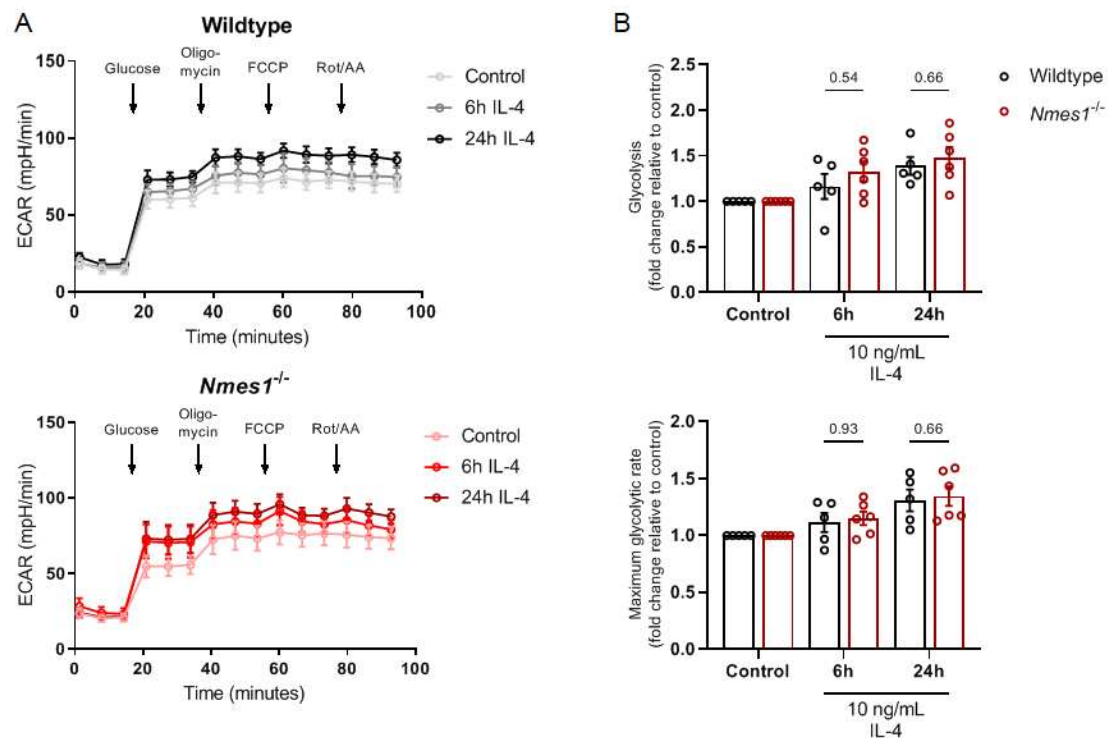


Figure 5: Ablation of *Aa467197* does not impact extracellular acidification rates (ECARs) of BMDMs. (A) ECAR curves of wildtype and *Nmes1*^{-/-} mice untreated or treated with 10ng/mL IL-4 for 6h or 24h. Points indicate mean \pm SEM, each point represents n=6 samples/mice. (B) Glycolysis and maximal glycolysis rates of BMDMs from wildtype and *Nmes1*^{-/-} mice 6h and 24h after treatment with 10ng/mL IL-4. Each data point represents one sample/mouse; n=6. Fold change relative to control is shown. Bars indicate mean \pm SEM. Indicated p-values were calculated using Mann-Whitney U test, comparing only the wildtype and *Nmes1*^{-/-} datasets at the indicated time point.

5.3.2 Modulation of *Aa467197* expression during phagocytosis

Preliminary experiments were performed to assess whether *Aa467197* expression in macrophages is altered during phagocytosis of apoptotic cells. As previously noted (chapter 2.2.2.2), anti-inflammatory macrophages express PtdSer receptors with which to recognise and uptake apoptotic cells, including TAM receptor tyrosin kinases. Notably, mice lacking AXL and MERTK show downregulation of tissue remodelling-associated genes in macrophages after stimulation with IL-4⁷³. Accordingly, it is possible that expression of *Aa467197* may be altered through sensing of PtdSer exposed on the surface of apoptotic cells by AXL and MERTK. To test this hypothesis, BMDMs were generated from mice in which *Axl* and *Mertk* are flanked by loxP sites and knocked out in cells expressing *Csf1r* through expression of Cre recombinase (*Axl*^{fl/fl}*Mertk*^{fl/fl}-*Csf1r*-Cre⁺), and control mice, which lack the Cre recombinase and therefore still express *Axl* and *Mertk* (*Axl*^{fl/fl}*Mertk*^{fl/fl}-*Csf1r*-Cre⁻). Cells were incubated with 10ng/mL IL-4 for 6h or 24h, then examined for their expression of *Aa467197*. No difference in *Aa467197* mRNA levels were detected between the Cre⁻ and Cre⁺ cells at either time point (Figure 6A).

Since no difference in *Aa467197* expression could be detected in cells with reduced phagocytic capacity using IL-4 alone, phagocytosis experiments were performed using aTs in addition to IL-4 to engage PtdSer receptors through a stronger stimulus. To this end, cells from wildtype mice were incubated with aTs for 1h prior to stimulation with 10ng/mL IL-4 for 6h to assess whether phagocytosis could increase

expression of *Aa467197*. BMDMs incubated with IL-4 alone for 6h served as a control. As an additional negative control, uptake of aTs was blocked by incubating the cells on ice (at 0°C) during coculture with aT, or by adding 10µg/mL CytD to the cells prior to adding the aT. Untreated controls and cells treated with IL-4 alone were also incubated at 0°C or with CytD as a further control. While the addition of IL-4 increased expression of *Aa467197*, as previously observed, addition of aT did not alter the expression of *Aa467197* further. However, incubation of cells at 0°C or addition of CytD did prevent upregulation of *Aa467197* by IL-4 (Figure 6B).

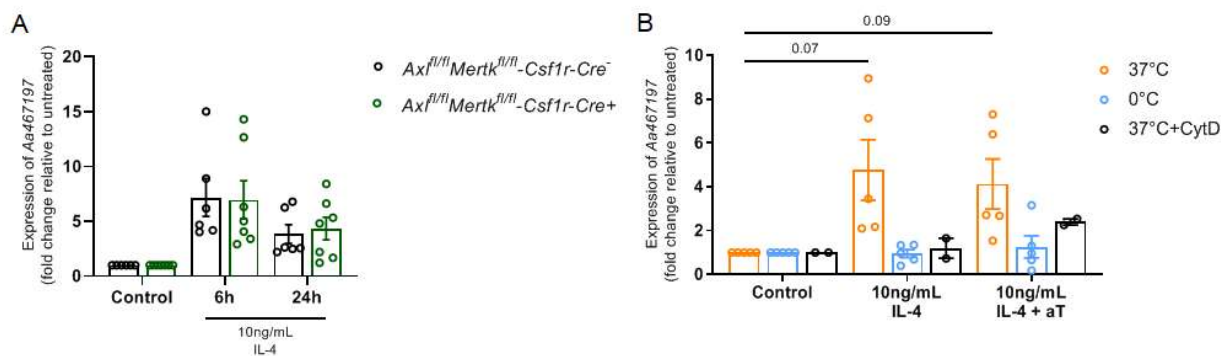


Figure 6: Phagocytosis of apoptotic cells does not regulate *Aa467197* expression. (A) Expression of *Aa467197* in BMDMs from *Ax1^{fl/fl}Mertk^{fl/fl}Csf1r-Cre⁻* and *Ax1^{fl/fl}Mertk^{fl/fl}Csf1r-Cre⁺* mice treated with 10ng/mL IL-4 for 6h or 24h. Control indicates untreated BMDMs. Each data point represents one sample/mouse; n=6-7. Fold change relative to untreated control is shown. Bars indicate mean ± SEM. p-values were calculated using Mann-Whitney U test, comparing only the *Cre⁻* and *Cre⁺* datasets at the indicated time point. Missing p-value bars indicate non-significance (p>0.05). (B) Expression of *Aa467197* in BMDMs from wildtype mice treated with 10ng/mL IL-4 alone for 1h and 10ng/mL IL-4 for 6h. Control indicates untreated BMDMs. Within each treatment group, cells were incubated on ice (0°C), at 37°C, or at 37°C with addition of 10µg/mL CytD during incubation with or without aT. Indicated p-values were calculated using Kruskal-Wallis test, with Dunn's test for multiple comparisons; treated samples were compared to the respective untreated control. Missing p-value bars indicate non-significance (p>0.05). Each data point represents one sample/mouse; n=2-5. Fold change relative to untreated control is shown. Bars indicate mean ± SEM.

5.4 Analysis of transcriptional profile of IL-4-stimulated cells with ablated *Aa467197*

Since it could be ruled out that *Aa467197* expression affects polarisation, mitochondrial function, and phagocytosis functions of IL-4-stimulated macrophages, a more unbiased approach was taken to investigate which IL-4-related pathways may be affected by *Aa467197*. To this end, RNAseq was performed on BMDMs from 3 pooled wildtype and 3 pooled *Nmes1^{-/-}* mice untreated or treated with IL-4 for 6h (the peak of *Aa467197* expression) or 24h (increased expression of tissue remodelling markers). For analysis, only genes with at least 1.5-fold upregulation after addition of IL-4 were included. The degree of differential expression of these genes was then compared between the wildtype and the *Nmes1^{-/-}* mice. The 50 genes with the strongest difference in upregulation between the wildtype and the *Nmes1^{-/-}* mice are shown in Figure 7A and B.

A selection of these genes (*Gata3*, *Ahr*, *Fzd4*, and *Socs5*) was chosen to confirm the observed RNAseq results by qPCR (Figure 7C). In addition, gene ontology (GO) term analysis was performed on genes at least 1.25-fold more upregulated in the wildtype versus the *Nmes1^{-/-}* cells to gain insight into the biological processes that are most strongly affected by ablation of *Aa467197* (Figure 7D).

Results

Notably, analysis of GO terms and upregulated genes revealed that after 6h several genes associated with alternatively activated macrophage functions (*Gata3*^{53,237}, *Tle1*²³⁸) were more strongly upregulated in wildtype BMDMs compared to *Nmes1*^{-/-} BMDMs. This was also the case for genes related to macrophages' response to microbial infection (*Gja1*, *Tarm1*, *Ahr*, *Socs5*), cell migration (*Aqp1*, *Gpr183*), and involvement in the Wnt signalling pathway (*Fzd4*²³⁹, *Srpk1*). After 24h, several genes related to the macrophage response to microbial infection were upregulated (*Ahr*, *Gja1*, *Socs5*), but also genes related to blood vessel development and angiogenesis (*Ahr*, *Sdc4*, *Ednrb*, *Hbegf*, *Pdgfc*). In addition, genes associated with monocyte chemotaxis (*Thrb*, *Ccr24*, *Ccr12*, *Ccr7*) were more strongly upregulated.

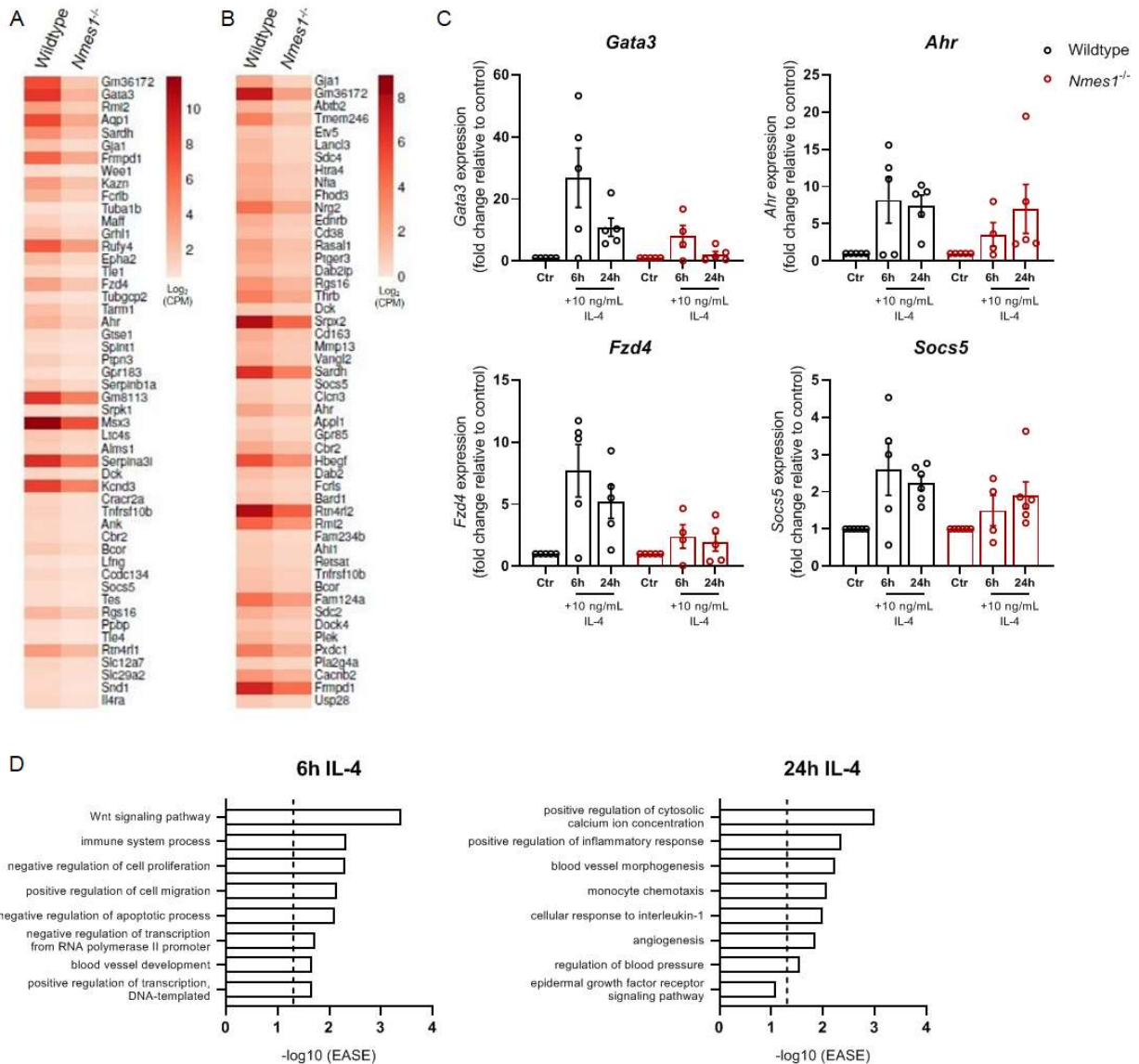


Figure 7: *Aa467197* expression affects the transcriptional profile of BMDMs untreated or treated with IL-4 for 6h and 24h. (A) Heatmap depicting the 50 most highly differentially expressed genes between wildtype and the *Nmes1*^{-/-} mice after incubation with 10ng/mL IL-4 for 6h and (B) 24h. Colour intensity shows log₂(CPM), with more intense colour indicating stronger upregulation. (C) Expression of *Gata3*, *Ahr*, *Fzd4*, and *Socs5* in BMDMs treated with 10ng/mL IL-4 for 6h or 24h. Ctr indicates untreated BMDMs. Each data point represents one sample/mouse; n=4-5. Fold change relative to respective untreated control is shown. Bars indicate mean ± SEM. (D) GO analysis of genes at least 1.25-fold more strongly upregulated in wildtype BMDMs compared to *Nmes1*^{-/-} BMDMs when treated with IL-4 for 6h or 24h. Bars indicate $-\log_{10}(\text{EASE})$, with higher values indicating lower p-values. Dotted line represents p=0.05.

Further analysis of the expression of *Gata3*, *Ahr*, *Fzd4*, and *Socs5* via qPCR revealed that expression of all four genes was increased in the untreated *Nmes1*^{-/-} BMDMs compared to the untreated wildtype cells, while expression levels were similar between wildtype and *Nmes1*^{-/-} BMDMs after treatment with IL-4 (both at 6h and at 24h) (Figure 8). This suggests that *Aa467197* may play a more prominent role in regulating macrophage gene expression in naïve macrophages, rather than stimulated macrophages.

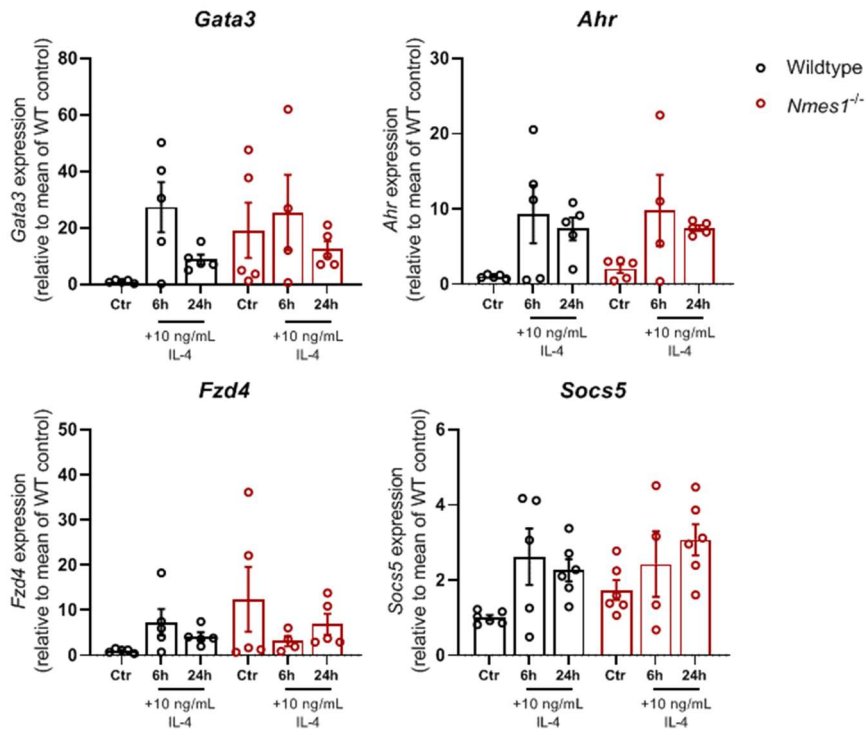


Figure 8: *Aa467197* affects expression of IL-4-induced macrophage genes even in untreated BMDMs. Expression of *Gata3*, *Ahr*, *Fzd4*, and *Socs5* in BMDMs treated with 10ng/mL IL-4 for 6h or 24h. Ctr indicates untreated BMDMs. Each data point represents one sample/mouse; n=4-5. Fold change relative to mean of untreated wildtype control is shown. Bars indicate mean ± SEM.

5.5 Expression of *NMES1* in human cells and tissue

Since *Aa467197* expression was induced in mouse BMDMs after addition of IL-4, the expression of the human homolog of *Aa467197* – *NMES1* – was examined in MDMs generated from human PBMCs through differentiation with M-CSF after incubation with IL-4. There was no significant difference between the expression of *NMES1* in untreated control MDMs and MDMs treated with IL-4 for 1h, 6h, or 24h (Figure 9A), which suggests that sensing of IL-4 by human MDMs does not induce expression of *NMES1*. However, as noted in chapter 2.3, miR-147b has been found to be downregulated in inflamed colon mucosa biopsies from patients with UC^{240–242} and in colorectal cancer (CRC) tissues^{90,91}. This suggests that dysregulation of miR-147b, and by extension *NMES1*, may be a contributing factor to the pathogenesis of IBD, which may be reversed in patients in which the inflammation is resolved. To investigate this, expression of *NMES1* was also examined in colon biopsies from patients suffering from or in remission from UC at the UKE. Compared to tissue from patients unaffected by UC and patients suffering from acute colitis, there was a trend for patients in remission from UC to express higher levels of *NMES1* in their colonic tissue (Figure 9B).

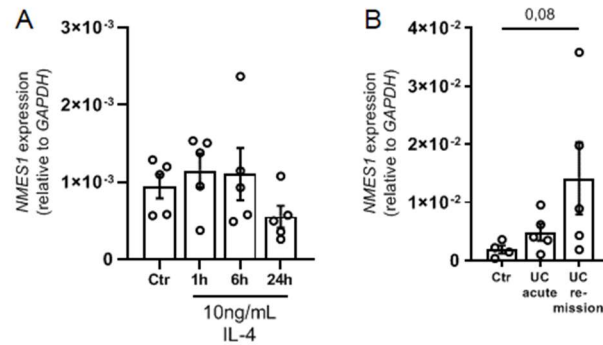


Figure 9: NMES1 expression is not induced in MDMs treated with IL-4, but is increased in colons of patients in remission from UC. (A) Expression of *NMES1* in MDMs generated from PBMCs untreated or treated with 10ng/mL IL-4 for 1h, 6h, or 24h. Each data point represents one sample; n=5. Expression relative to a housekeeping gene (*GAPDH*) is shown. Bars indicate mean \pm SEM. p-values were calculated using Kruskal-Wallis test, with Dunn's test for multiple comparisons. Missing p-value bars indicate non-significance ($p > 0.05$). (B) Expression of *NMES1* in total sigmoid colon tissue from healthy control patients, patients suffering from acute UC, or patients in remission from UC. Each data point represents one sample; n=4-5. Expression relative to a housekeeping gene (*GAPDH*) is shown. Bars indicate mean \pm SEM. Indicated p-values were calculated using Kruskal-Wallis test, with Dunn's test for multiple comparisons. Missing p-value bars indicate non-significance ($p > 0.05$).

With *NMES1* upregulated in human colons during recovery from UC, this suggested that a suitable murine *in vivo* model to study *Aa467197* could be DSS colitis. However, it was not yet known whether *Aa467197* was expressed in the mouse colon. In addition, while mice raised without intestinal microbiota (germ-free mice) develop severe epithelial damage upon administration of DSS, the inflammatory response normally associated with DSS treatment is not induced in these mice²⁴³⁻²⁴⁵. Therefore it would be important to investigate how microbiota affect expression of *Aa467197* in steady-state. Accordingly, a preliminary examination of steady-state *Aa467197* expression in intestinal tissues of wildtype mice raised under normal and germ-free conditions was performed. Among the intestinal tissues, expression of *Aa467197* was highest in colonic tissue, and expression of *Aa467197* was not altered in mice that lacked intestinal microbiota (germ-free mice).

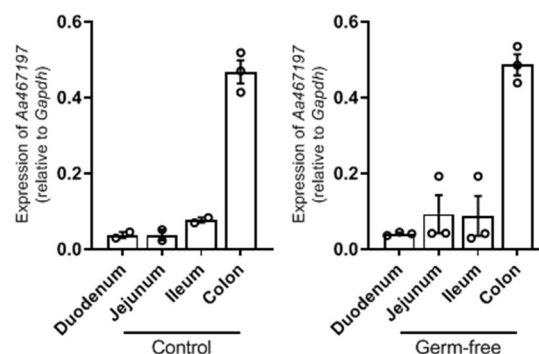


Figure 10: *Aa467197* is more highly expressed in mouse colons compared to other intestinal compartments, and expression is microbiota-independent. Expression of *Aa467197* in total tissue from duodenum, jejunum, ileum, and colon of wildtype mice and germ-free mice. Each data point represents one sample/mouse; n=2-3. Expression relative to a housekeeping gene (*Gapdh*) is shown. Bars indicate mean \pm SEM.

5.6 Analysis of *Aa467197* in a model of dextran sodium sulfate (DSS)-induced colitis

5.6.1 Expression of *Aa467197* during DSS colitis in wildtype mice

With expression of *Aa467197* being highest in colonic tissue in steady state, and expression of *NMES1* increasing in patients in remission from UC, it was decided that the model of DSS-induced colitis would be well-suited to study the effects of *Aa467197* in an *in vivo* system. In this model, colitis is induced in mice through oral application of DSS via drinking water, which is thought to compromise intestinal barrier integrity, thereby triggering the rapid induction of an inflammatory immune response^{246,247}. Among other symptoms, this is characterised by weight loss, bloody diarrhoea, and neutrophil infiltration²⁴⁸. Importantly, mice can recover from the induced colitis when given regular drinking water, regaining lost weight and slowly regenerating the colonic epithelium²⁴⁹, with macrophage tissue repair functions being crucial to this recovery process^{250–252}. Accordingly, using this model could provide insight into the mechanisms through which *Aa467197* mediates tissue remodelling functions in macrophages.

Initial experiments focussed on establishing the DSS colitis model as well as determining the expression pattern of *Aa467197* during colitis. To this end, wildtype mice received 1.5% DSS solution in place of drinking water for 7 days, before switching back to regular drinking water for another 7 days. Mice began to lose weight around day 5, with average weight loss being at 10% from day 7 to day 11. Mice began to recover weight on days 12 and 13, almost returning to normal levels (Figure 11A).

Mice were sacrificed at different time points during the course of the disease. Cells were isolated from the colons and CD45⁺ LY6G⁻ CD11b⁺ F4/80⁺ cells were FACS sorted from the colon at day 3 (d3), d7, d10, and d14 of DSS colitis, as well as from untreated controls. Analysis of *Aa467197* expression via qPCR reveals that *Aa467197* levels were increased in colon macrophages at d10 and d14 of DSS colitis compared to untreated controls (Figure 11B). In addition, colon cells were isolated at d7 and d14 and stained using the PrimeFlow™ method to analyse *Aa467197* mRNA expression via flow cytometry. The percentage of CD45⁺ Ly6G⁻ CD11b⁺ F4/80⁺ colon macrophages expressing *Aa467197* mRNA increased over the course of the colitis, with the highest proportion at d14 (55.9%), during which mice are recovering from colitis (Figure 11C).

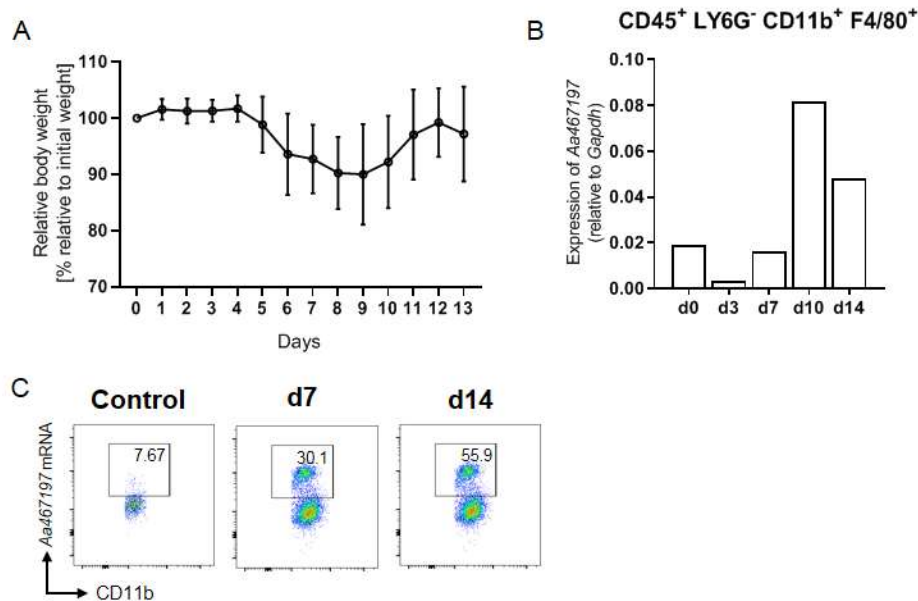


Figure 11: Aa467197 expression in mouse colon macrophages increases during the recovery phase of DSS colitis. (A) Weight loss of mice during DSS colitis. 1,5% DSS solution was given to wildtype mice in drinking water for 7 days, followed by regular drinking water for 7 days. Weight loss is shown relative to initial weight. Points indicate mean \pm SD, points at days 0 to 7 represent $n=16-22$ mice, points at days 8 to 13 represent $n=4-10$ mice. (B) Expression of *Aa467197* in sorted CD45⁺ Ly6G⁻ CD11b⁺ F4/80⁺ cells from colons of wildtype mice. Cells were pooled from $n=4-5$ mice. Each bar shows *Aa467197* mRNA levels relative to expression of a housekeeping gene (*Gapdh*). (C) Dot plots showing frequency of CD45⁺ Ly6G⁻ CD11b⁺ F4/80⁺ colon cells expressing *Aa467197* mRNA in wildtype mice. Cells were pooled from $n=5$ mice. Gates and frequencies indicate cells considered positive for *Aa467197* mRNA, based on FMO (not shown).

5.6.2 Phenotype of *Nmes1*^{-/-} mice during DSS colitis

Since expression of *Aa467197* could be observed in colon macrophages during acute colitis and recovery from colitis, DSS colitis experiments were performed on wildtype and *Nmes1*^{-/-} mice to assess the role of *Aa467197* on the progression of the disease and its impact on macrophage phenotypes and functions during colitis. Interestingly, despite being treated with 1,5% DSS in drinking water for 7 days, as previously established, both wildtype and *Nmes1*^{-/-} mice did not begin to lose weight until day 8 of the experiment, with peak weight loss at day 10 (95% of starting weight). Mice in both groups regained weight from day 11 to day 13 (Figure 12A).

Having observed that weight loss began later than anticipated, mice were sacrificed at d10 and d14 of the experiment. Cells were isolated from the colons, pooled, and sorted into CD45⁺ LY6G⁺ neutrophils, CD45⁺ LY6G⁻ CD11b⁺ F4/80⁺ CX3CR1⁻ macrophages, and CD45⁺ LY6G⁻ CD11b⁺ F4/80⁺ CX3CR1⁺ macrophages (Figure 12B). Expression of *Aa467197* was analysed via qPCR to quantify *Aa467197* levels in the sorted cell populations. In addition, *Arg1* and *Chil3* expression was analysed by qPCR to analyse potential changes in the cell phenotype due to altered levels of *Aa467197* (Figure 12C).

The results show that LY6G⁺ neutrophils and CX3CR1⁺ macrophages expressed *Aa467197* at d10 after DSS colitis treatment, with lower expression of *Aa467197* in CX3CR1⁻ macrophages. At d14, the differences in *Aa467197* between the cell populations were not as distinct, with all three populations showing similar levels of expression.

Arg1 expression was different between wildtype and *Nmes1^{-/-}* mice in all three sorted populations at d10, with *Arg1* being increased in *Nmes1^{-/-}* LY6G⁺ cells, but decreased in both macrophage populations. At d14, there were no differences between wildtype and *Nmes1^{-/-}* mice in the LY6G⁺ and CX3CR1⁻ populations, but increased *Arg1* in the CX3CR1⁺ *Nmes1^{-/-}* cells. Interestingly, CX3CR1⁻ cells showed almost no expression of *Arg1*. Expression of *Chil3* at d10 followed a similar pattern to *Arg1*, with increased levels in *Nmes1^{-/-}* LY6G⁺ neutrophils and decreased levels in *Nmes1^{-/-}* CX3CR1⁻ cells (but similar expression in CX3CR1⁺ cells). At d14, *Chil3* levels were decreased in the *Nmes1^{-/-}* LY6G⁺ and CX3CR1⁺ cells, but similar and higher overall in the CX3CR1⁻ macrophages. Overall, these data suggest that *Aa467197* regulates expression of *Arg1* and *Chil3*, and that it does so differently depending on the stage of colitis progression.

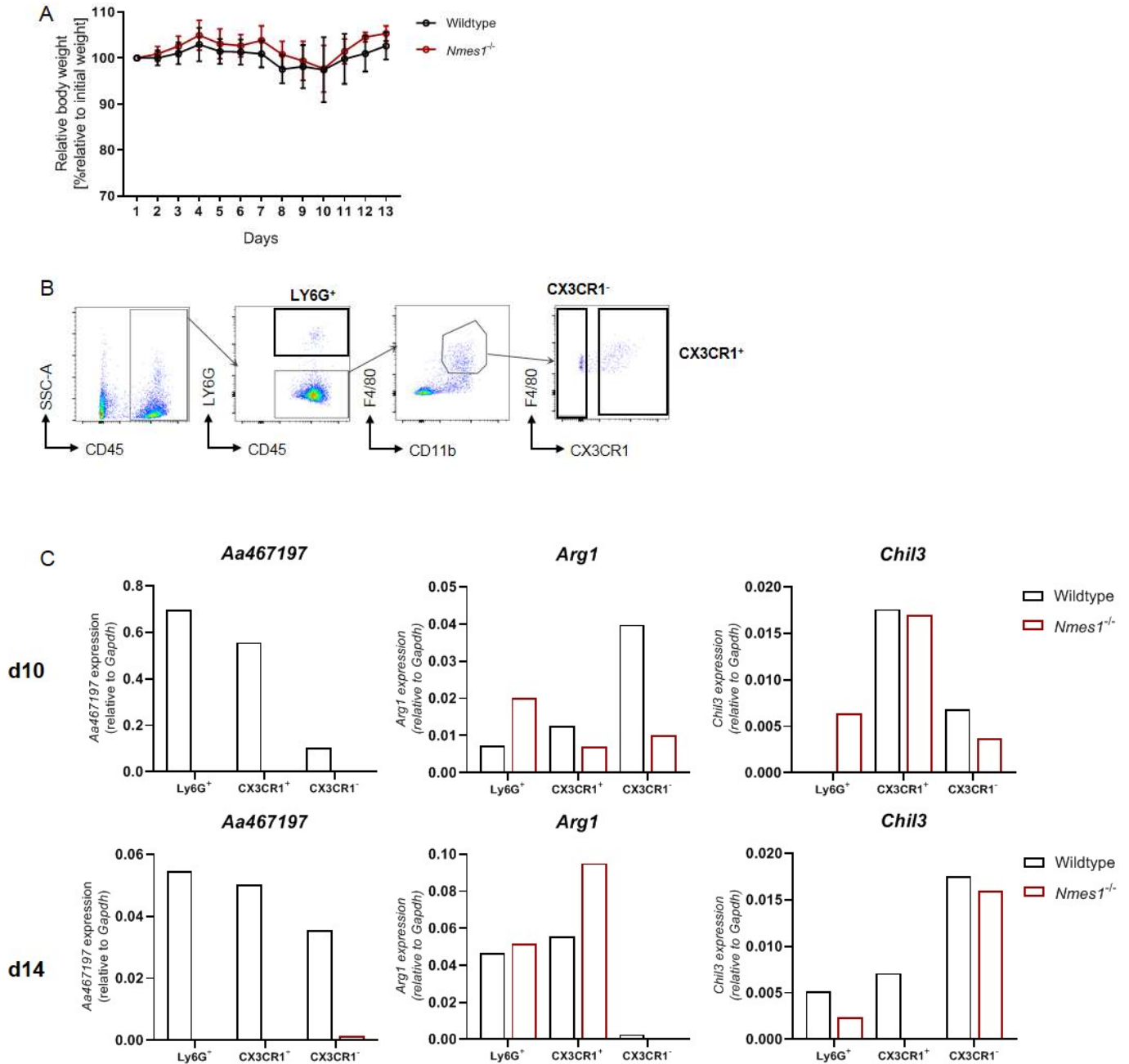


Figure 12: *Aa467197* protects co-housed wildtype and *Nmes1*^{-/-} mice from DSS-induced colitis and influences expression of *Arg1* and *Chil3* in myeloid colon cells. (A) Weight loss of mice during DSS colitis. 1.5% DSS solution was given to wildtype and *Nmes1*^{-/-} mice in drinking water for 7 days, followed by regular drinking water for 7 days. Weight loss is shown relative to initial weight. Points indicate mean ± SD, points at days 0 to 9 represent n=10 mice, points at days 10 to 13 represent n=5 mice. (B) Gating strategy for FACS of cells from colons of wildtype and *Nmes1*^{-/-} mice. Cells in bold gates were sorted, with indicated nomenclature used to identify the cell population. (C) Expression of *Aa467197* in cells sorted from colons of wildtype and *Nmes1*^{-/-} mice at d10 and d14 of DSS colitis. Cells were pooled from n=6 mice and sorted as indicated in B. Each bar shows the expression relative to expression of a housekeeping gene (*Gapdh*).

5.7 Analysis of *Aa467197* in a model of infection with *Schistosoma mansoni*

5.7.1 Expression of *Aa467197* in colons of mice during *S. mansoni* infection

To further examine the effects of *Aa467197 in vivo*, a second model in which intestinal damage occurs was chosen – infection with the helminth parasite *S. mansoni*. As described in chapter 2.4.2, chronic *S. mansoni* infection is characterised by a Th2-mediated response and an associated increase in levels of IL-4 and IL-13, as well as increased numbers of tissue remodelling macrophages. While these factors are essential for host survival of the initial inflammatory response^{127,227}, in later stages of the infection the increased levels of IL-13 and accumulation of tissue remodelling macrophages contribute to granuloma formation around *S. mansoni* eggs, which eventually leads to fibrosis development and tissue damage in the liver and intestine. Because macrophages with tissue remodelling functions play such a crucial role in this model, it is likely to be a good candidate with which to study the effects of *Aa467197*.

To examine the expression of *Aa467197* in the colon during infection, wildtype mice were infected with *S. mansoni* cercariae for 8 weeks (w8) or 14 weeks (w14), respectively. Colon cells were isolated from the mice at the two time points and *Aa467197* mRNA expression in CD45⁺ LY6G⁻ CD11b⁺ F4/80⁺ CX3CR1⁺ macrophages was analysed using the PrimeFlow™ method (Figure 13). Unlike in the DSS colitis model, there was no clear population of *Aa467197*⁺ cells (Figure 13A), through an increased proportion of macrophages expressing *Aa467197* could be observed at both w8 and w14. Interestingly, MFI analysis showed that while macrophages from uninfected and infected mice showed similar expression of *Aa467197* at w8, at w14 uninfected mice tended towards reduced expression of *Aa467197* in macrophages compared to infected mice (Figure 13B). This suggested that w14 would be the most suitable time point for further analysis of *Aa467197* in this model.

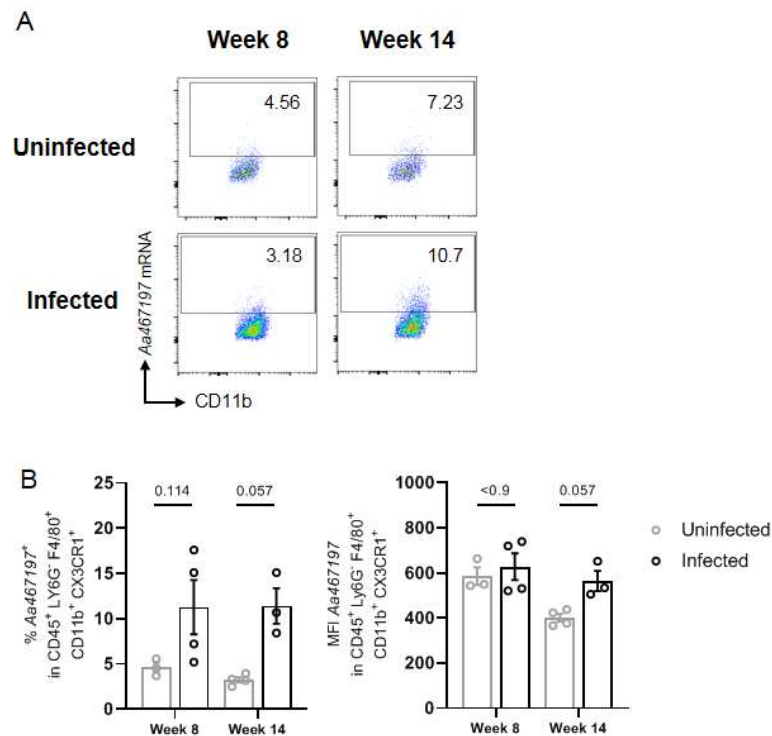


Figure 13: *Aa467197* expression is upregulated in mouse colon macrophages during infection with *S. mansoni*. (A) Representative dot plots of $CD45^+ LY6G^- CD11b^+ F4/80^+ CX3CR1^+$ colon macrophages from wildtype mice at w8 or w14 post infection with *S. mansoni*. Gates and frequencies indicate cells considered positive for *Aa467197* mRNA, based on FMO (not shown). (B) Population frequencies and MFIs of *Aa467197* in $CD45^+ LY6G^- CD11b^+ F4/80^+ CX3CR1^+$ colon macrophages of mice at w8 and w14 post infection with *S. mansoni*. Each data point represents one sample/mouse; n=3-4. Bars indicate mean \pm SEM. Indicated p-values were calculated using Mann-Whitney U test, comparing only the uninfected and infected datasets at the indicated time point.

5.7.2 Phenotype of *Nmes1*^{-/-} mice at week 14 of infection with *S. mansoni*

Having established that *Aa467197* expression was slightly elevated in mice at w14 of infection with *S. mansoni* compared to uninfected controls, wildtype and *Nmes1*^{-/-} mice were infected with *S. mansoni* for 14 weeks, then examined for differences in disease phenotype. In human schistosomiasis, egg counts in urine and stool have been used as a measure for infection intensity^{253,254}, and since much of the pathology of *S. mansoni* stems from granulomatous inflammation and fibrosis around trapped eggs, egg counts were determined as a measure of disease severity. Interestingly, *Nmes1*^{-/-} mice had reduced egg counts in the colon compared to wildtype mice (Figure 14A). Since *S. mansoni* eggs are known to induce formation of granuloma, and subsequent fibrotic lesions^{126,255}, the expression of genes related to extracellular matrix rearrangement (such as *Mmp13* or *Timp1*²¹⁷), or which have been described to contribute to fibrosis formation in schistosomiasis (such as *Arg1* and *IL-1 β* ^{60,230}) was examined in total colon tissue (Figure 14B). The expression of *Timp1* and *Arg1* was decreased, with a tendency for *IL-1 β* to be decreased as well. In contrast, expression of *Mmp13*, which has been described to play roles in collagen degradation and may have anti-fibrotic functions²⁵⁶, was similar in colons of wildtype and *Nmes1*^{-/-} mice.

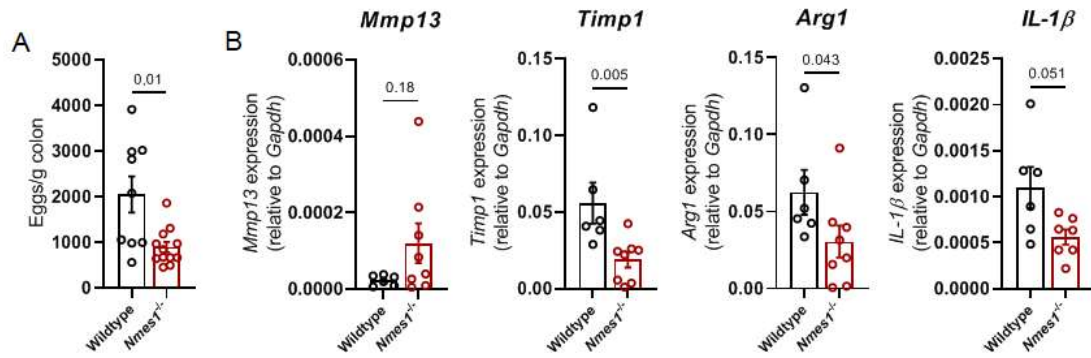


Figure 14: Aa467197 controls accumulation of *S. mansoni* eggs in the intestine and regulates fibrosis progression at w14 of *S. mansoni* infection. (A) Number of eggs per gram of colon tissue in wildtype and *Nmes1*^{-/-} mice. Each data point represents one sample/mouse; n=9-12. Bars indicate mean ± SEM. Indicated p-value was calculated using Mann-Whitney U test. (B) Expression of *Mmp13*, *Timp1*, *Arg1*, and *IL-1β* in total colon tissue of wildtype and *Nmes1*^{-/-} mice at w14 post infection with *S. mansoni*. Each data point represents one sample/mouse; n=6-8. Expression relative to a housekeeping gene (*Gapdh*) is shown. Bars indicate mean ± SEM. Indicated p-value was calculated using Mann-Whitney U test.

Since one of the main organs in which damage occurs during infection with *S. mansoni* is the liver due to granulomatous inflammation as a result of increased Th2 cytokine production in response to trapped *S. mansoni* eggs (see chapter 2.4.2.3), egg counts and expression of fibrosis-related markers were also determined in the liver. Here, there was no difference in the number of eggs in the *Nmes1*^{-/-} mice compared to the wildtype mice (Figure 15A), which suggests that Aa467197 does not control egg accumulation in the liver. Examination of fibrosis-associated markers showed no significant differences in expression of *Timp1*, *Arg1*, *IL-1β*, or *Mmp13* in the *Nmes1*^{-/-} mice compared to the wildtype mice (Figure 15B).

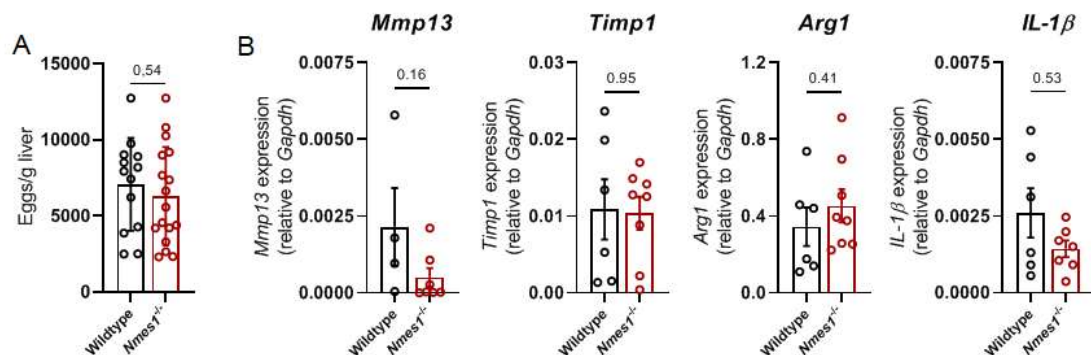


Figure 15: Aa467197 does not control accumulation of *S. mansoni* eggs in the liver at w14 of infection, and does not affect expression of fibrosis-associated markers in the liver. (A) Number of eggs per gram of liver tissue in wildtype and *Nmes1*^{-/-} mice. Each data point represents one sample/mouse; n=13-17. Bars indicate mean ± SEM. Indicated p-value was calculated using Mann-Whitney U test. (B) Expression of *Mmp13*, *Timp1*, *Arg1*, and *IL-1β* in total liver tissue of wildtype and *Nmes1*^{-/-} mice at w14 post infection with *S. mansoni*. Each data point represents one sample/mouse; n=6-8. Expression relative to a housekeeping gene (*Gapdh*) is shown. Bars indicate mean ± SEM. Indicated p-value was calculated using Mann-Whitney U test.

Another method with which to assess liver damage is by measuring the levels of alanine transaminase (ALT) in the sera, since ALT is released into the bloodstream when liver damage occurs²⁵⁷. Here, no significant differences in the ALT levels of wildtype mice and *Nmes1*^{-/-} mice were observed (Figure 16A). In addition to ALT levels, cytokine levels were measured in the sera using the LegendPlex™. An 8-plex was performed to measure levels of Th1 and Th2 cytokines in the sera of infected mice to gain a better understanding of which processes are mediated by *Aa467197*. No differences were detected in the concentrations of IFN- γ , IL-5, TNF- α , IL-2, IL-6, IL-4, and IL-10 between the wildtype and *Nmes1*^{-/-} sera (data not shown). However, the levels of IL-13 were strongly increased in the sera of *Nmes1*^{-/-} mice (Figure 16B). This suggests that *Aa467197* regulates secretion of IL-13. However, since mice with a total knockout of *Aa467197* were used in this study, it is not clear in which population of cells may be the cause of the observed phenotype. Since a major source of IL-13 in *S. mansoni* infection is CD4⁺ T cells^{207,258}, levels of IL-13 secreted by lymphocytes isolated from mesenteric lymph nodes of wildtype and *Nmes1*^{-/-} mice, then left unstimulated or stimulated with anti-CD3 ϵ , were measured via ELISA. No increase in IL-13 secretion was observed in the stimulated samples compared to the unstimulated samples (Figure 16C), which suggests that cells were not activated by addition of anti-CD3 ϵ . However, when samples were analysed for levels of IL-5, which has been shown to be essential to fibrosis progression through recruitment of eosinophils and promoting polarisation of macrophages towards a tissue remodelling phenotype^{259,260}, while there were no differences between wildtype and *Nmes1*^{-/-} mice, IL-5 production was induced in the samples stimulated with anti-CD3 ϵ (Figure 16D). This suggests that the analysed leukocytes did not increase production of IL-13, even upon stimulation. Alternatively, this may hint at a technical error in the performance of the ELISA.

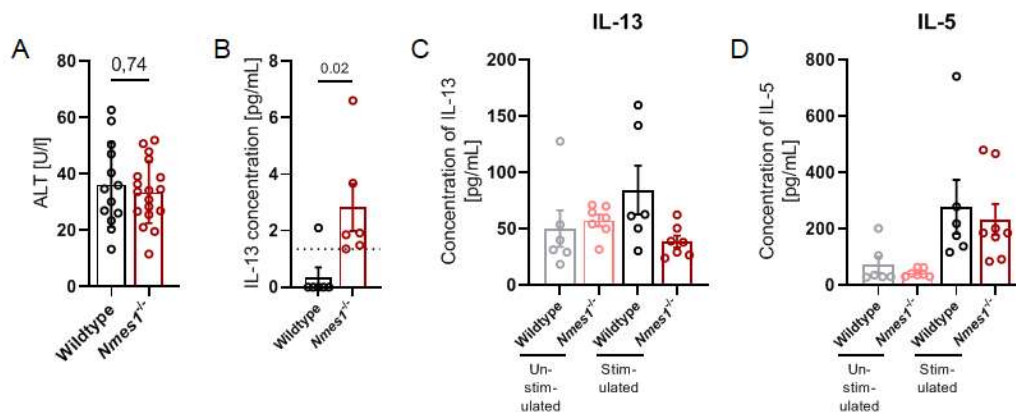


Figure 16: *Aa467197* does not affect liver damage caused by *S. mansoni* infection. (A) Alanine transaminase (ALT) levels in sera of wildtype and *Nmes1*^{-/-} mice at w14 post *S. mansoni* infection. Each data point represents one sample/mouse; n=13-17. Bars indicate mean \pm SEM. Indicated p-value was calculated using Mann-Whitney U test. (B) Concentration of IL-13 in sera of wildtype and *Nmes1*^{-/-} mice at w14 post *S. mansoni* infection. Each data point represents one sample/mouse; n=6-8. Bars indicate mean \pm SEM. Indicated p-value was calculated using Mann-Whitney U test. (C) Concentration of IL-13 and (D) IL-5 in supernatants of unstimulated or anti-CD3 ϵ -stimulated leukocytes isolated from mesenteric lymph nodes of wildtype and *Nmes1*^{-/-} mice at w14 post *S. mansoni* infection. Each data point represents one sample/mouse; n=6-8. Bars indicate mean \pm SEM.

5.7.3 Analysis of myeloid cell populations in *Nmes1^{-/-}* mice at week 14 of *S. mansoni* infection

5.7.3.1 Analysis of colon cell populations

Since the number of eggs found in the colons of *Nmes1^{-/-}* mice was significantly reduced compared to wildtype mice (Figure 14), and macrophages and monocytes have been shown to regulate egg-induced granuloma formation and fibrosis development in *S. mansoni* infection^{230,261,262}, macrophage and monocyte populations in the colons of infected wildtype and *Nmes1^{-/-}* mice were examined in greater detail. In addition, even though neutrophils are thought to play a less dominant role in *S. mansoni* infection compared to infection with *S. japonicum*, in which neutrophils are the predominant cell type in egg granuloma²⁶³, since *Aa467197* had been shown to be expressed in neutrophils during DSS colitis (Figure 12), infiltration of neutrophils was also analysed in *Nmes1^{-/-}* mice in comparison to wildtype mice.

Colon cells were isolated from infected mice at week 14 post infection with *S. mansoni* and analysed by flow cytometry. Different subsets of cells within the CD45⁺ subset were analysed. Within CD45⁺ cells, LY6G⁻ CD11b⁺ cells were further subdivided by expression of F4/80, a marker for macrophages. F4/80⁻ cells were then divided into subpopulations based on the expression of LY6C, as a marker for cells derived from infiltrating, inflammatory monocytes, and CX3CR1, a monocyte chemotaxis marker which is also highly expressed on resident intestinal macrophages²⁶⁴. In addition, frequencies of LY6G⁺ CD11b⁺ neutrophils were analysed (Figure 17A). No differences between wildtype and *Nmes1^{-/-}* mice were observed in the proportions of CD11b⁺ F4/80⁺ cells (Figure 17C) or infiltrating LY6C⁻, LY6C^{low}, or LY6C^{int} macrophages (Figure 17D-F). However, there was a strong reduction of CD45⁺ LY6G⁻ CD11b⁺ F4/80⁻ LY6C^{hi} CX3CR1^{low} infiltrating monocytes in the intestines of *Nmes1^{-/-}* mice (Figure 17G), as well as a non-significant reduction of infiltrating CD45⁺ LY6G⁺ CD11b⁺ neutrophils (Figure 17B). This suggests that *Aa467197* may play a role in driving migration of LY6C^{hi} monocytes to the intestine during infection with *S. mansoni*.

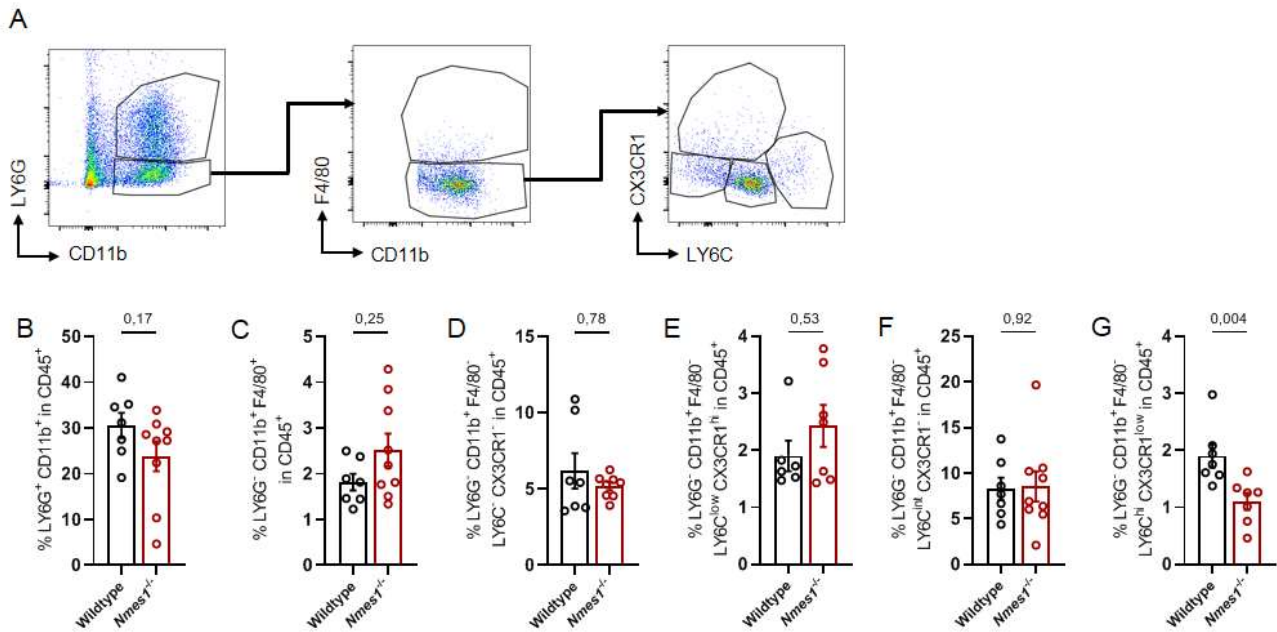


Figure 17: *Aa467197* regulates infiltration of neutrophils and monocytes into the colon at week 14 of infection with *S. mansoni*. (A) Gating strategy for analysis of colon cell populations. Population frequencies of (B) LY6G⁺ CD11b⁺ neutrophils, (C) LY6G⁻ CD11b⁺ F4/80⁺ macrophages, (D) LY6G⁻ CD11b⁺ F4/80⁻ LY6C⁻ CX3CR1⁻ cells, (E) LY6G⁻ CD11b⁺ F4/80⁻ LY6C^{low} CX3CR1^{hi} resident cells, (F) LY6G⁻ CD11b⁺ F4/80⁻ LY6C^{int} CX3CR1⁻ monocytes, and (G) LY6G⁻ CD11b⁺ F4/80⁻ LY6C^{hi} CX3CR1^{low} infiltrating monocytes in the CD45⁺ population. Each data point represents one sample/mouse; n=7-9. Bars indicate mean ± SEM. Indicated p-values were calculated using Mann-Whitney U test.

Due to the low frequencies of F4/80⁺ macrophages, LY6C^{hi} infiltrating monocytes, and CX3CR1^{hi} monocytes, expression of macrophage and monocyte activation markers was only analysed in the LY6G⁻ CD11b⁺ F4/80⁻ LY6C^{int} CX3CR1⁻ monocyte population (Figure 17F). Although expression of ARG1 and YM1 was not regulated by *Aa467197* in vitro (Figure 3), *Aa467197* expression had been found to influence mRNA expression of *Arg1* and *Chil3* in neutrophils and macrophages during DSS colitis (Figure 13). Therefore, frequencies and MFIs of ARG1 and YM1 were analysed in all colon subpopulations to investigate whether *Aa467197* can regulate their expression in *S. mansoni* infection. In addition, frequencies and MFIs of CD80, as a marker for pro-inflammatory macrophages²⁶⁵, CCR2, which is crucial for monocyte recruitment³⁴, and MHCII, as a measure for antigen presentation capacity, were measured.

The expression of MHCII and CD80 did not differ between wildtype and *Nmes1*^{-/-} mice (data not shown), nor did the proportions of ARG1⁺ or YM1⁺ cells within the LY6C^{int} CX3CR1⁻ monocyte population. However, there was a slight reduction in CCR2⁺ cells in the *Nmes1*^{-/-} mice (Figure 18A), though the MFI did not differ between wildtype and *Nmes1*^{-/-} mice (Figure 18B). This suggests that, while *Aa467197* does not influence the polarisation of monocytes or macrophages in the colon during infection with *S. mansoni*, it may regulate monocyte infiltration into the colon.

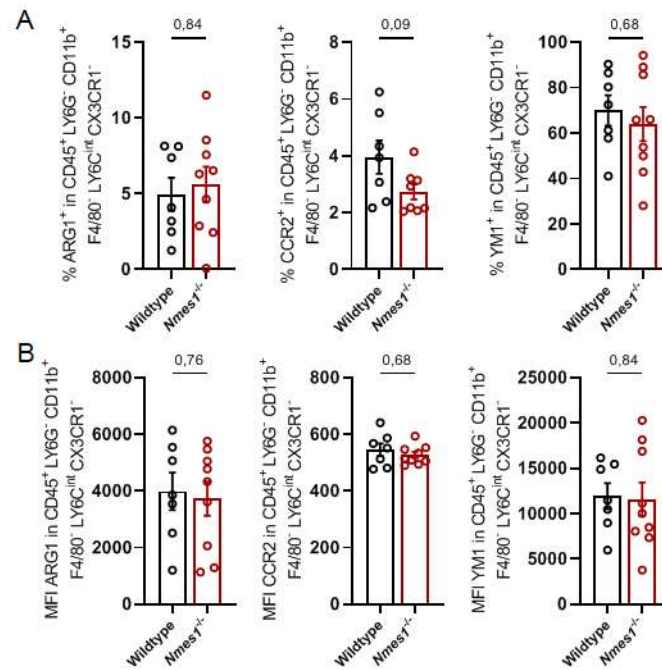


Figure 18: *Aa467197* regulates the infiltration of CCR2⁺ colon monocytes during infection with *S. mansoni*. (A) Population frequencies and (B) MFIs of ARG1, CCR2, and YM1 in CD45⁺ LY6G⁻ CD11b⁺ F4/80⁻ LY6C^{int} CX3CR1⁻ monocytes in the colon of wildtype and *Nmes1*^{-/-} mice at week 14 of infection with *S. mansoni*. Each data point represents one sample/mouse; n=7-9. Bars indicate mean ± SEM. Indicated p-values were calculated using Mann-Whitney U test.

In the neutrophils, in addition to ARG1, expression of CD44, MPO, and citrullinated Histone 3 (Histone 3) was analysed to assess whether *Aa467197* regulates their activation. There were no differences in the frequencies or MFIs of MPO⁺, Histone 3⁺, or ARG1⁺ cells between wildtype and *Nmes1*^{-/-} neutrophils, though there was a non-significant reduction in CD44⁺ cells (Figure 19A, B). However, all together this indicates that *Aa467197* does not modulate neutrophil activation in the colon.

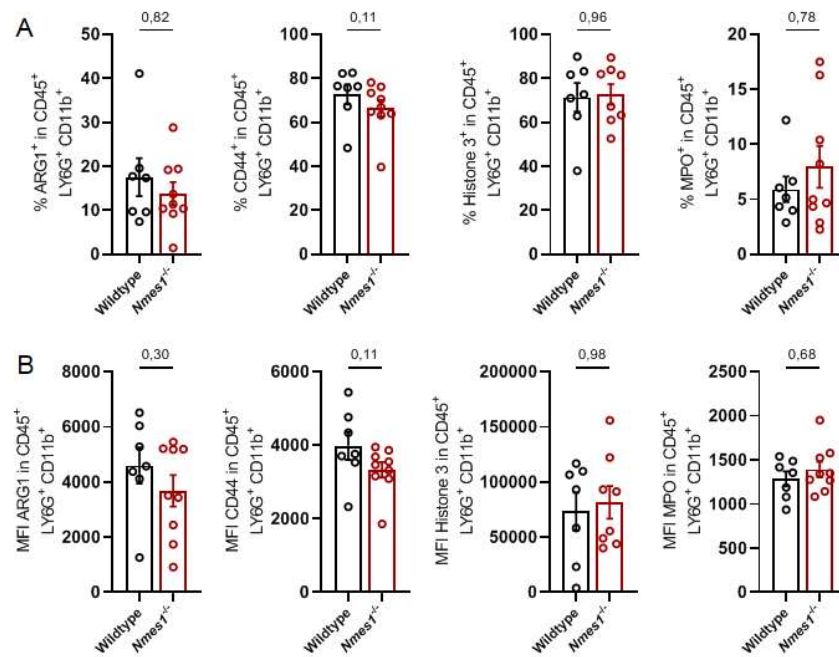


Figure 19: *Aa467197* does not modulate neutrophil activation in the colon at week 14 of *S. mansoni* infection. (A) Population frequencies and (B) MFIs of ARG1, CD44, MPO, and Histone 3 in CD45⁺ LY6G⁺ CD11b⁺ cells in the colon of wildtype and *Nmes1*^{-/-} mice at week 14 of infection with *S. mansoni*. Each data point represents one sample/mouse; n=7-9. Bars indicate mean \pm SEM. Indicated p-values were calculated using Mann-Whitney U test.

5.7.3.2 Analysis of liver cell populations

Since infiltrating monocytes and macrophages which exert tissue remodelling functions play key roles in promoting or restricting inflammation and fibrosis in the liver, depending on their activation status^{266,267}, liver cells were isolated from the infected mice and analysed by flow cytometry. Within CD45⁺ cells, frequencies of LY6C⁻ LY6G⁻ cells, which exclude neutrophils and infiltrating monocytes and most likely represent differentiated monocyte-derived macrophages and resident cells, and LY6C⁺ LY6G⁻ cells, which presented characteristics typical of infiltrating cells^{268,269}, were analysed in greater detail. Populations of LY6C⁻ LY6G⁻ cells and Ly6C⁺ Ly6G⁻ cells were further subdivided into populations based on the expression of CD11b, a marker for myeloid cells, and CD68, which is enriched in macrophages^{270,271} and considered a marker for liver-resident macrophages (Figure 21A).

In addition, since *Aa467197* had been shown to be expressed in colon neutrophils during DSS colitis (Figure 12), the expression of *Aa467197* in liver neutrophils was examined during infection with *S. mansoni*. CD45⁺ LY6G⁻ neutrophils were sorted from wildtype and *Nmes1*^{-/-} livers at week 14 of infection and examined for their expression of *Aa467197*, with CD45⁺ LY6G⁻ F4/80⁺ CD11b⁺ macrophages for comparison. *Aa467197* was expressed in the sorted LY6G⁺ cells, and was even higher than in the F4/80⁺ CD11b⁺ cells (Figure 20). This suggested that *Aa467197* could also modulate neutrophil infiltration and functions in infection with *S. mansoni*. Accordingly, the infiltration of neutrophils into livers of mice infected with *S. mansoni* was also analysed.

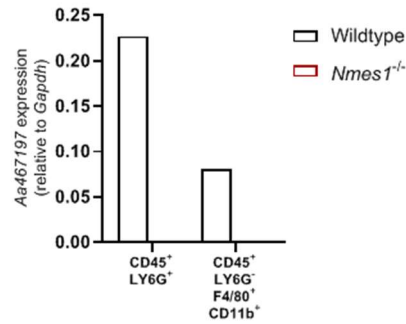


Figure 20: *Aa467197* is expressed in liver neutrophils of mice during infection with *S. mansoni*. Expression of *Aa467197* in CD45⁺ LY6G⁺ neutrophils and CD45⁺ LY6G⁻ F4/80⁺ CD11b⁺ macrophages sorted from livers of wildtype and *Nmes1*^{-/-} mice at w14 post infection with *S. mansoni*. Cells were pooled from n=6-8 mice. Each bar shows the expression relative to expression of a housekeeping gene (*Gapdh*).

There were no significant differences between wildtype and *Nmes1*^{-/-} mice in the proportions of CD45⁺ LY6C⁺ CD11b⁺ CD68⁻ infiltrating monocytes (Figure 21C) or of CD45⁺ LY6C⁻ CD11b⁺ CD68⁺ or CD68⁻ resident cells (Figure 21D) in the liver at week 14 of infection with *S. mansoni*, as well as a non-significant reduction of CD45⁺ LY6G⁺ CD11b⁺ neutrophils in the livers of *Nmes1*^{-/-} mice (Figure 21B). Similarly, there was a non-significant reduction in the proportion of CD45⁺ LY6C⁺ CD11b⁺ CD68⁺ cells in *Nmes1*^{-/-} livers (Figure 21C). These cells are most likely non-resident macrophages, differentiated from bone marrow monocytes^{269,272}. However, overall *Aa467197* does not appear to affect recruitment of monocyte or neutrophil populations into the liver during *S. mansoni* infection.

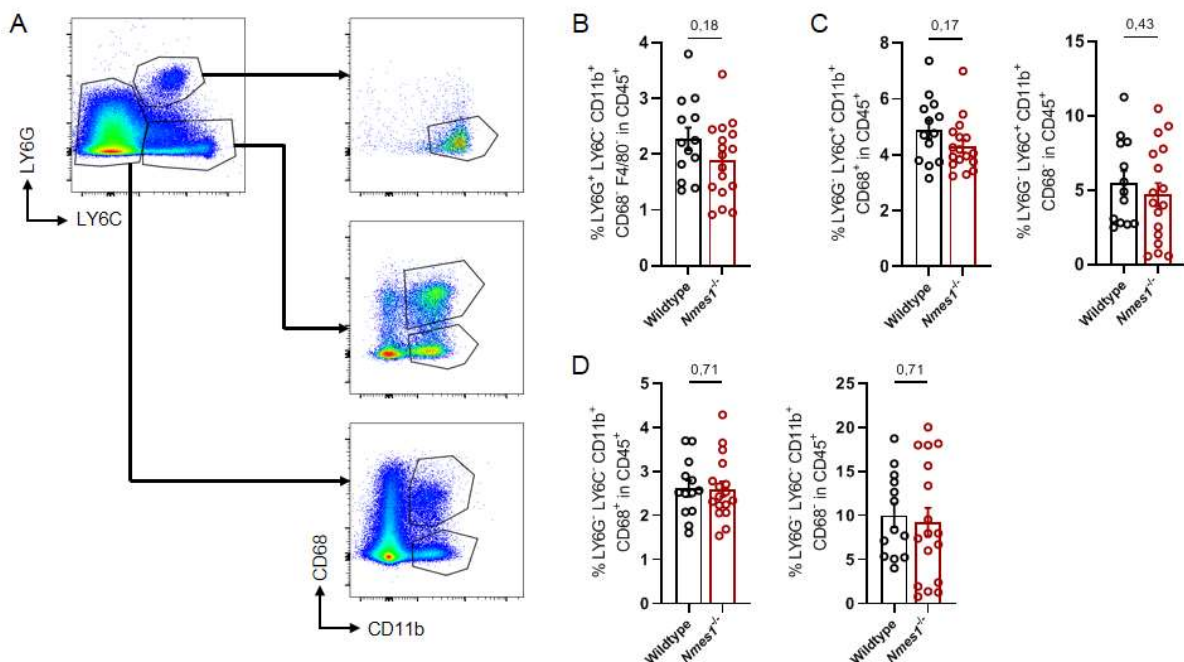


Figure 21: *Aa467197* does not modulate frequencies of resident or infiltrating myeloid cell populations in the liver at week 14 of infection with *S. mansoni*. (A) Gating strategy for analysis of liver cell populations. Population frequencies of (B) LY6G⁺ CD11b⁺ CD68⁻ neutrophils, (C) LY6G⁻ LY6C⁺ CD11b⁺ CD68⁺ and CD68⁻ cells, and (D) LY6G⁻ LY6C⁻ CD11b⁺ CD68⁺ and CD68⁻ cells in CD45⁺ population. Each data point represents one sample/mouse; n=13-17. Bars indicate mean \pm SEM. Indicated p-values were calculated using Mann-Whitney U test.

As in the colon, the different monocyte and macrophage populations in the liver were analysed for the expression of ARG1, YM1, CD80, CR2, and MHCII. The amounts of CCR2⁺ and CD80⁺ cells in wildtype and *Nmes1*^{-/-} mice were similar in all of the populations analysed, as were the proportions of ARG1⁺, MHCII⁺, and YM1⁺ cells in the CD68⁺ resident and infiltrating macrophage subpopulations (data not shown). There was also no difference in the proportions (Figure 22A, C) or MFIs (Figure 22B, D) of YM1⁺ or MHCII⁺ cells in the CD68⁻ cell subpopulations, though there was a non-significant reduction in the MFI of MHCII in the CD45⁺ LY6G⁻ CD11b⁺ CD68⁻ LY6C⁻ population (Figure 22B). However, in the CD45⁺ LY6G⁻ CD11b⁺ CD68⁻ LY6C⁺ blood-derived macrophages, there was a significant increase in the proportion of ARG1⁺ cells in the *Nmes1*^{-/-} livers compared to the wildtype livers (Figure 22C). This was similar, but not significant, in the CD45⁺ LY6G⁻ CD11b⁺ CD68⁻ LY6C⁻ cells (Figure 22A). Overall, this indicates that *Aa467197* plays a role in modulating ARG1 expression in blood-derived macrophages during infection with *S. mansoni*, and may therefore affect their tissue remodelling functions within the damaged tissue.

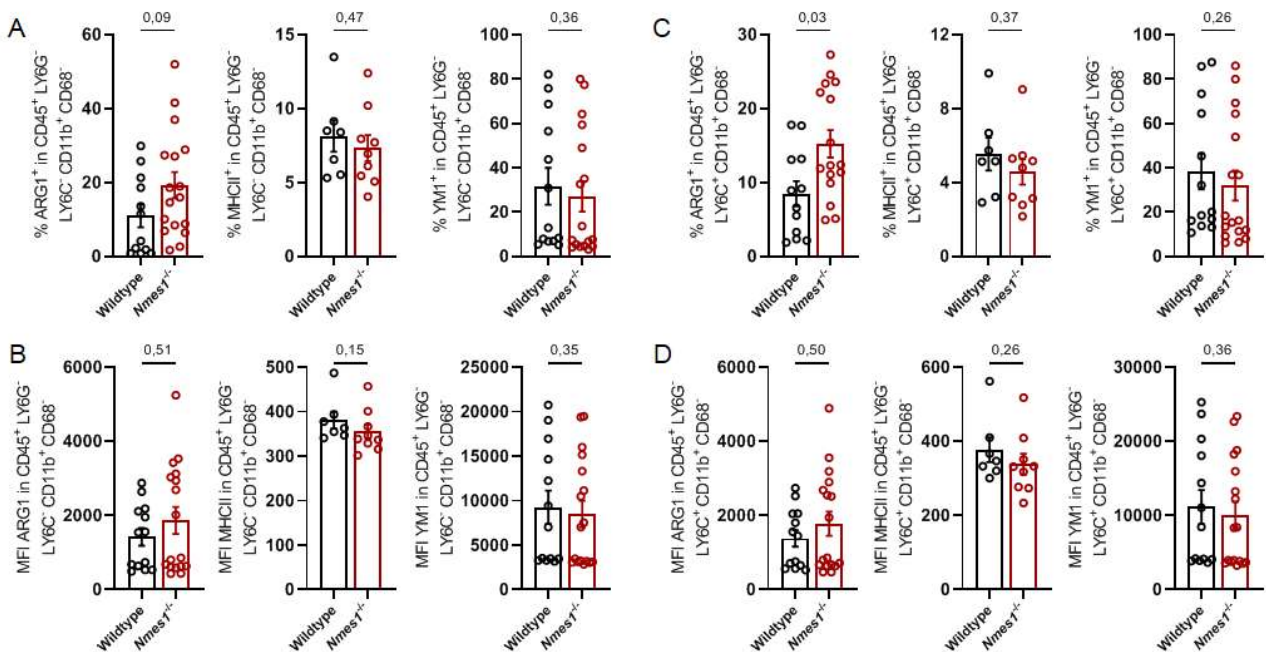


Figure 22: *Aa467197* regulates the expression of ARG1 in blood-derived liver macrophages during infection with *S. mansoni*. (A) Population frequencies and (B) MFIs of ARG1, MHCII, and YM1 in CD45⁺ LY6G⁻ LY6C⁻ CD11b⁺ CD68⁻ cells in the liver of wildtype and *Nmes1*^{-/-} mice at week 14 of infection with *S. mansoni*. (C) Population frequencies and (D) MFIs of ARG1, MHCII, and YM1 in CD45⁺ LY6G⁻ LY6C⁺ CD11b⁺ CD68⁻ cells in the liver of wildtype and *Nmes1*^{-/-} mice at week 14 of infection with *S. mansoni*. Each data point represents one sample/mouse; n=13-17. Bars indicate mean \pm SEM. Indicated p-values were calculated using Mann-Whitney U test.

Within the neutrophil population, population frequencies and MFIs of ARG1 and neutrophil activation markers (CD44, MPO, and Histone 3) were examined. While there was no difference in the frequency or MFI of ARG1⁺, MPO⁺, or Histone 3⁺ cells between the wildtype and *Nmes1*^{-/-} mice (Figure 23A, B), there was a non-significant decrease in the amount of neutrophils positive for CD44 in the *Nmes1*^{-/-} livers (Figure 23A). This indicates that *Aa467197* expression may mediate CD44-dependent neutrophil

activation in the livers of *S. mansoni*-infected mice to a minor extent, specifically the recruitment and polarisation of neutrophils^{273,274}.

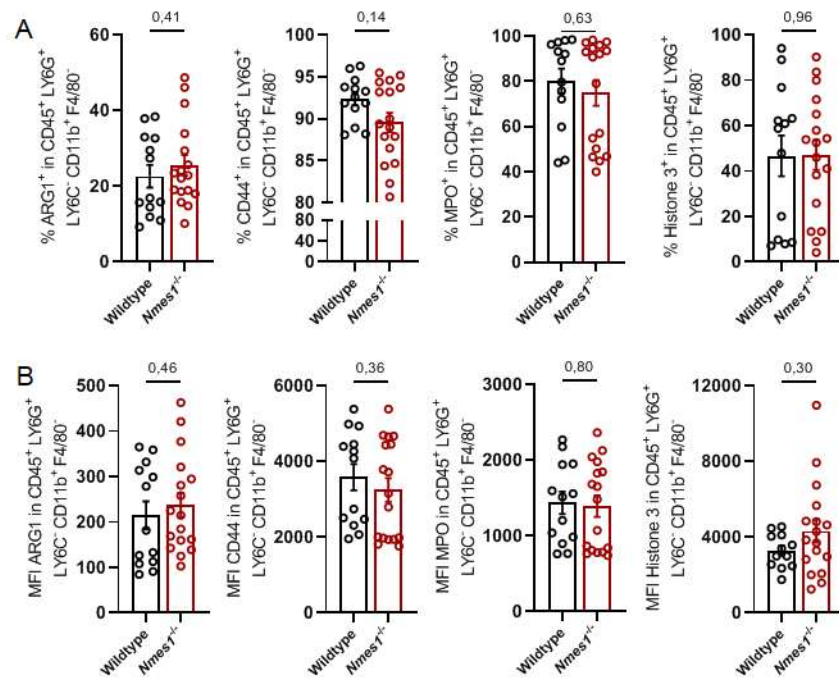


Figure 23: *Aa467197* does not modulate neutrophil activation in the liver at week 14 of *S. mansoni* infection. (A) Population frequencies and (B) MFIs of ARG1, CD44, MPO, and Histone 3 in CD45⁺ LY6G⁺ CD11b⁺ F4/80⁻ cells in the colon of wildtype and *Nmes1*^{-/-} mice at week 14 of infection with *S. mansoni*. Each data point represents one sample/mouse; n=13-17. Bars indicate mean ± SEM. Indicated p-values were calculated using Mann-Whitney U test.

5.8 Expression of *Aa467197* in *in vitro*-cultured neutrophils derived from bone marrow

Since *Aa467197* had been found to be expressed in liver neutrophils at w14 post infection, expression of *Aa467197* was examined in neutrophils isolated from bone marrow and incubated with IL-4 *in vitro*. Unlike in BMDMs, no significant change in expression of *Aa467197* could be detected (Figure 24A), though expression of *Chil3* was significantly increased 24h post addition of IL-4 (Figure 24B), which indicates that these neutrophils were able to respond to IL-4. Accordingly, sensing of IL-4 does not lead to induction of *Aa467197*, which in turn suggests that *Aa467197* does not play a role in mediating IL-4-induced functions in neutrophils.

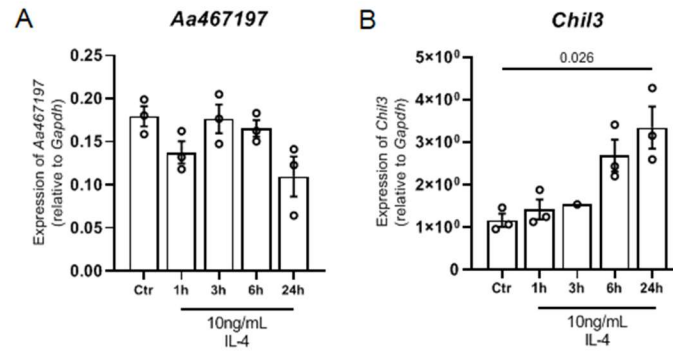


Figure 24: IL-4 does not induce *Aa467197* expression in neutrophils *in vitro*. (A) Expression of *Aa467197* and (B) *Chil3* in neutrophils stimulated with 10ng/mL IL-4 for the indicated lengths of time. Each data point represents one sample/mouse; n=3. Expression relative to a housekeeping gene (*Gapdh*) is shown. Bars indicate mean \pm SEM. p-values were calculated using Kruskal-Wallis test, with Dunn's test for multiple comparisons. Missing bars indicate non-significance ($p > 0.05$). All treated samples were compared to the untreated control.

6. Discussion

It has been established that myeloid cells, and macrophages in particular, are crucial for the development of an organism, the maintenance of homeostasis, and recovery from inflammation. The latter function is particularly important to prevent the occurrence of chronic inflammatory disease. Accordingly, understanding the mechanisms through which macrophages mediate anti-inflammatory responses and tissue remodelling, and the molecules involved in these processes, could be critical in developing new forms of treatment.

In this thesis, the focus has been on a candidate gene – *Aa467197* – which had previously been established to be downregulated in macrophages with impaired tissue remodelling functions⁷³ and to play a role in dampening the inflammatory response of LPS-activated macrophages⁹⁹. The studies presented here were performed with the aim to better understand the conditions upon which *Aa467197* is expressed, shed light on macrophage functions regulated by *Aa467197*, establish models with which to study the impact of *Aa467197* during disease, and investigate the function of *Aa467197* during the course of chronic disease.

Overall, this study showed that *Aa467197* may contribute to macrophage polarisation early after sensing of IL-4, and may play a role in mediating tissue remodelling functions of macrophages, including macrophage migration, monocyte chemotaxis, and angiogenesis. In addition, *Aa467197* may also contribute to intestinal disease progression. This is supported by the finding that expression of *NMES1*, the human homolog to *Aa467197*, is increased in colons of patients in remission from UC. In DSS colitis, ablation of *Aa467197* protected mice against colitis, and in *S. mansoni* infection, mice lacking *Aa467197* had lower egg counts fibrosis marker expression, and monocyte infiltration in the colon.

6.1 The role of *Aa467197* in macrophage polarisation after stimulation with IL-4

The results generated during this thesis indicate that *Aa467197* may contribute to macrophage polarisation shortly after stimulation with IL-4. *Aa467197* is only upregulated in macrophages after 6h of exposure to IL-4, and ablation of *Aa467197* only significantly reduces the expression of *Chil3* at 24h post IL-4 treatment. This reduction is much less pronounced 48h after addition of IL-4 (Figure 1). Together, these results suggest that *Aa467197* can regulate the expression of individual tissue remodelling genes at specific time points. One explanation for this transient change in gene expression only during early polarisation with IL-4 could be genetic compensation²⁷⁵, a well-documented phenomenon across many model organisms in which knockdown of a gene may lead to upregulation of a functionally similar gene, which subsequently compensates for the loss of function. For example, mice with genetic ablation for the ribosomal gene *Rpl22* show almost no translational defects due to a compensatory increase in *Rpl22l1*, which in turn is regulated by *RPL22*²⁷⁶. Accordingly, for our study a next important step would be to analyse genes upregulated in *Nmes1*^{-/-} macrophages compared to the wildtype during the response to IL-4, and investigate whether the listed genes may play a functionally similar role to *Aa467197*.

In addition, it is possible that that genetic ablation of *Aa467197* changes the expression kinetics of genes that induce macrophage polarisation, rather than the strength of the tissue remodelling response.

Altered downstream expression kinetics or delayed functionality after genetic ablation have also been described for other knockout models, such as mice lacking solute carrier 11a1, which show a delayed wound healing response due to reduced expression of secretory leukocyte protease inhibitor (SLPI) in macrophages²⁷⁷. Based on these initial results, a broad spectrum RNAseq analysis was performed to investigate the transcriptome and expression kinetics of genes regulated by *Aa467197*. RNAseq analysis showed strong upregulation of genes and pathways associated with the induction of IL-4-induced macrophage responses in the wildtype compared to the *Nmes1^{-/-}* after 6h, but not 24h, of exposure to IL-4 (Figure 7). Of particular note is the difference in upregulation of *Gata3*, a master regulator of Th2 cytokine expression and function in tissue remodelling macrophages^{53,237,278}, and several genes associated with the Wnt signalling pathways, such as *Fzd4*²³⁹. In macrophages, components of the Wnt/ β -catenin signalling pathway are highly upregulated in tissue remodelling macrophages and Wnt signalling promotes the polarisation of macrophages towards a tissue remodelling phenotype^{279,280}. Together, this indicates that *Aa467197* only plays a role in macrophage polarisation early after sensing of IL-4. Further evidence to support this hypothesis lies in the extracellular flux analysis performed on wildtype and *Nmes1^{-/-}* cells (Figure 5). IL-4-polarised macrophages have been shown to have increased OCR rates and ATP production compared to unstimulated cells due to increased activity of the oxidative phosphorylation (OXPHOS) cycle⁴⁶. Accordingly, the increased OCRs and rates of maximal respiration observed at 24h post IL-4 induction in the wildtype and *Nmes1^{-/-}* cells were anticipated. However, the *Nmes1^{-/-}* cells also showed a non-significant increase in the OCRs of unstimulated and 6h-stimulated cells. This implies that the *Aa467197* cells may already be primed towards higher OXPHOS.

In addition, the finding that the differences between wildtype and *Nmes1^{-/-}* in the upregulation of *Gata3*, *Ahr*, *Fzd4*, and *Socs5* upon stimulation with IL-4 were not caused by increased expression at 6h or 24h, but due to the high basal expression of the genes in the untreated *Nmes1^{-/-}* cells (Figure 8) implies that while *Aa467197* may play a role in driving macrophage polarisation after exposure to IL-4, it also functions as a regulator of tissue remodelling gene expression in unpolarised macrophages. Notably, naïve bone marrow macrophages and resting tissue macrophages play an intrinsically anti-inflammatory role¹⁵, with fewer differentially expressed genes³⁶ and more similar morphology²⁸¹ to tissue healing macrophages than inflammatory macrophages. Accordingly, *Aa467197* may play a role in suppressing expression of tissue remodelling genes in macrophages that have not been exposed to anti-inflammatory cytokines. This may be important to prevent excess production and activity of pro-fibrotic mediators, such as proline production through ARG1, as discussed in chapter 2.4.2.3, or growth factors that could contribute to tumour formation outside the context of wound healing, such as VEGF, which plays essential functions in angiogenesis in cancer²⁸². Regulating polarisation may also ensure that naïve macrophages are better able to respond to inflammatory stimuli, though anti-inflammatory macrophages were found to be easily repolarised into inflammatory macrophages after stimulation with LPS and IFN- γ ²⁸³.

Another important aspect to the regulation of macrophage polarisation by *Aa467197* is that *in vitro* it only appears to have an effect on differential expression of the tissue remodelling marker *Chil3* at the mRNA level (Figure 2), but not at protein level (Figure 3). For *Aa467197* in particular, there are two possibilities through which it is most likely to impact mRNA expression of these genes. *Aa467197* has

been described to encode for a microRNA, miR-147b, so it is possible that the microRNA directly regulates the expression of tissue remodelling-associated genes by binding to their already transcribed mRNA, thus reducing their stability or inhibiting their expression. However, since the *Nmes1*^{-/-} macrophages had decreased levels of *Chil3* mRNA, it is unlikely that *Aa467197* modifies its expression in this manner. Accordingly, it is more likely that *Aa467197* indirectly influences tissue remodelling gene expression by regulating expression of transcriptional regulators, though it is unlikely to itself be a transcriptional regulator, since the protein encoded by the *Aa467197* sequence does not appear to have a DNA-binding site^{87,89}. A concrete example of this is *Gata3*, which is a master regulator of gene expression in tissue remodelling macrophages and is downregulated in *Nmes1*^{-/-} BMDMs. Accordingly, *Aa467197* probably regulates expression of other regulators through the encoded miRNA, or as a result of the expressed protein, NMES1, impacting other functions.

Interestingly, one of the key targets described for miR-147b, *Ndufa4*, is a subunit of the cytochrome c oxidase in the mitochondrial electron transport chain²⁸⁴ and in fact a recent study reported that NMES1 itself can replace NDUFA4 in the cytochrome c oxidase during inflammation, reducing production of ROS and dampening the immune response²⁸⁵. NDUFA4 has also been described to contribute to glycolysis in colon cancer cells by upregulating PDK1, PFK1 and PKM2⁹¹. This would indicate that one method through which *Aa467197* might regulate macrophage differentiation is by blocking ROS production and shifting their metabolic profile towards OXPHOS, which in macrophages is known to lead to a more M2-like phenotype⁴⁶. However, in this thesis, *Nmes1*^{-/-} BMDMs only showed non-significant increases in OCR in comparison to wildtype BMDMs when untreated or after incubation with IL-4 for 6h, and no differences in ECAR (Figure 5). There were also no differences in ATP-linked respiration, maximal respiration, glycolysis, or maximum glycolysis. However, the influence of *Aa467197* on the function of cytochrome c oxidase in macrophages has not yet been examined. Therefore, while *Aa467197* does not appear to modulate mitochondrial function in mice *in vitro*, this needs to be examined in greater detail.

Importantly, since protein levels of ARG1, RELMa, and YM1 were unchanged in *Nmes1*^{-/-} compared to the wildtype (Figure 3), despite *Aa467197* affecting transcription rates or mRNA stability of *Chil3* (Figure 2), it is likely that translational control mechanisms were engaged. Multiple methods of translation control have been described, with regulation of translation initiation through changes in the phosphorylation state of initiation factors and regulation of 40S ribosome recruitment being common pathways through which translation is inhibited or enhanced^{286,287}. Less commonly, the elongation and termination steps can also be subject to control, with elongation rates affecting proper protein folding²⁸⁸, and selenocysteine insertion into proteins involving recoding of the UGA stop codon^{289,290}. And, as noted above, binding of microRNA to mRNA can lead to translational repression or destabilisation of the target mRNA^{291,292}. In fact, several microRNAs have been shown to promote macrophage polarisation, such as miR-155 and miR-125b in inflammatory macrophage polarisation, and miR-124 and miR-142-5p in anti-inflammatory macrophages²⁹³. Therefore it is possible that translational control mechanisms are engaged when *Nmes1*^{-/-} macrophages are polarised with IL-4, thus balancing out the expression of tissue remodelling proteins to reach levels similar to the wildtype.

Notably, in the *in vivo* model of *S. mansoni* infection, the proportion of ARG1⁺ cells within the CD45⁺ LY6G⁻ CD11b⁺ CD68⁻ LY6C⁺ and LY6C⁻ liver populations was increased in *Nmes1*^{-/-} mice compared to wildtype controls. This may indicate that *Aa467197* can mediate the expression of some tissue remodelling-associated genes at protein level, but requires additional factors to do so, such as worm or egg-derived components like IPSE/alpha-1, or factors derived from other cells, such as T cells, basophils, or neutrophils. Since this study used mice with total ablation of *Aa467197*, pathways within other cell types may also have been affected, and may have contributed to the altered expression of ARG1. Accordingly, more studies are needed to pinpoint which factors are involved in *Aa467197*-mediated expression of tissue remodelling genes.

6.2 Macrophage tissue remodelling functions may be influenced by *Aa467197*

During an immune response, tissue remodelling-associated macrophages perform a number of functions to limit the damage caused by the initial, pro-inflammatory immune response and initiate and drive processes that lead to regeneration of damaged tissue. In this thesis, the contribution of *Aa467197* in driving a number of tissue remodelling functions in macrophages was examined in greater detail.

6.2.1 *Aa467197* may play a role in regulating macrophage migration, chemotaxis of cells to sites of inflammation, and the response to microbial infection

The results presented in this thesis provide evidence that *Aa467197* is involved in the regulation of cell chemotaxis and migration upon stimulation with IL-4 and during an immune response. RNAseq and GO term analysis (Figure 7) showed that several genes related to macrophage migration were upregulated in wildtype mice stimulated with IL-4 for 6h compared to *Nmes1*^{-/-} mice. For instance, G-protein-coupled receptor 183 (GPR183, also known as EBI2) is a chemotactic receptor expressed on lymphoid and myeloid immune cells, best characterised for positioning of B cells through binding of oxysterols²⁹⁴, and has also been shown to regulate macrophage migration induced by mouse astrocyte-conditioned media²⁹⁵. Interestingly, GPR183 expression in macrophages has also been shown to regulate growth of *Mycobacterium tuberculosis* and is associated with higher disease severity^{296,297}, indicating that it may also have functions in regulating the immune response during infection. Similarly, in addition to suppressing migration of resting macrophages²⁹⁸, aquaporin-1 (AQP1) has been shown to attenuate macrophage-mediated inflammatory responses in LPS-induced acute kidney injury²⁹⁹. Intriguingly, *Aqp1*^{-/-} macrophages show increased arginase activity and a redistribution of CD206 into cellular extensions, indicating a shift towards an IL-4-induced, anti-inflammatory phenotype²⁹⁸. This may hint at a mechanism through which unstimulated *Nmes1*^{-/-} macrophages upregulate tissue remodelling-associated genes.

While *Aa467197* may play a role in macrophage migration during the early response to IL-4, after incubation with IL-4 for 24h, genes encoding a number of chemokines known to regulate monocyte chemotaxis were found to be more highly upregulated in wildtype mice compared to *Nmes1*^{-/-} mice, specifically CC chemokine ligands CCL7, CCL12, and CCL24. Interestingly, while CCL12 has been shown to be specific to monocytes³⁰⁰, CCL7 and CCL24 have also been shown to attract other cell types, with CCL7 also recruiting macrophages, neutrophils, and eosinophils³⁰¹⁻³⁰³, and CCL24 recruiting

basophils, eosinophils, and Th2 cells³⁸ in addition to monocytes. Similar to GPR183 and AQP1, all three chemokines have been shown to play roles in immune regulation in addition to their chemotactic properties. CCL7 has protective functions in West Nile virus and Leishmania infections^{302,304}, but is also elevated in *S. mansoni* pulmonary granulomas³⁰¹. CCL24 also plays a protective function in Leishmaniasis, contributing to the maintenance of anti-inflammatory macrophages in the dermis through recruitment of eosinophils³⁰⁵. In contrast, CCL12 has been characterised as an inflammatory marker, contributing to chronic inflammation in periodontitis by decreasing fibroblast migration and limiting collagen production³⁰⁶. Together, this suggests that one pathway through which *Aa467197* modulates the immune function of macrophages is by regulating chemokine secretion. In addition, the decrease in the proportion of CCR2-expressing LY6C^{int} cells in the colons of *S. mansoni*-infected *Nmes1^{-/-}* mice (Figure 18) indicates that *Aa467197* can also regulate chemokine sensing in monocytes. The CCR2 ligand CCL2, which is known to drive chemotaxis of myeloid and lymphoid cells, has also been shown to be expressed upon induction by Th2 cytokines and to promote macrophage accumulation in early *S. mansoni* granuloma formation³⁰⁷. Accordingly, the decreased expression of CCR2 is also a likely explanation for the observed decreased proportions of infiltrating Ly6C^{hi} cells into the colons of *Nmes1^{-/-}* mice during *S. mansoni* infection during the later, chronic stage of the infection (Figure 17), though the direct link between the two has yet to be established. While no differences in the percentage of F4/80⁺ macrophages could be detected at this stage of infection, their prevalence in the liver and colon should also be analysed at earlier time points during *S. mansoni* infection to assess whether macrophage migration kinetics are affected by genetic ablation of *Aa467197*. In addition, chemokine expression in the liver and colon and chemokine levels in the sera should be analysed to better characterise how *Aa467197* affects chemokine production.

Overall, these data suggest that *Aa467197* plays a role in modulating macrophage migration during the early response to IL-4, and later contributes to chemokine production and recruitment of immune cells like monocytes and neutrophils to sites of inflammation. In addition, these modulations most likely contribute to immune functions of macrophages during infection, alongside expression of other genes induced during microbial infection such as connexin-43 (*Cx43*, also known as *Gja1*³⁰⁸), the aryl hydrocarbon receptor (*Ahr*^{309,310}), or suppressor of cytokine signalling (*Socs*^{311,312}) proteins.

6.2.2 *Aa467197* may act as a regulator of blood vessel development and angiogenesis

In addition to monocyte chemotaxis, the RNAseq analysis indicated that *Aa467197* may contribute to tissue remodelling functions of macrophages by inducing expression of genes involved in blood vessel development and angiogenesis, which are essential to the wound healing process. As described in chapter 2.2.2.2, wound healing macrophages aid in angiogenesis primarily through induction of growth factors like VEGF, EGF, and PDGF^{61,62}, some of which were found to be less strongly upregulated in *Nmes1^{-/-}* BMDMs (*Hbegf*, *Pdgfc*). This was also the case for syndecan-4 (*Sdc4*), which contributes to wound repair and angiogenesis by enhancing PDGF-BB activity^{313,314}, *Ahr*, which has been shown to regulate vascular development, angiogenesis, and blood pressure^{315,316}, and endothelin receptor type B (*Ednrb*), which binds endothelin-1 (ET-1) and signalling through which is vital for blood pressure control and prevention of hypertension^{317,318}.

While macrophage-mediated angiogenesis and vascular remodelling are crucial to wound healing processes, they can also contribute to disease pathology. This has been best characterised in tumour development, in which secretion of angiogenic factors such as VEGF, basic fibroblast growth factor (bFGF), TGF- β , and TNF- α by tumour-associated macrophages contribute to tumour growth and vascularisation, as well as promoting metastasis by providing access to the vascular system^{282,319–321}. However, dysregulated vascular growth is also a hallmark of a number of inflammatory conditions, such as rheumatoid arthritis, hepatitis, obesity, and IBD^{321,322}. Crucially, liver fibrosis has been shown to require formation of new blood vessels and vascular remodelling^{323,324}, with anti-angiogenic therapies slowing liver fibrosis progression³²⁵. Accordingly, it is possible that the decrease in expression of *Timp1* and *Arg1*, which have been characterised as pro-fibrotic markers in *S. mansoni* infection, observed in colons of infected *Nmes1^{-/-}* mice (Figure 14) could be mediated by decreased expression of genes related to angiogenesis and vascular remodelling.

Overall, there are some indications that *Aa467197* may induce expression of genes that contribute to blood vessel development and angiogenesis, and that this may contribute to disease pathology in *S. mansoni* infection.

6.2.3 *Aa467197* expression may depend on macrophage cytoskeletal functions

Finally, the suppression of *Aa467197* expression in cells treated with IL-4 after application of cold or the actin polymerisation inhibitor CytD indicates that cytoskeletal function may contribute to expression of *Aa467197* (Figure 6).

Cytoskeletal rearrangement is crucial for a number of macrophage functions, including motility, phagocytosis, and antigen presentation³²⁶, and can even influence macrophage polarisation³²⁷. Actin stabiliser chondramide A has been suggested as a cancer therapeutic due to its cytotoxicity to tumour cells through activation of inflammatory pathways in macrophages³²⁸. Accordingly, impairment of cytoskeletal function through cold stress, which leads to microtubule and actin filament disruption³²⁹, has been shown to lead to a suppressive phenotype in macrophages, with lower phagocytic capacity, decreased TNF- α and IL-6, but increased IL-10 production^{330,331}. Similarly, while CytD has been best characterised for its ability to impair macrophage phagocytosis^{332,333}, it also inhibits production of TNF in macrophages after LPS treatment³³⁴. Therefore, it is likely that macrophage functions that involve cytoskeletal rearrangement also involve *Aa467197*.

One such function is phagocytosis, which was examined through co-culture of BMDMs with aTs. Phagocytosis of aT did not further increase expression of *Aa467197* in wildtype BMDMs, which indicates that uptake of apoptotic cells does not play a role in modulating *Aa467197* expression. However, additional studies in this group (unpublished data, PhD thesis) have shown that the identity of an apoptotic cell, defined by soluble mediators and contents released upon death, as well as shape, size, and ligand density^{327,335–339}, can differentially affect gene expression in macrophages and, in consequence, the function they perform after ingesting the apoptotic cell³⁴⁰. Accordingly, it is possible that the type of apoptotic cell may influence the expression of *Aa467197*.

In addition, the expression of *Aa467197* in BMDMs with genetic ablation of the phagocytic receptors *Axl* and *Mertk* was analysed. Given that AXL and MERTK are PtdSer receptors, and BMDM cultures have

been described to contain a small population of cells which express PtdSer due to apoptosis while in culture⁷³, differential expression of *Aa467197* was expected in this model even without addition of exogenous apoptotic cells. However, *Aa467197* mRNA levels were similar in both the *Ax^{fl/fl}Mertk^{fl/fl}-Csf1r-Cre⁺* and the *Ax^{fl/fl}Mertk^{fl/fl}-Csf1r-Cre⁻* mice, which suggests that engagement of AXL and MERTK does not play a role in inducing *Aa467197* expression. However, since *Aa467197* expression has previously been found to be downregulated in macrophages of mice lacking AXL and MERTK, but during *in vivo* infection with *N. braziliensis*⁷³, additional factors present in the *in vivo* system which cannot be replicated *in vitro* may also be involved. Therefore, additional experiments should be performed using *Ax^{fl/fl}Mertk^{fl/fl}-Csf1r-Cre^{+/-}* mice to better characterise the influence of these phagocytic receptors on *Aa467197* expression.

6.3 The role of *Aa467197* in models of chronic disease

6.3.1 Expression of *Aa467197* may affect microbiota composition, which leads to stronger colitis induction by DSS

For this project, the murine model of DSS-induced colitis was chosen to analyse colitis progression during both the acute stage and the recovery and wound healing stage of the disease. In addition, the DSS colitis model mirrors the clinical and histological symptoms of human UC^{248,341}, in which increased expression of NMES1 was observed in patients in remission (Figure 9). The similar expression pattern of *Aa467197* in the DSS colitis model increasing during acute colitis and during recovery from colitis (Figure 11) does indeed seem to confirm that this model would be suitable to mimic the human condition.

However, when the model was applied to co-housed wildtype and *Nmes1^{-/-}* mice, it was no longer possible to induce the disease phenotype, as evidenced by a lack of weight loss (Figure 12). This was particularly striking in the case of the wildtype mice, in which *Aa467197* should retain its original function, and which was shown to be expressed in the sorted macrophage and neutrophil populations. The most likely explanation for this phenotype applying to both mouse strains is that genetic ablation of *Aa467197* alters the composition of the intestinal microbiota, which was then adopted by the co-housed wildtype mice. This in turn conferred protection from DSS colitis. A similar phenomenon has been described for a number of other knockout mouse models. Co-housing of DSS-treated wildtype mice with healthy wildtype mice has been shown to induce faster recovery through normalisation of the microbiota composition, which was not the case when co-housed with *PTPN22^{-/-}* mice. Conversely, colitis recovery in *PTPN22^{-/-}* mice was not affected by co-housing with wildtype mice³⁴². On the other hand, *Casp3/11^{-/-}* mice have been shown to be protected from DSS colitis, but gain susceptibility to the disease when co-housed with wildtype mice, as evidenced by greater weight loss³⁴³. This indicates that, while microbiota of co-housed mice may normalise, it is unclear whether this will have a protective or disease-enhancing effect on the mice, and appears to be dependent on the genetic differences between the mice.

Unfortunately, since colitis was not properly induced in the mice, it was not possible to fully examine the impact of *Aa467197* on the disease phenotype. However, some differences could still be observed in the expression of *Arg1* and *Chil3* in sorted cell populations during administration of DSS. Neutrophils, CX3CR1⁺ macrophages, and CX3CR1⁻ macrophages were isolated and sorted at d10, considered

equivalent to the acute stage of colitis, and d14, during the recovery stage, and analysed for expression of tissue remodelling markers *Arg1* and *Chil3*.

As described in chapter 2.2.2.2, the function of *Chil3*/YM1 in macrophages and neutrophils has not yet been characterised in detail. Accordingly, it is interesting that decreased *Chil3* expression could be observed in *Nmes1^{-/-}* CX3CR1⁺ macrophages at d14 of DSS colitis, since this implies that these macrophages are less strongly polarised towards the tissue remodelling phenotype than the corresponding wildtype macrophages during the tissue remodelling stage of colitis. In addition, *Chil3* was the only macrophage tissue remodelling marker downregulated in *Nmes1^{-/-}* BMDMs after 24h of incubation with IL-4 (Figure 2). This indicates that *Aa467197* may play a role in regulating *Chil3*/YM1 expression in particular, and which may give some indications as to the function of *Chil3*/YM1 in tissue remodelling macrophages, which has not yet been addressed. Similarly, *Chil3* expression was increased in *Nmes1^{-/-}* neutrophils at d10 of DSS colitis, which indicates that it may play a role in regulating neutrophil function during acute colitis, though one that is distinct from its function in macrophages. Interestingly, there is evidence that YM1 plays a significant role in driving Th2-mediated responses during helminth infections. For instance, in the lungs of mice infected with *N. braziliensis*, YM1 has been shown to play different roles depending on the time point of the infection, driving the tissue repair response during early infection, but later acting to limit excessive immune activation³⁴⁴. In addition, production of YM1 and YM2 in response to IL-13 has been shown to promote Th2 cytokine production and allergic airway inflammation by inhibiting the production of 12-hydroxyeicosatetraenoic acid by 12/15(S)-lipoygenase³⁴⁵. Although no changes in YM1 expression could be observed in *S. mansoni* infection during this study (Figure 18, Figure 22), these may be pathways through which expression of *Chil3*/YM1 – and by extension *Aa467197* – mediates tissue remodelling responses in macrophages and neutrophils in other models as well.

In contrast to YM1, the function of ARG1 as a driver of ornithine production and as a marker of an anti-inflammatory phenotype in macrophages has been thoroughly established (see chapter 2.2.2.2). Interestingly, *Arg1* expression was elevated in *Nmes1^{-/-}* CX3CR1⁺ cells at d14, while *Chil3* was downregulated. This may indicate that, similarly to *Chil3*, *Aa467197* may regulate the expression of *Arg1* in macrophages, but with different activation kinetics. Furthermore, the exact role of ARG1 in macrophage tissue remodelling has not been fully established, and there is evidence that ARG1 may also contribute to pro-inflammatory mechanisms. For instance, ARG1 has been found to mediate LPS-induced retinal inflammation³⁴⁶, and inhibition of ARG1 activity was found to improve excisional wound healing in mice³⁴⁷.

While the lack of a disease phenotype in the above experiments means little can be concluded from the observed differences in expression here, more research is needed not only to examine the role of *Aa467197* in macrophages during colitis, but also to further establish the contributions of YM1 and ARG1 to disease progression and/or recovery.

6.3.2 Expression of *Aa467197* may affect egg retention in the colon as well as parasite maturation during *S. mansoni* infection

In parallel to the DSS colitis model, infection with *S. mansoni* was considered as an alternative *in vivo* model to investigate the role of *Aa467197* in disease. This model has several advantages in this investigation: it is known that intestinal damage is induced during infection, but not so much that it becomes difficult to isolate colon cells, as is an established problem for helminth infection models^{348–350}. In addition, high concentrations of Th2 cytokines are produced during chronic infection, which suits the intended aim of analysing the effect of *Aa467197* in IL-4-polarised macrophages. Much like with the DSS colitis model, the first step was to investigate whether *Aa467197* expression can be induced and to determine the best time point during the infection at which to study the effects of *Aa467197*. It was decided that 14 weeks post infection would be the most suitable time point, since this is where both the proportion of cells expressing *Aa467197* in the infected is increased, but also the amount of *Aa467197* in each cell, as evidenced by the MFI (Figure 13). Accordingly, subsequent infection experiments focussed on the 14 weeks p.i. time point.

Strikingly, egg counts in the colon (Figure 14), but not the liver (Figure 15), were found to be reduced in the *Nmes1^{-/-}* mice. There are several potential explanations for the decreased egg count in the colon: egg excretion may have been more efficient in mice with ablated *Aa467197*, adult *S. mansoni* females may have laid fewer eggs in the *Nmes1^{-/-}* mice, or the clearance of eggs trapped in the intestinal tissues may have been more efficient in the *Nmes1^{-/-}* mice. Other experiments in this study provide some evidence that *Aa467197* may play a role in supporting extravasation of *S. mansoni* eggs by inducing angiogenesis, which has been found to promote worm load and hepatic egg deposition²⁰⁹. In addition, GO term analysis of RNAseq data showed that angiogenesis-related genes were found to be more highly upregulated in IL-4-treated wildtype mice compared to *Nmes1^{-/-}* mice (Figure 7).

This study also found that expression of *Timp1* and *Arg1*, which have been characterised as markers of fibrosis in *S. mansoni* infection, was decreased in the intestine at week 14 of the infection. Fibrosis in schistosomiasis is largely a consequence of granuloma formation around the egg deposited in the affected tissue, with excessive granuloma formation leading to the eggs becoming trapped and the formation of fibrotic lesions (see chapter 2.4.2.3). Accordingly, it is possible that the reduced levels of fibrosis markers and the reduced egg counts in the colons of the *Nmes1^{-/-}* mice point to sufficiently reduced granuloma formation for eggs to be transported to the intestinal lumen quickly enough to avoid entrapment in the intestinal tissue. A further supporting factor is the decreased infiltration of monocytes and neutrophils observed in the colon (Figure 17), which has been shown to lead to reduced granuloma size in *S. mansoni* infection³⁵¹. While a complete lack of granuloma formation around *Schistosoma* eggs has been described to be detrimental to the host due to toxic secretions and an elevated pro-inflammatory immune response, as described for mice with macrophages and neutrophils lacking IL-4Ra, which cannot sense IL-4 or IL-13^{215,220,227,352} (see chapter 2.4.2.3), at this stage of the infection, the reduction in infiltrating cells is likely playing a protective role, leading to smaller granuloma formation around the eggs, and thus potentially enabling more efficient migration of the eggs through the intestinal wall.

It is also possible that the reduced number of eggs in the *Nmes1^{-/-}* colons was caused due to an altered response to the parasite during the early stages of infection, resulting in a lower worm burden in these mice. While early infection with *S. mansoni* is characterised by an inflammatory, Th1-mediated immune response, *S. mansoni* worms have been shown to prime CD4⁺ T cells and basophils to produce IL-4 in response to egg antigens well before the onset of egg deposition³⁵³ and activity of CD4⁺ T cells has been shown to be crucial for proper *S. mansoni* maturation³⁵⁴. Accordingly, it is possible that ablation of *Aa467197* may have impacted worm maturation through alteration of CD4⁺ T cell activity. However, since wildtype and *Nmes1^{-/-}* mice had similar egg counts in the liver, it is not likely that the reduction of eggs in the colon is caused by *Aa467197* affecting parasite fitness.

6.3.3 *Aa467197* expression exacerbates fibrosis in the intestine through upregulation of pro-fibrotic pathways and recruitment of monocytes to the colon during schistosomiasis

With egg counts decreased in the colons of *Nmes1^{-/-}* mice, fibrosis marker expression was examined in colon and liver tissue. In the colon expression of *Timp1* and *Arg1* was found to be significantly decreased, with a tendency towards decreased *Il-1 β* expression. As previously described, increased levels of ARG1 have been associated with liver fibrosis progression in schistosomiasis^{60,126}. TIMP1 levels have been shown to peak during the chronic stage of infection with *S. mansoni*^{217,218} and serve as a predictor of hepatic fibrosis in human *S. japonicum* infection³⁵⁵. While it is thought to contribute to fibrosis induction through inhibition of MMPs, which digest and degrade extracellular matrix components such as collagen, its role in fibrosis development is controversial, since other studies have found that fibrotic pathology of *S. mansoni*-infected TIMP1-deficient mice is no different to that of wildtype mice³⁵⁶. Nevertheless, this may indicate that modulation of ARG1 and TIMP1 levels may affect granuloma formation in the colon as well as the liver. Studies focussing on granuloma formation in the intestine during *S. mansoni* infection are rarer, but it is known that the cell composition of the granuloma differs between different organs, with intestinal granuloma containing a higher proportion of macrophages^{216,357}. Accordingly, it is likely that the observed differences in *Arg1* and *Timp1* expression in the colons of wildtype and *Nmes1^{-/-}* mice are mediated by macrophage-specific pathways under the control of *Aa467197*.

In addition, some of the pathways indicated by GO term analysis of the RNAseq data shed light on other processes, driven specifically by anti-inflammatory macrophages, that could contribute to fibrosis progression during *S. mansoni* infection. In particular, the role of *Aa467197* in promoting macrophage and monocyte recruitment as well as angiogenesis should be examined in more detail, and may be key pathways through which *Aa467197* contributes to the disease pathology. In addition, Wnt signalling through macrophage-derived Wnt ligands has also been implicated in accelerating mucosal tissue regeneration, but also exacerbating fibrosis in the intestine and lung³⁵⁸, and Wnt signalling in hepatocytes has been associated with increased fibrosis in *S. japonicum* infection³⁵⁹. Wnt signalling components, including *Fzd4*, which was less strongly upregulated in IL-4-treated *Nmes1^{-/-}* BMDMs, have also been shown to be increased in macrophages in several infection models, including *T. cruzi*, *Staphylococcus aureus*, and *M. tuberculosis*²³⁹.

Another method through which *Aa467197* may contribute to fibrosis development in the infected colon is by driving recruitment of LY6C^{hi} monocytes, which were significantly reduced in *Nmes1^{-/-}* mice, and potentially neutrophils, which were also reduced in *Nmes1^{-/-}* mice, but not to a significant degree (Figure 17). This is further supported by the observation that a lower proportion of LY6C^{int} monocytes expressed CCR2, a monocyte chemotaxis marker (Figure 18). In *S. mansoni* infection, infiltration of Ly6C⁺ monocytes into the liver has been described to play a protective role due to the subsequent differentiation of these monocytes into anti-inflammatory macrophages, which protect the host from the acute Th1 response during early infection³⁵¹. However, they have also been identified as a factor in fibrosis development^{360,361}. In addition, decreased infiltration of monocytes and neutrophils has been shown to lead to reduced granuloma size in *S. mansoni* infection³⁵¹, which may be playing a protective role here, leading to smaller granuloma around the eggs, and thus potentially enabling more efficient excretion, as discussed above in chapter 6.3.2. In addition, the reduction in infiltrating cells may act as an additional protective element, potentially counteracting pro-fibrotic effects caused by the increased levels of IL-13 in the sera (Figure 16). Together with the RNAseq analysis suggesting that *Aa467197* may play a role in regulating monocyte chemotaxis, it is likely that alterations in chemokine secretion and sensing play a role in this context, as discussed in chapter 6.2.1. Interestingly, although a previous study observed that mice lacking CCR2 had increased numbers of LY6G^{hi} neutrophils in the liver during *S. mansoni* infection³⁵¹, ablation of *Aa467197* did not lead to an increase in neutrophil infiltration into the colons of infected mice. This suggests that *Aa467197* regulates the chemotaxis of other cell types in addition to monocytes, in line with our finding that CCL7 and CCL24, which function as chemoattractants for other cell types (see chapter 6.2.1), are upregulated in wildtype mice compared to *Nmes1^{-/-}* mice at 24h post stimulation with IL.4 (Figure 7). Alternatively, the mechanism by which CCR2 expression suppresses neutrophil infiltration during *S. mansoni* infection could be specific to the liver, with other mechanisms playing a role in the colon.

Taken together, there are strong indications that *Aa467197* plays a role in colonic fibrosis development in *S. mansoni* infection through ARG1 and TIMP1-driven pathways and by inducing infiltration of monocytes into the colon of infected mice, but potentially also through regulation of other anti-inflammatory macrophage functions.

6.3.4 *Aa467197* may contribute to fibrosis development in the liver by blocking expression of ARG1 in macrophages

Curiously, unlike in the colon, egg counts in the liver were not reduced in *Nmes1^{-/-}* mice, and the expression of *Mmp13*, *Timp1*, *Arg1*, and *Il-1 β* was unchanged compared to the wildtype. This indicates that *Aa467197* may only play a minor role in fibrosis development in the liver. However, while ablation of *Aa467197* did not appear to change the tissue remodelling capacities of monocytes and macrophages in the colon, as evidenced by the similar expression of ARG1 and YM1 (Figure 18), there was a higher proportion of ARG1⁺ LY6C⁺ CD68⁻ liver monocytes in the *Nmes1^{-/-}* mice (Figure 22). As noted in chapter 2.4.2.3, anti-inflammatory macrophages, and their increased expression of ARG1 during the early Th2 response in particular, have been shown to play a protective role in chronic *S. mansoni* infection by suppressing fibrosis development^{229,230}. Accordingly, the observed increased expression of ARG1 in the *Nmes1^{-/-}* mice implies that *Aa467197* contributes to the pathology of *S. mansoni* in the liver. However,

this did not lead to reduced egg counts or ALT levels, which are considered markers for liver disease severity in schistosomiasis. It is possible, therefore, that the increased expression of ARG1 at this late stage of the infection does not contribute substantially to disease pathology.

Alternatively, the increased expression of ARG1 may be counteracting the potentially pro-fibrotic effects of the observed increased expression of IL-13 (Figure 16). Considering that IL-13 has been established to be the main driver of fibrosis development in *S. mansoni*²²⁰⁻²²², this seems to be at odds with the observed decrease in fibrosis marker expression in the colon and the lack of differences between the wildtype and *Nmes1^{-/-}* livers. However, bearing in mind the *in vitro* results of this study, which indicate that genetic ablation of *Aa467197* may lead to alteration of gene expression kinetics, and that Th2 cytokine-induced activation of macrophages is essential for host survival of acute schistosomiasis^{127,227}, it is possible that the increased IL-13 levels observed in *Nmes1^{-/-}* mice are indicative that the mice are still at an earlier stage of the disease, in which IL-13 is still playing a protective role in these mice, rather than a pro-fibrotic role. To investigate this, mice should be examined at earlier and later stages of the infection to assess the potential shift in disease progression. In addition, it is possible that IL-13 regulators may be increased in the *Nmes1^{-/-}* mice alongside IL-13 itself. A potential candidate for this is IL-13R α 2, which has been shown to mitigate fibrosis in *S. mansoni* infection through high-affinity binding to IL-13²²². In addition, reduced expression of IL-13R α 2 has been shown to increase IL-13 expression, but also expression of MMP13, which has antifibrotic functions in *S. mansoni* infection²⁵⁶. Accordingly, the role of IL-13 and its regulators should be examined more closely in future experiments.

Taken together, it appears that *Aa467197* contributes to the pathology of chronic *S. mansoni* infection in both the colon and the liver, but does so in different ways. It is possible that this difference between the liver and colon may be caused by different strategies to handle the *S. mansoni* eggs, which can be cleared from the colon, but not the liver. Accordingly, while ablation of *Aa467197* led to increased clearance of eggs from the colon, potentially through reduction of infiltrating cells, other elements were induced in the liver to protect the host from the trapped eggs. Accordingly, ablation of *Aa467197* led to increased production of ARG1 in liver macrophages, which have been shown to regulate fibrosis development.

6.3.5 *Aa467197* does not modulate neutrophil infiltration or function during infection with *S. mansoni*

Lastly, despite high basal expression of *Aa467197* in colon neutrophils (Figure 10) and expression in liver neutrophils at week 14 of infection with *S. mansoni* (Figure 20), ablation of *Aa467197* did not lead to altered expression of neutrophil activation markers in either organ during infection with *S. mansoni* (Figure 19, Figure 23). This indicates that *Aa467197* does not modulate neutrophil function at this particular time point. However, it cannot be ruled out that *Aa467197* does so at other time points during infection, in particular during the acute stage of the infection. It has also been described that proteins secreted by larval and adult *S. mansoni* parasites³⁶² as well as eggs³⁶³ inhibit neutrophil migration and function, which suggests that *S. mansoni* infection may not be the most suitable model with which to study the function of neutrophils in schistosomiasis. In contrast, neutrophils have been shown to be the main drivers of pathology in *S. japonicum* infection through induction of hepatic necrosis and liver

damage^{364,365}, and make up a significant portion of the granuloma²⁶³. This suggests that early infection with *S. japonicum* may be a suitable model to study the effect of *Aa467197* in neutrophils.

6.4 *NMES1* may contribute to recovery from UC by promoting accumulation and wound healing functions of macrophages

Finally, the increased expression of *NMES1* in human colon tissue in patients in remission from UC (Figure 9) indicates that this gene may contribute to the wound healing process in colitis. As noted previously, UC is characterised by a dysregulated Th2-like response, with increased levels of IL-5 and IL-13^{174,175}. In addition, macrophages in UC patients showed constitutive expression of the pro-inflammatory cytokine IL-12³⁶⁶. Resolving the inflammatory response is considered a crucial step in IBD remission, with induction of a proper wound healing response in macrophages considered essential in this process^{367,368}. The data accumulated throughout this study suggest that *NMES1* may contribute to induction of the wound healing response in macrophages in several ways, in particular by driving recruitment and differentiation of monocytes into anti-inflammatory macrophages, and promoting the induction of wound healing pathways such as angiogenesis. However, further studies in human samples or cell lines are needed to confirm this hypothesis.

7. Conclusion and future perspectives

The results of this thesis suggest that *Aa467197* can be considered a contributing factor to the establishment and performance of macrophage tissue remodelling functions. *Aa467197* has been shown to regulate macrophage polarisation in the early stage after sensing of IL-4, altering expression of genes associated with the macrophage tissue remodelling phenotype and functions. In addition, there is evidence that *Aa467197* contributes to the induction of crucial tissue remodelling functions, such as macrophage and monocyte migration as well as blood vessel formation and angiogenesis. In addition, although *Aa467197* expression does not appear to be modulated by macrophages' phagocytosis of apoptotic cells, other functions that require cytoskeletal remodelling might regulate *Aa467197* expression in macrophages. *Aa467197* has also been shown to contribute to the pathogenesis of DSS-induced colitis and *S. mansoni* infection. In DSS colitis, genetic ablation of *Aa467197* protected co-housed knockout and wildtype mice from colitis, indicating that *Aa467197* alters microbiota composition and this is the source of the protective effect. In *S. mansoni* infection, *Nmes1^{-/-}* mice showed reduced egg burdens and expression of *Timp1*, *Arg1*, and *IL-1 β* in the colon, as well as decreased infiltration of monocytes, indicating that these mice were protected from fibrosis and that the immune response to *S. mansoni* in the colon was altered in an *Aa467197*-dependent manner. In addition, *Aa467197* expression may alter the kinetics of disease progression and expression of ARG1 in the liver. Finally, despite *Aa467197* not affecting colitis progression in a murine model of the disease, expression of *NMES1*, the human homolog to *Aa467197*, was higher in patients in remission from UC compared to patients with acute UC. Together, these results show that *Aa467197* may play a role during the immune response to intestinal damage, and in particular that it may affect macrophage tissue remodelling functions in several ways.

However, there are still many open questions that need to be addressed. While *Aa467197* did not appear to affect macrophage metabolism *in vitro*, a recent study revealed that human NMES1 functions as a negative regulator of inflammatory responses by replacing the cytochrome c subunit NDUFA4 and by targeting *Ndufa4* mRNA through miR-147b²⁸⁵. Therefore, studies on cytochrome c oxidase function should be performed in *Nmes1^{-/-}* BMDMs to fully elucidate the role of *Aa467197* in macrophage mitochondrial function. In addition, the unbiased approach of analysing the transcriptional profile of wildtype BMDMs in comparison to *Nmes1^{-/-}* BMDMs revealed a number of pathways *Aa467197* may be involved in, most of which have yet to be explored. Accordingly, specific experimental approaches are needed to examine the role of *Aa467197* in monocyte and macrophage migration as well as angiogenesis. A number of *in vitro* methods with which to analyse cell migration have been described, such as transwell migration assays^{369,370} or cell migration through three-dimensional fibrin gel or Matrigel^{371,372}. Co-culture of macrophages with tumour spheroids has also been used to assess tissue infiltration³⁷³. In addition, secretion of cytokines and chemokines by wildtype and *Nmes1^{-/-}* macrophages could be compared to better assess their capacity to induce chemotaxis in other cells. For example, co-culture experiments of macrophages with other cell types, such as monocytes or neutrophils, could also give insight into the effect *Aa467197* may have on cell chemotaxis and help identify specific chemokine-chemokine receptor interactions which might be controlled by *Aa467197* expression in macrophages. *In vitro* studies of angiogenesis have generally focussed on studying proliferation, migration, and

differentiation of endothelial cells when incubated with angiogenic or anti-angiogenic agents^{374–376}. Accordingly, analysing endothelial cell functions and phenotypes during co-culture with *Nmes1^{-/-}* macrophages or macrophage components, such as extracellular vesicles³⁷⁷, could indicate whether pro or anti-angiogenic factors are affected by expression of *Aa467197*. Alternatively, live imaging approaches have been used to study macrophage phenotypes in wound angiogenesis³⁷⁸, and a similar approach could be considered using *Nmes1^{-/-}* macrophages.

The role of *Aa467197* in phagocytosis also has yet to be fully explored. While expression of *Aa467197* was unchanged in cells lacking AXL and MERTK after incubation with IL-4 alone, this may not be the case after co-culture with additional apoptotic cells. In addition, phagocytosis experiments should be performed with other types of apoptotic cells in addition to thymocytes, such as neutrophils, to gain a fuller picture of whether and how phagocytosis affects expression of *Aa467197 in vitro*. Measuring the expression of phagocytic receptors on *Nmes1^{-/-}* mice, and performing phagocytosis assays with *Nmes1^{-/-}* mice should also provide information on how *Aa467197* affects phagocytic functions of macrophages. The initial experiments performed to examine the role of phagocytosis on *Aa467197* expression also revealed that cytoskeletal remodelling-related functions may involve *Aa467197*. These include not only macrophage migration and phagocytosis, but also T cell activation. Accordingly, co-culture experiments with T cells and *Nmes1^{-/-}* macrophages should be performed to assess the capacity of macrophages lacking *Aa467197* to activate T cells.

The initial DSS colitis experiments performed in this thesis indicated that the expression of *Aa467197* may affect the intestinal microbiota composition of mice. To further investigate this, DSS colitis should be induced both in co-housed wildtype and *Nmes1^{-/-}* mice, but also in both strains separately. Analysis of the microbiome composition of these mice through 16s rRNA sequencing^{379,380} may also help pin down how the microbiome is affected by *Aa467197* expression and what implications this has for development of colitis. In addition, the DSS colitis protocol needs to be adjusted to account for the protective effect caused by the ablation of *Aa467197*, then repeated to properly investigate the effect of *Aa467197* on the phenotype and function of macrophages during colitis.

In the model of *S. mansoni* infection, the most striking observation was that egg counts and expression of fibrosis markers *Timp1* and *Arg1* were significantly decreased in the colons of *Nmes1^{-/-}* mice. This was most likely mediated by decreased infiltration of monocytes into the colon, and the subsequent reduced production of these factors in the colon, as well as more efficient excretion of *S. mansoni* eggs. An important next step would therefore be to investigate whether chemokine levels are reduced in the colons of infected *Nmes1^{-/-}* mice, and to investigate whether the decreased infiltration of LY6C^{hi} cells into the colon is directly linked to a decreased expression of CCR2 on these cells. In addition, the source of the increased IL-13 levels in the sera should be elucidated. Since mice with total genetic ablation of *Aa467197* were used in this thesis, it is possible that this may have led to altered cytokine expression by cell types other than macrophages, such as T cells. While this was accounted for, and no increased secretion of IL-13 could be measured in the supernatants of stimulated lymphocytes isolated from mesenteric lymph nodes of *S. mansoni*-infected mice in this case, other *Nmes1^{-/-}* cell populations should be examined for their capacity to produce cytokines, in particular IL-13. As mentioned previously, it is also possible that ablation of *Aa467197* altered the kinetics of disease progression caused by

S. mansoni, and with that the function of IL-13 in the *Nmes1*^{-/-} mice. Examination of other stages of the disease, such as the acute stage at 8 weeks or earlier, or a later stage of the chronic disease, should help characterise the effect of *Aa467197* on disease progression during *S. mansoni* infection.

While there was no change in the infiltration of neutrophils in this infection model, the high expression of *Aa467197* in neutrophils implies that it may also modulate their function. Accordingly, additional mouse models with specific ablations in macrophages, such as *Aa467197*^{fl/fl}-*Csf1r-Cre*^{+/-}, or neutrophils, such as *Aa467197*^{fl/fl}-*Ly6g-Cre*^{+/-} or *Aa467197*^{fl/fl}-*Mrp8-Cre*^{+/-}³⁸¹, may help dissect the function of *Aa467197* in these individual cells. In addition, since neutrophils are a more prominent feature of granuloma in infection with *S. japonicum*, rather than *S. mansoni*²⁶³, an alternative infection model should be used to study the effects of *Aa467197* in neutrophils.

Finally, as noted above, additional studies should be performed in human tissues to fully assess conditions in which *NMES1* is expressed and how it affects macrophage tissue remodelling. In particular, while there are indications that *NMES1* plays a role in recovery from colitis, additional patient samples are needed to strengthen the observations presented here. In addition, the expression of *NMES1* in human schistosomiasis has not yet been examined. However, acquiring colonic tissue samples from patients is an invasive procedure, and only a limited amount of tissue can be procured from each patient. Accordingly, finding a suitable *in vitro* model to study the effects of *NMES1* would be of great importance. Unfortunately, attempts to establish an *in vitro* model with which to further examine the role of *NMES1* in human macrophages were unsuccessful, as expression of *NMES1* could not be induced *in vitro* upon stimulation of PBMC-derived macrophages with IL-4 (Figure 24). Accordingly, a broader analysis of potential triggers of *NMES1* expression should be performed to investigate under which conditions *NMES1* is expressed in human cells. There are also a number of human monocyte cell lines, such as THP-1 or U937 cells³⁸²⁻³⁸⁴, which can be differentiated into macrophages and which have not yet been examined for their capacity to express *NMES1*. In addition, human organoid models could be used for more organ-specific examinations into the function of *NMES1*, and in particular in human macrophages. The advantage of this approach would be that organoid models more closely resemble their tissue of origin in 3D structure and cell composition, and are thus a more accurate representation of the *in vivo* situation than 2D cell culture. In this case, colon organoids could be of particular interest to study the effect of *NMES1*. In addition, it would be possible to induce selective ablation of *NMES1* in human macrophages using the CRISPR-Cas9 genome editing system^{385,386}, and then study their effect within the context of intestinal organoids.

In conclusion, it is clear that *Aa467197* plays a role in modulating macrophage tissue remodelling functions in response to inflammation, and that further studies into *Aa467197* may contribute to the base of knowledge needed to develop new approaches to treating chronic inflammatory diseases.

8. References

1. Takeuchi, O. & Akira, S. Pattern Recognition Receptors and Inflammation. *Cell* **140**, 805–820 (2010).
2. Medzhitov, R. Origin and physiological roles of inflammation. *Nature* **454**, 428–435 (2008).
3. Nathan, C. Neutrophils and immunity: Challenges and opportunities. *Nature Reviews Immunology* **6**, 173–182 (2006).
4. Geginat, J. *et al.* Plasticity of human CD4 T cell subsets. *Frontiers in Immunology* **5**, 630 (2014).
5. Chaplin, D. D. Overview of the immune response. *J. Allergy Clin. Immunol.* **125**, S3 (2010).
6. Ma, C. S. *et al.* Deficiency of Th17 cells in hyper IgE syndrome due to mutations in STAT3. *J. Exp. Med.* **205**, 1551–1557 (2008).
7. Tesmer, L. A., Lundy, S. K., Sarkar, S. & Fox, D. A. Th17 cells in human disease. *Immunological Reviews* **223**, 87–113 (2008).
8. Sallusto, F. & Lanzavecchia, A. Heterogeneity of CD4⁺ memory T cells: Functional modules for tailored immunity. *Eur. J. Immunol.* **39**, 2076–2082 (2009).
9. Mosser, D. M. & Edwards, J. P. Exploring the full spectrum of macrophage activation. *Nature Reviews Immunology* **8**, 958–969 (2008).
10. McCormick, S. M. & Heller, N. M. Commentary: IL-4 and IL-13 receptors and signaling. *Cytokine* **75**, 38–50 (2015).
11. Ponzoni, M., Pastorino, F., Di Paolo, D., Perri, P. & Brignole, C. Targeting macrophages as a potential therapeutic intervention: Impact on inflammatory diseases and cancer. *International Journal of Molecular Sciences* **19**, (2018).
12. Lumeng, C. N., Bodzin, J. L. & Saltiel, A. R. Obesity induces a phenotypic switch in adipose tissue macrophage polarization. *J. Clin. Invest.* **117**, 175–184 (2007).
13. Fricker, M. & Gibson, P. G. Macrophage dysfunction in the pathogenesis and treatment of asthma. *Eur. Respir. J.* **50**, 1700196 (2017).
14. Krenkel, O. & Tacke, F. Liver macrophages in tissue homeostasis and disease. *Nat. Rev. Immunol.* **17**, 306–321 (2017).
15. Murray, P. J. & Wynn, T. A. Protective and pathogenic functions of macrophage subsets. *Nat. Rev. Immunol.* **11**, 723–737 (2011).
16. Stanley, E. R. & Chitu, V. CSF-1 receptor signaling in myeloid cells. *Cold Spring Harbor Perspectives in Biology* **6**, (2014).
17. Dai, X. M. *et al.* Targeted disruption of the mouse colony-stimulating factor 1 receptor gene results in osteopetrosis, mononuclear phagocyte deficiency, increased primitive progenitor cell frequencies, and reproductive defects. *Blood* **99**, 111–120 (2002).
18. Pridans, C. *et al.* Pleiotropic Impacts of Macrophage and Microglial Deficiency on Development

- in Rats with Targeted Mutation of the *Csf1r* Locus . *J. Immunol.* **201**, 2683–2699 (2018).
19. Erlich, B., Zhu, L., Etgen, A. M., Dobrenis, K. & Pollard, J. W. Absence of colony stimulation factor-1 receptor results in loss of microglia, disrupted brain development and olfactory deficits. *PLoS One* **6**, (2011).
 20. Paolicelli, R. C. *et al.* Synaptic pruning by microglia is necessary for normal brain development. *Science (80-.)*. **333**, 1456–1458 (2011).
 21. Squarzoni, P. *et al.* Microglia Modulate Wiring of the Embryonic Forebrain. *Cell Rep.* **8**, 1271–1279 (2014).
 22. Zigmond, E. *et al.* Macrophage-restricted interleukin-10 receptor deficiency, but not IL-10 deficiency, causes severe spontaneous colitis. *Immunity* **40**, 720–733 (2014).
 23. A-Gonzalez, N. & Castrillo, A. Origin and specialization of splenic macrophages. *Cell. Immunol.* **330**, 151–158 (2018).
 24. Sheng, J., Ruedl, C. & Karjalainen, K. Most Tissue-Resident Macrophages Except Microglia Are Derived from Fetal Hematopoietic Stem Cells. *Immunity* **43**, 382–393 (2015).
 25. Hoeffel, G. *et al.* C-Myb⁺ Erythro-Myeloid Progenitor-Derived Fetal Monocytes Give Rise to Adult Tissue-Resident Macrophages. *Immunity* **42**, 665–678 (2015).
 26. Gomez Perdiguero, E. *et al.* Tissue-resident macrophages originate from yolk-sac-derived erythro-myeloid progenitors. *Nature* **518**, 547–551 (2015).
 27. Okabe, Y. & Medzhitov, R. Tissue-specific signals control reversible program of localization and functional polarization of macrophages. *Cell* **157**, 832–844 (2014).
 28. Lavin, Y. *et al.* Tissue-resident macrophage enhancer landscapes are shaped by the local microenvironment. *Cell* **159**, 1312–26 (2014).
 29. Kang, B. *et al.* Commensal microbiota drive the functional diversification of colon macrophages. *Mucosal Immunol.* **13**, 216–229 (2020).
 30. Shaw, T. N. *et al.* Tissue-resident macrophages in the intestine are long lived and defined by Tim-4 and CD4 expression. *J. Exp. Med.* **215**, 1507–1518 (2018).
 31. Bonnardel, J. *et al.* Stellate Cells, Hepatocytes, and Endothelial Cells Imprint the Kupffer Cell Identity on Monocytes Colonizing the Liver Macrophage Niche. *Immunity* **51**, 638-654.e9 (2019).
 32. Shi, C. & Pamer, E. G. Monocyte recruitment during infection and inflammation. *Nature Reviews Immunology* **11**, 762–774 (2011).
 33. Ingersoll, M. A., Platt, A. M., Potteaux, S. & Randolph, G. J. Monocyte trafficking in acute and chronic inflammation. *Trends in Immunology* **32**, 470–477 (2011).
 34. Tsou, C. L. *et al.* Critical roles for CCR2 and MCP-3 in monocyte mobilization from bone marrow and recruitment to inflammatory sites. *J. Clin. Invest.* **117**, 902–909 (2007).
 35. Auffray, C. *et al.* Monitoring of blood vessels and tissues by a population of monocytes with

- patrolling behavior. *Science* (80-.). **317**, 666–670 (2007).
36. Jablonski, K. A. *et al.* Novel markers to delineate murine M1 and M2 macrophages. *PLoS One* **10**, 5–11 (2015).
 37. Benoit, M., Desnues, B. & Mege, J.-L. Macrophage Polarization in Bacterial Infections. *J. Immunol.* **181**, 3733–3739 (2008).
 38. Mantovani, A. *et al.* The chemokine system in diverse forms of macrophage activation and polarization. *Trends Immunol.* **25**, 677–86 (2004).
 39. Yao, Y., Xu, X. H. & Jin, L. Macrophage polarization in physiological and pathological pregnancy. *Frontiers in Immunology* **10**, 792 (2019).
 40. Murray, P. J. *et al.* Macrophage Activation and Polarization: Nomenclature and Experimental Guidelines. *Immunity* **41**, 14–20 (2014).
 41. Martinez, F. O. & Gordon, S. The M1 and M2 paradigm of macrophage activation: time for reassessment. *F1000Prime Rep.* **6**, 13 (2014).
 42. Kawasaki, T. & Kawai, T. Toll-like receptor signaling pathways. *Frontiers in Immunology* **5**, 461 (2014).
 43. Shuai, K. *et al.* Polypeptide signalling to the nucleus through tyrosine phosphorylation of Jak and Stat proteins. *Nature* **366**, 580–583 (1993).
 44. Bode, J. G., Ehrling, C. & Häussinger, D. The macrophage response towards LPS and its control through the p38 MAPK-STAT3 axis. *Cellular Signalling* **24**, 1185–1194 (2012).
 45. Viola, A., Munari, F., Sánchez-Rodríguez, R., Sclaro, T. & Castegna, A. The metabolic signature of macrophage responses. *Frontiers in Immunology* **10**, (2019).
 46. Van den Bossche, J., Baardman, J. & de Winther, M. P. J. Metabolic Characterization of Polarized M1 and M2 Bone Marrow-derived Macrophages Using Real-time Extracellular Flux Analysis. *J. Vis. Exp.* (2015). doi:10.3791/53424
 47. Mills, C. D., Kincaid, K., Alt, J. M., Heilman, M. J. & Hill, A. M. M-1/M-2 Macrophages and the Th1/Th2 Paradigm. *J. Immunol.* **164**, 6166–6173 (2000).
 48. Tisoncik, J. R. *et al.* Into the Eye of the Cytokine Storm. *Microbiol. Mol. Biol. Rev.* **76**, 16–32 (2012).
 49. McGonagle, D., Sharif, K., O'Regan, A. & Bridgewood, C. The Role of Cytokines including Interleukin-6 in COVID-19 induced Pneumonia and Macrophage Activation Syndrome-Like Disease. *Autoimmunity Reviews* **19**, 102537 (2020).
 50. Stearns-Kurosawa, D. J., Osuchowski, M. F., Valentine, C., Kurosawa, S. & Remick, D. G. The pathogenesis of sepsis. *Annu. Rev. Pathol. Mech. Dis.* **6**, 19–48 (2011).
 51. Junttila, I. S. Tuning the cytokine responses: An update on interleukin (IL)-4 and IL-13 receptor complexes. *Front. Immunol.* **9**, (2018).

52. Luzina, I. G. *et al.* Regulation of inflammation by interleukin-4: a review of “alternatives”. *J. Leukoc. Biol.* **92**, 753–764 (2012).
53. Zheng, W. P. & Flavell, R. A. The transcription factor GATA-3 is necessary and sufficient for Th2 cytokine gene expression in CD4 T cells. *Cell* **89**, 587–596 (1997).
54. El-Arabey, A. A. *et al.* GATA3 as a master regulator for interactions of tumor-associated macrophages with high-grade serous ovarian carcinoma. *Cell. Signal.* **68**, 109539 (2020).
55. Bouhlef, M. A. *et al.* PPAR γ Activation Primes Human Monocytes into Alternative M2 Macrophages with Anti-inflammatory Properties. *Cell Metab.* **6**, 137–143 (2007).
56. Gordon, S. Alternative activation of macrophages. *Nat. Rev. Immunol.* **3**, 23–35 (2003).
57. Mantovani, A., Biswas, S. K., Galdiero, M. R., Sica, A. & Locati, M. Macrophage plasticity and polarization in tissue repair and remodelling. *J. Pathol.* **229**, 176–185 (2013).
58. Novak, M. L. & Koh, T. J. Macrophage phenotypes during tissue repair. *J. Leukoc. Biol.* **93**, 875–881 (2013).
59. Modolell, M., Corraliza, I. M., Link, F., Soler, G. & Eichmann, K. Reciprocal regulation of the nitric oxide synthase/arginase balance in mouse bone marrow-derived macrophages by TH 1 and TH 2 cytokines. *Eur. J. Immunol.* **25**, 1101–1104 (1995).
60. Hesse, M. *et al.* Differential Regulation of Nitric Oxide Synthase-2 and Arginase-1 by Type 1/Type 2 Cytokines In Vivo: Granulomatous Pathology Is Shaped by the Pattern of L-Arginine Metabolism. *J. Immunol.* **167**, 6533–6544 (2001).
61. Nucera, S., Bizziato, D. & De Palma, M. The interplay between macrophages and angiogenesis in development, tissue injury and regeneration. *Int. J. Dev. Biol.* **55**, 495–503 (2011).
62. Corliss, B. A., Azimi, M. S., Munson, J. M., Peirce, S. M. & Murfee, W. L. Macrophages: An Inflammatory Link Between Angiogenesis and Lymphangiogenesis. *Microcirculation* **23**, 95–121 (2016).
63. Mantovani, A., Locati, M., Vecchi, A., Sozzani, S. & Allavena, P. Decoy receptors: A strategy to regulate inflammatory cytokines and chemokines. *Trends in Immunology* **22**, 328–336 (2001).
64. Gratchev, A. *et al.* Alternatively activated macrophages differentially express fibronectin and its splice variants and the extracellular matrix protein β IG-H3. *Scand. J. Immunol.* **53**, 386–392 (2001).
65. Bae, J. S. *et al.* β ig-h3 supports keratinocyte adhesion, migration, and proliferation through α 3 β 1 integrin. *Biochem. Biophys. Res. Commun.* **294**, 940–948 (2002).
66. Kim, H. J. & Kim, I. S. Transforming growth factor- β -induced gene product, as a novel ligand of integrin α M β 2, promotes monocytes adhesion, migration and chemotaxis. *Int. J. Biochem. Cell Biol.* **40**, 991–1004 (2008).
67. LeBaron, R. G. *et al.* β IG-H3, a novel secretory protein inducible by transforming growth factor- β , is present in normal skin and promotes the adhesion and spreading of dermal fibroblasts in

- vitro. *J. Invest. Dermatol.* **104**, 844–849 (1995).
68. Fadok, V. A. *et al.* Exposure of phosphatidylserine on the surface of apoptotic lymphocytes triggers specific recognition and removal by macrophages. *J. Immunol.* **148**, 2207–16 (1992).
69. Nagata, S., Suzuki, J., Segawa, K. & Fujii, T. Exposure of phosphatidylserine on the cell surface. *Cell Death Differ.* **23**, 952–961 (2016).
70. Penberthy, K. K. & Ravichandran, K. S. Apoptotic cell recognition receptors and scavenger receptors. *Immunol. Rev.* **269**, 44–59 (2016).
71. Lai, C. & Lemke, G. An extended family of protein-tyrosine kinase genes differentially expressed in the vertebrate nervous system. *Neuron* **6**, 691–704 (1991).
72. Lemke, G. Phosphatidylserine Is the Signal for TAM Receptors and Their Ligands. *Trends in Biochemical Sciences* **42**, 738–748 (2017).
73. Bosurgi, L. *et al.* Macrophage function in tissue repair and remodeling requires IL-4 or IL-13 with apoptotic cells. *Science (80-.)*. **356**, 1072–1076 (2017).
74. Raes, G. *et al.* Differential expression of FIZZ1 and Ym1 in alternatively versus classically activated macrophages. *J. Leukoc. Biol.* **71**, 597–602 (2002).
75. Stütz, A. M. *et al.* The Th2 Cell Cytokines IL-4 and IL-13 Regulate Found in Inflammatory Zone 1/Resistin-Like Molecule α Gene Expression by a STAT6 and CCAAT/Enhancer-Binding Protein-Dependent Mechanism. *J. Immunol.* **170**, 1789–1796 (2003).
76. Nair, M. G. *et al.* Alternatively activated macrophage-derived RELM- α is a negative regulator of type 2 inflammation in the lung. *J. Exp. Med.* **206**, 937–952 (2009).
77. Pesce, J. T. *et al.* Retn1a (Relma/Fizz1) suppresses helminth-induced Th2- type immunity. *PLoS Pathog.* **5**, 1000393 (2009).
78. Osborne, L. C. *et al.* Resistin-like Molecule α Promotes Pathogenic Th17 Cell Responses and Bacterial-Induced Intestinal Inflammation. *J. Immunol.* **190**, 2292–2300 (2013).
79. Munitz, A. *et al.* Resistin-Like Molecule α Decreases Glucose Tolerance during Intestinal Inflammation. *J. Immunol.* **182**, 2357–2363 (2009).
80. Welch, J. S. *et al.* T H2 cytokines and allergic challenge induce Ym1 expression in macrophages by a STAT6-dependent mechanism. *J. Biol. Chem.* **277**, 42821–42829 (2002).
81. Harbord, M. *et al.* Ym1 is a neutrophil granule protein that crystallizes in p47phox-deficient mice. *J. Biol. Chem.* **277**, 5468–5475 (2002).
82. Chang, N. C. A. *et al.* A Macrophage Protein, Ym1, Transiently Expressed during Inflammation Is a Novel Mammalian Lectin. *J. Biol. Chem.* **276**, 17497–17506 (2001).
83. Röszer, T. Understanding the Mysterious M2 Macrophage through Activation Markers and Effector Mechanisms. *Mediators Inflamm.* **2015**, 1–16 (2015).
84. Sutherland, T. E. *et al.* Chitinase-like proteins promote IL-17-mediated neutrophilia in a tradeoff

- between nematode killing and host damage. *Nat. Immunol.* **15**, 1116–1125 (2014).
85. Gundra, U. M. *et al.* Alternatively activated macrophages derived from monocytes and tissue macrophages are phenotypically and functionally distinct. *Blood* **123**, e110-22 (2014).
86. Bult, C. J. *et al.* Mouse Genome Database (MGD) 2019. *Nucleic Acids Res.* **47**, D801–D806 (2019).
87. Bateman, A. *et al.* UniProt: The universal protein knowledgebase in 2021. *Nucleic Acids Res.* **49**, D480–D489 (2021).
88. Zhou, J. *et al.* A novel gene, NMES1, downregulated in human esophageal squamous cell carcinoma. *Int. J. Cancer* **101**, 311–316 (2002).
89. Uniprot website - Nmes1. *UniProt website* (2021). Available at: <https://www.uniprot.org/uniprot/Q810Q5>. (Accessed: 21st March 2021)
90. Yi, L. *et al.* MicroRNA-147b Promotes Proliferation and Invasion of Human Colorectal Cancer by Targeting RAS Oncogene Family (RAP2B). *Pathobiology* **86**, 173–181 (2019).
91. Cui, S., Yang, X., Zhang, L., Zhao, Y. & Yan, W. LncRNA MAFG-AS1 promotes the progression of colorectal cancer by sponging miR-147b and activation of NDUFA4. *Biochem. Biophys. Res. Commun.* **506**, 251–258 (2018).
92. Chatterjee, V. *et al.* MicroRNA-147b regulates vascular endothelial barrier function by targeting ADAM15 expression. *PLoS One* **9**, e110286 (2014).
93. Lee, C. G., McCarthy, S., Gruidl, M., Timme, C. & Yeatman, T. J. MicroRNA-147 Induces a Mesenchymal-To-Epithelial Transition (MET) and Reverses EGFR Inhibitor Resistance. *PLoS One* **9**, e84597 (2014).
94. Zhang, Y., Zhang, H. & Liu, Z. MicroRNA-147 suppresses proliferation, invasion and migration through the AKT/mTOR signaling pathway in breast cancer. *Oncol. Lett.* **11**, 405–410 (2016).
95. Sui, C. J. *et al.* MicroRNA-147 suppresses human hepatocellular carcinoma proliferation migration and chemosensitivity by inhibiting HOXC6. *Am. J. Cancer Res.* **6**, 2787–2798 (2016).
96. Zhang, E. *et al.* MicroRNA miR-147b promotes tumor growth via targeting UBE2N in hepatocellular carcinoma. *Oncotarget* **8**, 114072 (2017).
97. El-Guendy, N. M. *et al.* The Liver MicroRNA Expression Profiles Associated With Chronic Hepatitis C Virus (HCV) Genotype-4 Infection: A Preliminary Study. *Hepat. Mon.* **16**, (2016).
98. Zhang, W. C. *et al.* miR-147b-mediated TCA cycle dysfunction and pseudohypoxia initiate drug tolerance to EGFR inhibitors in lung adenocarcinoma. *Nat. Metab.* **1**, 460–474 (2019).
99. Liu, G. *et al.* miR-147, a microRNA that is induced upon Toll-like receptor stimulation, regulates murine macrophage inflammatory responses. *Proc. Natl. Acad. Sci.* **106**, 15819–15824 (2009).
100. Lin, J. Da *et al.* Single-cell analysis of fate-mapped macrophages reveals heterogeneity, including stem-like properties, during atherosclerosis progression and regression. *JCI insight* **4**, (2019).

101. Zhang, L. *et al.* Chemokine CXCL16 regulates neutrophil and macrophage infiltration into injured muscle, promoting muscle regeneration. *Am. J. Pathol.* **175**, 2518–2527 (2009).
102. Kim, M. J. *et al.* CXCL16 positively correlated with M2-macrophage infiltration, enhanced angiogenesis, and poor prognosis in thyroid cancer. *Sci. Rep.* **9**, 1–10 (2019).
103. Das, A. *et al.* Endothelial Antioxidant-1: A Key Mediator of Copper-dependent Wound Healing in vivo. *Sci. Rep.* **6**, 1–16 (2016).
104. Chen, G. F. *et al.* Copper Transport Protein Antioxidant-1 Promotes Inflammatory Neovascularization via Chaperone and Transcription Factor Function. *Sci. Rep.* **5**, (2015).
105. Kim, D. W. *et al.* Tat-ATOX1 inhibits inflammatory responses via regulation of MAPK and NF- κ B pathways. *BMB Rep.* **51**, 654–659 (2018).
106. Jia, W., Kidoya, H., Yamakawa, D., Naito, H. & Takakura, N. Galectin-3 accelerates M2 macrophage infiltration and angiogenesis in tumors. *Am. J. Pathol.* **182**, 1821–1831 (2013).
107. Di Gregoli, K. *et al.* Galectin-3 Identifies a Subset of Macrophages with a Potential Beneficial Role in Atherosclerosis. *Arterioscler. Thromb. Vasc. Biol.* **40**, 1491–1509 (2020).
108. Cassaglia, P. *et al.* Genetic Deletion of Galectin-3 Alters the Temporal Evolution of Macrophage Infiltration and Healing Affecting the Cardiac Remodeling and Function after Myocardial Infarction in Mice. *Am. J. Pathol.* **190**, 1789–1800 (2020).
109. Jin, C., Henao-Mejia, J. & Flavell, R. A. Innate immune receptors: Key regulators of metabolic disease progression. *Cell Metabolism* **17**, 873–882 (2013).
110. Ferrucci, L. & Fabbri, E. Inflammageing: chronic inflammation in ageing, cardiovascular disease, and frailty. *Nature Reviews Cardiology* **15**, 505–522 (2018).
111. Heneka, M. T., Kummer, M. P. & Latz, E. Innate immune activation in neurodegenerative disease. *Nature Reviews Immunology* **14**, 463–477 (2014).
112. Funes, S. C., Rios, M., Escobar-Vera, J. & Kalergis, A. M. Implications of macrophage polarization in autoimmunity. *Immunology* **154**, 186–195 (2018).
113. Miller, A. H. & Raison, C. L. The role of inflammation in depression: From evolutionary imperative to modern treatment target. *Nature Reviews Immunology* **16**, 22–34 (2016).
114. Brundin, L., Bryleva, E. Y. & Thirtamara Rajamani, K. Role of Inflammation in Suicide: From Mechanisms to Treatment. *Neuropsychopharmacology* **42**, 271–283 (2017).
115. Furman, D. *et al.* Chronic inflammation in the etiology of disease across the life span. *Nat. Med.* **25**, 1822–1832 (2019).
116. Roth, G. A. *et al.* Global, regional, and national age-sex-specific mortality for 282 causes of death in 195 countries and territories, 1980–2017: a systematic analysis for the Global Burden of Disease Study 2017. *Lancet* **392**, 1736–1788 (2018).
117. Lumeng, C. N. & Saltiel, A. R. Inflammatory links between obesity and metabolic disease. *Journal of Clinical Investigation* **121**, 2111–2117 (2011).

118. Gregor, M. F. & Hotamisligil, G. S. Inflammatory Mechanisms in Obesity. *Annu. Rev. Immunol.* **29**, 415–445 (2011).
119. Kamdar, K. *et al.* Genetic and Metabolic Signals during Acute Enteric Bacterial Infection Alter the Microbiota and Drive Progression to Chronic Inflammatory Disease. *Cell Host Microbe* **19**, 21–31 (2016).
120. Lok, A. S. F. Chronic Hepatitis B. *N. Engl. J. Med.* **346**, 1682–1683 (2002).
121. Seeff, L. B. Natural history of chronic hepatitis C. *Hepatology* **36**, s35–s46 (2002).
122. Deeks, S. G., Lewin, S. R. & Havlir, D. V. The end of AIDS: HIV infection as a chronic disease. *The Lancet* **382**, 1525–1533 (2013).
123. Pérez-Molina, J. A. & Molina, I. Chagas disease. *Lancet* **391**, 82–94 (2018).
124. Martin, D. & Tarleton, R. Generation, specificity, and function of CD8+ T cells in *Trypanosoma cruzi* infection. *Immunological Reviews* **201**, 304–317 (2004).
125. Anuradha, R. *et al.* Parasite Antigen-Specific Regulation of Th1, Th2, and Th17 Responses in *Strongyloides stercoralis* Infection. *J. Immunol.* **195**, 2241–2250 (2015).
126. Pearce, E. J. & MacDonald, A. S. The immunobiology of schistosomiasis. *Nature Reviews Immunology* **2**, 499–511 (2002).
127. Brunet, L. R., Finkelman, F. D., Cheever, A. W., Kopf, M. A. & Pearce, E. J. IL-4 protects against TNF-alpha-mediated cachexia and death during acute schistosomiasis. *J. Immunol.* **159**, (1997).
128. Cheever, A. W., Hoffmann, K. F. & Wynn, T. A. Immunopathology of schistosomiasis mansoni in mice and men. *Immunology Today* **21**, 465–466 (2000).
129. CDC. CDC | Inflammatory bowel disease. Available at: <https://www.cdc.gov/ibd/what-is-IBD.htm>. (Accessed: 28th March 2021)
130. Kaser, A., Zeissig, S. & Blumberg, R. S. Inflammatory bowel disease. *Annual Review of Immunology* **28**, 573–621 (2010).
131. Cordain, L. *et al.* Origins and evolution of the Western diet: health implications for the 21st century. *Am. J. Clin. Nutr.* **82**, 483 (2005).
132. Franzosa, E. A. *et al.* Gut microbiome structure and metabolic activity in inflammatory bowel disease. *Nat. Microbiol.* **4**, 293–305 (2019).
133. Zuo, T. & Ng, S. C. The Gut Microbiota in the Pathogenesis and Therapeutics of Inflammatory Bowel Disease. *Front. Microbiol.* **9**, 2247 (2018).
134. Axelrad, J. E., Lichtiger, S. & Yajnik, V. Inflammatory bowel disease and cancer: The role of inflammation, immunosuppression, and cancer treatment. *World Journal of Gastroenterology* **22**, 4794–4801 (2016).
135. Uko, V., Thangada, S. & Radhakrishnan, K. Liver disorders in inflammatory bowel disease. *Gastroenterology Research and Practice* **2012**, (2012).

136. Halling, M. L., Kjeldsen, J., Knudsen, T., Nielsen, J. & Hansen, L. K. Patients with inflammatory bowel disease have increased risk of autoimmune and inflammatory diseases. *World J. Gastroenterol.* **23**, 6137–6146 (2017).
137. Restellini, S., Chazouillères, O. & Frossard, J. L. Hepatic manifestations of inflammatory bowel diseases. *Liver International* **37**, 475–489 (2017).
138. Wilson, J. C., Furlano, R. I., Jick, S. S. & Meier, C. R. Inflammatory Bowel Disease and the Risk of Autoimmune Diseases. *J. Crohn's Colitis* **10**, 186–193 (2016).
139. Langer-Gould, A., Albers, K. B., Van Den Eeden, S. K. & Nelson, L. M. Autoimmune diseases prior to the diagnosis of multiple sclerosis: A population-based case-control study. *Mult. Scler.* **16**, 855–861 (2010).
140. Bernstein, C. N., Wajda, A. & Blanchard, J. F. The clustering of other chronic inflammatory diseases in inflammatory bowel disease: A population-based study. *Gastroenterology* **129**, 827–836 (2005).
141. Zéphir, H. *et al.* Milder multiple sclerosis course in patients with concomitant inflammatory bowel disease. *Mult. Scler. J.* **20**, 1135–1139 (2014).
142. Alatab, S. *et al.* The global, regional, and national burden of inflammatory bowel disease in 195 countries and territories, 1990–2017: a systematic analysis for the Global Burden of Disease Study 2017. *Lancet Gastroenterol. Hepatol.* **5**, 17–30 (2020).
143. Kawalec, P. Indirect costs of inflammatory bowel diseases: Crohn's disease and ulcerative colitis. A systematic review. *Arch. Med. Sci.* **12**, 295–302 (2016).
144. Park, K. T. *et al.* The Cost of Inflammatory Bowel Disease: An Initiative from the Crohn's & Colitis Foundation. *Inflamm. Bowel Dis.* **26**, 1–10 (2020).
145. Rogler, G. *et al.* Role of biological therapy for inflammatory bowel disease in developing countries. *Gut* **61**, 706–712 (2012).
146. Magro, F. *et al.* European consensus on the histopathology of inflammatory bowel disease. *J. Crohn's Colitis* **7**, 827–851 (2013).
147. Hendrickson, B. A., Gokhale, R. & Cho, J. H. Clinical aspects and pathophysiology of inflammatory bowel disease. *Clinical Microbiology Reviews* **15**, 79–94 (2002).
148. Xavier, R. J. & Podolsky, D. K. Unravelling the pathogenesis of inflammatory bowel disease. *Nature* **448**, 427–434 (2007).
149. Hugot, J. P. *et al.* Association of NOD2 leucine-rich repeat variants with susceptibility to Crohn's disease. *Nature* **411**, 599–603 (2001).
150. Ogura, Y. *et al.* A frameshift mutation in NOD2 associated with susceptibility to Crohn's disease. *Nature* **411**, 603–606 (2001).
151. Ogura, Y. *et al.* Nod2, a Nod1/Apaf-1 Family Member That Is Restricted to Monocytes and Activates NF- κ B. *J. Biol. Chem.* **276**, 4812–4818 (2001).

152. Girardin, S. E. *et al.* Nod2 is a general sensor of peptidoglycan through muramyl dipeptide (MDP) detection. *J. Biol. Chem.* **278**, 8869–8872 (2003).
153. Eckmann, L. & Karin, M. NOD2 and Crohn's disease: Loss or gain of function? *Immunity* **22**, 661–667 (2005).
154. Lu, Y., Li, X., Liu, S., Zhang, Y. & Zhang, D. Toll-like receptors and inflammatory bowel disease. *Frontiers in Immunology* **9**, 72 (2018).
155. Fukata, M. & Abreu, M. T. Role of Toll-like receptors in gastrointestinal malignancies. *Oncogene* **27**, 234–243 (2008).
156. Toiyama, Y. *et al.* The expression patterns of toll-like receptors in the ileal pouch mucosa of postoperative ulcerative colitis patients. *Surg. Today* **36**, 287–290 (2006).
157. Brand, S. *et al.* The Role of Toll-like Receptor 4 Asp299Gly and Thr399Ile Polymorphisms and CARD15/NOD2 Mutations in the Susceptibility and Phenotype of Crohn's Disease. *Inflamm. Bowel Dis.* **11**, 645–652 (2005).
158. Franchimont, D. *et al.* Deficient host-bacteria interactions in inflammatory bowel disease? the toll-like receptor (TLR)-4 Asp299gly polymorphism is associated with Crohn's disease and ulcerative colitis. *Gut* **53**, 987–992 (2004).
159. Hoshi, N. *et al.* MyD88 signalling in colonic mononuclear phagocytes drives colitis in IL-10-deficient mice. *Nat. Commun.* **3**, 1–10 (2012).
160. Arumugam, M. *et al.* Enterotypes of the human gut microbiome. *Nature* **473**, 174–180 (2011).
161. Peterson, D. A., Frank, D. N., Pace, N. R. & Gordon, J. I. Metagenomic Approaches for Defining the Pathogenesis of Inflammatory Bowel Diseases. *Cell Host and Microbe* **3**, 417–427 (2008).
162. Manichanh, C., Borruel, N., Casellas, F. & Guarner, F. The gut microbiota in IBD. *Nature Reviews Gastroenterology and Hepatology* **9**, 599–608 (2012).
163. Nishida, A. *et al.* Gut microbiota in the pathogenesis of inflammatory bowel disease. *Clinical Journal of Gastroenterology* **11**, 1–10 (2018).
164. Kim, M. *et al.* Critical Role for the Microbiota in CX3CR1 + Intestinal Mononuclear Phagocyte Regulation of Intestinal T Cell Responses. *Immunity* **49**, 151-163.e5 (2018).
165. Buisine, M. P. *et al.* Abnormalities in mucin gene expression in Crohn's disease. *Inflamm. Bowel Dis.* **5**, 24–32 (1999).
166. Larsson, J. M. H. *et al.* Altered O-glycosylation profile of MUC2 mucin occurs in active ulcerative colitis and is associated with increased inflammation. *Inflamm. Bowel Dis.* **17**, 2299–2307 (2011).
167. Salim, S. Y. & Söderholm, J. D. Importance of disrupted intestinal barrier in inflammatory bowel diseases. *Inflammatory Bowel Diseases* **17**, 362–381 (2011).
168. Neurath, M. F. Cytokines in inflammatory bowel disease. *Nat. Rev. Immunol.* **14**, 329–342 (2014).

169. Sadlack, B. *et al.* Ulcerative colitis-like disease in mice with a disrupted interleukin-2 gene. *Cell* **75**, 253–261 (1993).
170. Kühn, R., Löhler, J., Rennick, D., Rajewsky, K. & Müller, W. Interleukin-10-deficient mice develop chronic enterocolitis. *Cell* **75**, 263–274 (1993).
171. Olsen, T. *et al.* TH1 and TH17 interactions in untreated inflamed mucosa of inflammatory bowel disease, and their potential to mediate the inflammation. *Cytokine* **56**, 633–640 (2011).
172. Yen, D. *et al.* IL-23 is essential for T cell-mediated colitis and promotes inflammation via IL-17 and IL-6. *J. Clin. Invest.* **116**, 1310–1316 (2006).
173. van Dullemen, H. M. *et al.* Treatment of Crohn's disease with anti-tumor necrosis factor chimeric monoclonal antibody (cA2). *Gastroenterology* **109**, 129–135 (1995).
174. Fuss, I. J. *et al.* Disparate CD4⁺ lamina propria (LP) lymphokine secretion profiles in inflammatory bowel disease. Crohn's disease LP cells manifest increased secretion of IFN- γ , whereas ulcerative colitis LP cells manifest increased secretion of IL-5. *J. Immunol.* **157**, (1996).
175. Heller, F. *et al.* Interleukin-13 Is the Key Effector Th2 Cytokine in Ulcerative Colitis That Affects Epithelial Tight Junctions, Apoptosis, and Cell Restitution. *Gastroenterology* **129**, 550–564 (2005).
176. Smythies, L. E. *et al.* Human intestinal macrophages display profound inflammatory anergy despite avid phagocytic and bacteriocidal activity. *J. Clin. Invest.* **115**, 66–75 (2005).
177. Ogino, T. *et al.* Increased Th17-inducing activity of CD14⁺ CD163^{low} myeloid cells in intestinal lamina propria of patients with Crohn's disease. *Gastroenterology* **145**, (2013).
178. Singh, U. P. *et al.* Chemokine and cytokine levels in inflammatory bowel disease patients. *Cytokine* **77**, 44–49 (2016).
179. Matsushima, K., Larsen, C. G., DuBois, G. C. & Oppenheim, J. J. Purification and characterization of a novel monocyte chemotactic and activating factor produced by a human myelomonocytic cell line. *J. Exp. Med.* **169**, 1485–1490 (1989).
180. Reinecker, H. C. *et al.* Monocyte-chemoattractant protein 1 gene expression in intestinal epithelial cells and inflammatory bowel disease mucosa. *Gastroenterology* **108**, 40–50 (1995).
181. Khan, W. I. *et al.* Critical role of MCP-1 in the pathogenesis of experimental colitis in the context of immune and enterochromaffin cells. *Am. J. Physiol. - Gastrointest. Liver Physiol.* **291**, (2006).
182. Popivanova, B. K. *et al.* Blockade of a chemokine, CCL2, reduces chronic colitis-associated carcinogenesis in mice. *Cancer Res.* **69**, 7884–7892 (2009).
183. Watanabe, N. *et al.* Elimination of local macrophages in intestine prevents chronic colitis in interleukin-10-deficient mice. *Dig. Dis. Sci.* **48**, 408–414 (2003).
184. Kamada, N. *et al.* Abnormally Differentiated Subsets of Intestinal Macrophage Play a Key Role in Th1-Dominant Chronic Colitis through Excess Production of IL-12 and IL-23 in Response to

- Bacteria. *J. Immunol.* **175**, 6900–6908 (2005).
185. Takeda, K. *et al.* Enhanced Th1 activity and development of chronic enterocolitis in mice devoid of stat3 in macrophages and neutrophils. *Immunity* **10**, 39–49 (1999).
186. Rugtveit, J. *et al.* Respiratory burst of intestinal macrophages in inflammatory bowel disease is mainly caused by CD14+L1+ monocyte derived cells. *Gut* **37**, 367–373 (1995).
187. Rugtveit, J. *et al.* Cytokine profiles differ in newly recruited and resident subsets of mucosal macrophages from inflammatory bowel disease. *Gastroenterology* **112**, 1493–1505 (1997).
188. Kamada, N. *et al.* Unique CD14+ intestinal macrophages contribute to the pathogenesis of Crohn disease via IL-23/IFN- γ axis. *J. Clin. Invest.* **118**, 2269–2280 (2008).
189. Lissner, D. *et al.* Monocyte and M1 Macrophage-induced Barrier Defect Contributes to Chronic Intestinal Inflammation in IBD. *Inflamm. Bowel Dis.* **21**, 1297 (2015).
190. Jones, G. R. *et al.* Dynamics of colon monocyte and macrophage activation during colitis. *Front. Immunol.* **9**, (2018).
191. Cummings, R. J. *et al.* Different tissue phagocytes sample apoptotic cells to direct distinct homeostasis programs. *Nature* **539**, 565–569 (2016).
192. Bosurgi, L. *et al.* Paradoxical role of the proto-oncogene Axl and Mer receptor tyrosine kinases in colon cancer. *Proc. Natl. Acad. Sci. U. S. A.* **110**, 13091–13096 (2013).
193. WHO - Schistosomiasis. Available at: https://www.who.int/health-topics/schistosomiasis#tab=tab_1. (Accessed: 31st March 2021)
194. CDC - Schistosomiasis. Available at: <https://www.cdc.gov/parasites/schistosomiasis/index.html>. (Accessed: 31st March 2021)
195. WHO | Schistosomiasis interactive case map. Available at: https://apps.who.int/neglected_diseases/ntddata/sch/sch.html. (Accessed: 31st March 2021)
196. King, C. H., Dickman, K. & Tisch, D. J. Reassessment of the cost of chronic helminthic infection: A meta-analysis of disability-related outcomes in endemic schistosomiasis. *Lancet* **365**, 1561–1569 (2005).
197. Corbett, E. L., Butterworth, A. E., Fulford, A. J. C., Ouma, J. H. & Sturrock, R. F. Nutritional status of children with schistosomiasis mansoni in two different areas of Machakos district, Kenya. *Trans. R. Soc. Trop. Med. Hyg.* **86**, 266–273 (1992).
198. Adenowo, A. F., Oyinloye, B. E., Ogunyinka, B. I. & Kappo, A. P. Impact of human schistosomiasis in sub-Saharan Africa. *Brazilian Journal of Infectious Diseases* **19**, 196–205 (2015).
199. Vale, N. *et al.* Praziquantel for schistosomiasis: Single-drug metabolism revisited, mode of action, and resistance. *Antimicrobial Agents and Chemotherapy* **61**, (2017).
200. Nelwan, M. L. Schistosomiasis: Life Cycle, Diagnosis, and Control. *Curr. Ther. Res.* **91**, 5–9 (2019).

201. Braun, L., Grimes, J. E. T. & Templeton, M. R. The effectiveness of water treatment processes against schistosome cercariae: A systematic review. *PLoS Negl. Trop. Dis.* **12**, e0006364 (2018).
202. Cheever, A. W., Macedonia, J. G., Mosimann, J. E. & Cheever, E. A. Kinetics of egg production and egg excretion by *Schistosoma mansoni* and *S. japonicum* in mice infected with a single pair of worms. *Am. J. Trop. Med. Hyg.* **50**, 281–295 (1994).
203. Schramm, G. *et al.* Molecular characterization of an interleukin-4-inducing factor from *Schistosoma mansoni* eggs. *J. Biol. Chem.* **278**, 18384–18392 (2003).
204. Schramm, G. *et al.* Cutting Edge: IPSE/alpha-1, a Glycoprotein from *Schistosoma mansoni* Eggs, Induces IgE-Dependent, Antigen-Independent IL-4 Production by Murine Basophils In Vivo. *J. Immunol.* **178**, 6023–6027 (2007).
205. Jauréguiberry, S., Paris, L. & Caumes, E. Acute schistosomiasis, a diagnostic and therapeutic challenge. *Clinical Microbiology and Infection* **16**, 225–231 (2010).
206. De Jesus, A. R. *et al.* Clinical and immunologic evaluation of 31 patients with acute schistosomiasis mansoni. *J. Infect. Dis.* **185**, 98–105 (2002).
207. Knuhr, K. *et al.* *Schistosoma mansoni* egg-released IPSE/alpha-1 dampens inflammatory cytokine responses via basophil interleukin (IL)-4 and IL-13. *Front. Immunol.* **9**, (2018).
208. Barron, L. & Wynn, T. A. Macrophage activation governs schistosomiasis-induced inflammation and fibrosis. *European Journal of Immunology* **41**, 2509–2514 (2011).
209. Costain, A. H., MacDonald, A. S. & Smits, H. H. Schistosome Egg Migration: Mechanisms, Pathogenesis and Host Immune Responses. *Frontiers in Immunology* **9**, 3042 (2018).
210. Schwartz, C. & Fallon, P. G. *Schistosoma* “Eggs-iting” the host: Granuloma formation and egg excretion. *Frontiers in Immunology* **9**, 2492 (2018).
211. Nation, C. S., Da’dara, A. A., Marchant, J. K. & Skelly, P. J. Schistosome migration in the definitive host. *PLoS Negl. Trop. Dis.* **14**, e0007951 (2020).
212. Burke, M. L. *et al.* Immunopathogenesis of human schistosomiasis. *Parasite Immunology* **31**, 163–176 (2009).
213. Friedman, S. L. Hepatic stellate cells: Protean, multifunctional, and enigmatic cells of the liver. *Physiological Reviews* **88**, 125–172 (2008).
214. An, P. *et al.* Hepatocyte mitochondria-derived danger signals directly activate hepatic stellate cells and drive progression of liver fibrosis. *Nat. Commun.* **11**, 1–15 (2020).
215. Hams, E., Aviello, G. & Fallon, P. G. The *Schistosoma* Granuloma: Friend or Foe? *Front. Immunol.* **4**, 89 (2013).
216. Weinstock, J. V & Boros, D. L. Organ-dependent differences in composition and function observed in hepatic and intestinal granulomas isolated from mice with *Schistosomiasis mansoni*. *J. Immunol.* **130**, 418 LP – 422 (1983).
217. Singh, K. P., Gerard, H. C., Hudson, A. P. & Boros, D. L. Dynamics of collagen, MMP and TIMP

- gene expression during the granulomatous, fibrotic process induced by *Schistosoma mansoni* eggs. *Ann. Trop. Med. Parasitol.* **98**, 581–593 (2004).
218. Singh, K. P., Gerard, H. C., Hudson, A. P. & Boros, D. L. Differential expression of collagen, MMP, TIMP and fibrogenic-cytokine genes in the granulomatous colon of *Schistosoma mansoni*-infected mice. *Ann. Trop. Med. Parasitol.* **100**, 611–620 (2006).
219. Kumar, R. *et al.* Th2 CD4⁺ T Cells Are Necessary and Sufficient for *Schistosoma*- Pulmonary Hypertension. *J. Am. Heart Assoc.* **8**, (2019).
220. Fallon, P. G., Richardson, E. J., McKenzie, G. J. & McKenzie, A. N. J. Schistosome Infection of Transgenic Mice Defines Distinct and Contrasting Pathogenic Roles for IL-4 and IL-13: IL-13 Is a Profibrotic Agent. *J. Immunol.* **164**, 2585–2591 (2000).
221. Jankovic, D. *et al.* Schistosome-Infected IL-4 Receptor Knockout (KO) Mice, in Contrast to IL-4 KO Mice, Fail to Develop Granulomatous Pathology While Maintaining the Same Lymphokine Expression Profil. *J. Immunol.* 337–342 (1999).
222. Chiamonte, M. G., Donaldson, D. D., Cheever, A. W. & Wynn, T. A. An IL-13 inhibitor blocks the development of hepatic fibrosis during a T-helper type 2-dominated inflammatory response. *J. Clin. Invest.* **104**, 777–785 (1999).
223. Ariyaratne, A. & Finney, C. A. M. Eosinophils and macrophages within the Th2-induced granuloma: Balancing killing and healing in a tight space. *Infect. Immun.* **87**, (2019).
224. Wynn, T. A. Fibrotic disease and the TH1/TH2 paradigm. *Nature Reviews Immunology* **4**, 583–594 (2004).
225. Chun Geun Lee *et al.* Interleukin-13 induces tissue fibrosis by selectively stimulating and activating transforming growth factor β 1. *J. Exp. Med.* **194**, 809–821 (2001).
226. Borthwick, L. A. *et al.* Macrophages are critical to the maintenance of IL-13-dependent lung inflammation and fibrosis. *Mucosal Immunol.* **9**, 38–55 (2016).
227. Herbert, D. R. *et al.* Alternative macrophage activation is essential for survival during schistosomiasis and downmodulates T helper 1 responses and immunopathology. *Immunity* **20**, 623–635 (2004).
228. de Souza, V. C. A. *et al.* Adoptive Transfer of Bone Marrow-Derived Monocytes Ameliorates *Schistosoma mansoni* -Induced Liver Fibrosis in Mice. *Sci. Rep.* **9**, 1–11 (2019).
229. Vannella, K. M. *et al.* Incomplete Deletion of IL-4R α by LysMCre Reveals Distinct Subsets of M2 Macrophages Controlling Inflammation and Fibrosis in Chronic Schistosomiasis. *PLoS Pathog.* **10**, (2014).
230. Pesce, J. T. *et al.* Arginase-1-expressing macrophages suppress Th2 cytokine-driven inflammation and fibrosis. *PLoS Pathog.* **5**, (2009).
231. Nair, M. G. *et al.* Alternatively activated macrophage-derived RELM- α is a negative regulator of type 2 inflammation in the lung. *J. Exp. Med.* **206**, 937–952 (2009).

-
232. Pelczar, P. *et al.* A pathogenic role for T cell-derived IL-22BP in inflammatory bowel disease. *Science (80-)*. **354**, 358–362 (2016).
233. Schmittgen, T. D. & Livak, K. J. Analyzing real-time PCR data by the comparative C(T) method. *Nat. Protoc.* **3**, 1101–8 (2008).
234. Metsalu, T. & Vilo, J. ClustVis: A web tool for visualizing clustering of multivariate data using Principal Component Analysis and heatmap. *Nucleic Acids Res.* **43**, W566–W570 (2015).
235. Huang, D. W., Sherman, B. T. & Lempicki, R. A. Systematic and integrative analysis of large gene lists using DAVID bioinformatics resources. *Nat. Protoc.* **4**, 44–57 (2009).
236. Huang, D. W., Sherman, B. T. & Lempicki, R. A. Bioinformatics enrichment tools: Paths toward the comprehensive functional analysis of large gene lists. *Nucleic Acids Res.* **37**, 1–13 (2009).
237. Zhong, Y. & Yi, C. MicroRNA-720 suppresses M2 macrophage polarization by targeting GATA3. *Biosci. Rep.* **36**, 363 (2016).
238. De Paoli, F. *et al.* Transducin-like enhancer of split-1 is expressed and functional in human macrophages. *FEBS Lett.* **590**, 43–52 (2016).
239. Ljungberg, J. K., Kling, J. C., Tran, T. T. & Blumenthal, A. Functions of the WNT Signaling Network in Shaping Host Responses to Infection. *Frontiers in Immunology* **10**, 2521 (2019).
240. Lin, J. *et al.* Novel MicroRNA Signature to Differentiate Ulcerative Colitis from Crohn Disease: A Genome-Wide Study Using Next Generation Sequencing. *MicroRNA (Sharjah, United Arab Emirates)* **5**, 222–229 (2016).
241. Valmiki, S., Ahuja, V. & Paul, J. MicroRNA exhibit altered expression in the inflamed colonic mucosa of ulcerative colitis patients. *World J. Gastroenterol.* **23**, 5324–5332 (2017).
242. Dubois-Camacho, K. *et al.* Inhibition of miR-378a-3p by Inflammation Enhances IL-33 Levels: A Novel Mechanism of Alarmin Modulation in Ulcerative Colitis. *Front. Immunol.* **10**, 2449 (2019).
243. Hudcovic, T., Štěpánková, R., Cebra, J. & Tlaskalová-Hogenová, H. The Role of Microflora in the Development of Intestinal Inflammation: Acute and Chronic Colitis Induced by Dextran Sulfate in Germ-Free and Conventionally Reared Immunocompetent and Immunodeficient Mice. *Folia Microbiol. (Praha)*. **46**, 565–572 (2001).
244. Kitajima, S., Morimoto, M., Sagara, E., Shimizu, C. & Ikeda, Y. Dextran Sodium Sulfate-Induced Colitis in Germ-Free IqI/Jic Mice. *Exp. Anim.* **50**, 387–395 (2001).
245. Hernández-Chirlaque, C. *et al.* Germ-free and Antibiotic-treated Mice are Highly Susceptible to Epithelial Injury in DSS Colitis. *J. Crohn's Colitis* **10**, 1324–1335 (2016).
246. Cooper, H., Murthy, S., Shah, R. & Sedergran, D. Clinicopathologic study of dextran sulfate sodium experimental murine colitis. *Lab. Invest.* **69**, 238–49 (1993).
247. Wirtz, S. *et al.* Chemically induced mouse models of acute and chronic intestinal inflammation. *Nat. Protoc.* **12**, 1295–1309 (2017).
248. Okayasu, I. *et al.* A novel method in the induction of reliable experimental acute and chronic

- ulcerative colitis in mice. *Gastroenterology* **98**, 694–702 (1990).
249. Dieleman, L. A. *et al.* Chronic experimental colitis induced by dextran sulphate sodium (DSS) is characterized by Th1 and Th2 cytokines. *Clin. Exp. Immunol.* **114**, 385–91 (1998).
250. Horuluoglu, B. H., Kayraklioglu, N., Tross, D. & Klinman, D. PAM3 protects against DSS-induced colitis by altering the M2:M1 ratio. *Sci. Rep.* **10**, 1–8 (2020).
251. Lin, Y. *et al.* Chemerin aggravates DSS-induced colitis by suppressing M2 macrophage polarization. *Cell. Mol. Immunol.* **11**, 355–366 (2014).
252. Weisser, S. B. *et al.* SHIP-deficient, alternatively activated macrophages protect mice during DSS-induced colitis. *J. Leukoc. Biol.* **90**, 483–492 (2011).
253. Prada, J. M. *et al.* Understanding the relationship between egg- and antigen-based diagnostics of *Schistosoma mansoni* infection pre- and post-treatment in Uganda. *Parasites and Vectors* **11**, 21 (2018).
254. Munisi, D. Z., Buza, J., Mpolya, E. A. & Kinung’hi, S. M. Intestinal Schistosomiasis among Primary Schoolchildren in Two On-Shore Communities in Rorya District, Northwestern Tanzania: Prevalence, Intensity of Infection and Associated Risk Factors. *J. Parasitol. Res.* **2016**, (2016).
255. Wilson, M. S. *et al.* Immunopathology of schistosomiasis. *Immunol. Cell Biol.* **85**, 148–154 (2007).
256. Madala, S. K. *et al.* Matrix Metalloproteinase 12-Deficiency Augments Extracellular Matrix Degrading Metalloproteinases and Attenuates IL-13-Dependent Fibrosis. *J. Immunol.* **184**, 3955–3963 (2010).
257. Giannini, E. G., Testa, R. & Savarino, V. Liver enzyme alteration: A guide for clinicians. *CMAJ* **172**, 367–379 (2005).
258. Schwartz, C., Oeser, K., Prazeres da Costa, C., Layland, L. E. & Voehringer, D. T Cell-Derived IL-4/IL-13 Protects Mice against Fatal *Schistosoma mansoni* Infection Independently of Basophils. *J. Immunol.* **193**, 3590–3599 (2014).
259. Wynn, T. Cellular and molecular mechanisms of fibrosis. *J. Pathol.* **214**, 199–210 (2008).
260. Reiman, R. M. *et al.* Interleukin-5 (IL-5) augments the progression of liver fibrosis by regulating IL-13 activity. *Infect. Immun.* **74**, 1471–1479 (2006).
261. de Souza, V. C. A. *et al.* Adoptive Transfer of Bone Marrow-Derived Monocytes Ameliorates *Schistosoma mansoni* -Induced Liver Fibrosis in Mice. *Sci. Rep.* **9**, 1–11 (2019).
262. Vannella, K. M. *et al.* Incomplete Deletion of IL-4R α by LysMCre Reveals Distinct Subsets of M2 Macrophages Controlling Inflammation and Fibrosis in Chronic Schistosomiasis. *PLoS Pathog.* **10**, e1004372 (2014).
263. Llanwarne, F. & Helmbj, H. Granuloma formation and tissue pathology in *Schistosoma japonicum* versus *Schistosoma mansoni* infections. *Parasite Immunol.* **43**, e12778 (2021).
264. Bain, C. C. & Mowat, A. M. The monocyte-macrophage axis in the intestine. *Cell. Immunol.* **291**,

- 41–48 (2014).
265. Martinez, F. O., Sica, A., Mantovani, A. & Locati, M. Macrophage activation and polarization. *Front. Biosci.* **13**, 453–61 (2008).
266. Souza, C. O. S., Gardinassi, L. G., Rodrigues, V. & Faccioli, L. H. Monocyte and Macrophage-Mediated Pathology and Protective Immunity During Schistosomiasis. *Frontiers in Microbiology* **11**, 1973 (2020).
267. Barron, L. & Wynn, T. A. Macrophage activation governs schistosomiasis-induced inflammation and fibrosis. *Eur. J. Immunol.* **41**, 2509–2514 (2011).
268. Tacke, F. & Zimmermann, H. W. Macrophage heterogeneity in liver injury and fibrosis. *Journal of Hepatology* **60**, 1090–1096 (2014).
269. Blériot, C. & Ginhoux, F. Understanding the Heterogeneity of Resident Liver Macrophages. *Front. Immunol.* **10**, 2694 (2019).
270. Betjes, M. G. H., Haks, M. C., Tuk, C. W. & Beelen, R. H. J. Monoclonal Antibody EBM11 (Anti-CD68) Discriminates between Dendritic Cells and Macrophages after Short-Term Culture. *Immunobiology* **183**, 79–87 (1991).
271. Gottfried, E. *et al.* Expression of CD68 in non-myeloid cell types. *Scand. J. Immunol.* **67**, 453–463 (2008).
272. Elchaninov, A. V., Fatkhudinov, T. K., Vishnyakova, P. A., Lokhonina, A. V. & Sukhikh, G. T. Phenotypical and Functional Polymorphism of Liver Resident Macrophages. *Cells* **8**, 1–22 (2019).
273. Alstergren, P. *et al.* Polarization and directed migration of murine neutrophils is dependent on cell surface expression of CD44. *Cell. Immunol.* **231**, 146–157 (2004).
274. Khan, A. I. *et al.* Role of CD44 and Hyaluronan in Neutrophil Recruitment. *J. Immunol.* **173**, 7594–7601 (2004).
275. El-Brolosy, M. A. & Stainier, D. Y. R. Genetic compensation: A phenomenon in search of mechanisms. *PLoS Genetics* **13**, e1006780 (2017).
276. O'Leary, M. N. *et al.* The Ribosomal Protein Rpl22 Controls Ribosome Composition by Directly Repressing Expression of Its Own Paralog, Rpl22i1. *PLoS Genet.* **9**, e1003708 (2013).
277. Thuraingam, T. *et al.* Delayed cutaneous wound healing in mice lacking solute carrier 11a1 (formerly Nramp1): Correlation with decreased expression of secretory leukocyte protease inhibitor. *J. Invest. Dermatol.* **126**, 890–901 (2006).
278. Yang, M. *et al.* Deficiency of GATA3-Positive Macrophages Improves Cardiac Function Following Myocardial Infarction or Pressure Overload Hypertrophy. *J. Am. Coll. Cardiol.* **72**, 885–904 (2018).
279. Yang, Y. *et al.* Crosstalk between hepatic tumor cells and macrophages via Wnt/ β -catenin signaling promotes M2-like macrophage polarization and reinforces tumor malignant behaviors.

- Cell Death Dis.* **9**, 1–14 (2018).
280. Cosín-Roger, J. *et al.* M2 Macrophages Activate WNT Signaling Pathway in Epithelial Cells: Relevance in Ulcerative Colitis. *PLoS One* **8**, e78128 (2013).
281. Liu, Y. *et al.* Dissonant response of M0/M2 and M1 bone-marrow-derived macrophages to RhoA pathway interference. *Cell Tissue Res.* **366**, 707–720 (2016).
282. Carmeliet, P. VEGF as a key mediator of angiogenesis in cancer. *Oncology* **69**, 4–10 (2005).
283. Van den Bossche, J. *et al.* Mitochondrial Dysfunction Prevents Repolarization of Inflammatory Macrophages. *Cell Rep.* **17**, 684–696 (2016).
284. Balsa, E. *et al.* NDUFA4 Is a Subunit of Complex IV of the Mammalian Electron Transport Chain. *Cell Metab.* **16**, 378–386 (2012).
285. Lee, C. Q. E. *et al.* Coding and non-coding roles of MOCCI (C15ORF48) coordinate to regulate host inflammation and immunity. *Nat. Commun.* **12**, 1–22 (2021).
286. Gebauer, F. & Hentze, M. W. Molecular mechanisms of translational control. *Nature Reviews Molecular Cell Biology* **5**, 827–835 (2004).
287. Kelen, K. Van Der, Beyaert, R., Inzé, D. & Veylder, L. De. Translational control of eukaryotic gene expression. *Critical Reviews in Biochemistry and Molecular Biology* **44**, 143–168 (2009).
288. Cabrita, L. D., Dobson, C. M. & Christodoulou, J. Protein folding on the ribosome. *Current Opinion in Structural Biology* **20**, 33–45 (2010).
289. Hershey, J. W. B., Sonenberg, N. & Mathews, M. B. Principles of Translational Control: An Overview. *Cold Spring Harb. Perspect. Biol.* **4**, a011528–a011528 (2012).
290. Copeland, P. R. Regulation of gene expression by stop codon recoding: Selenocysteine. *Gene* **312**, 17–25 (2003).
291. Lodish, H. F., Zhou, B., Liu, G. & Chen, C.-Z. Micromanagement of the immune system by microRNAs. *Nat. Rev. Immunol.* **8**, 120–30 (2008).
292. Mohr, A. M. & Mott, J. L. Overview of microRNA biology. *Semin. Liver Dis.* **35**, 3–11 (2015).
293. Self-Fordham, J. B., Naqvi, A. R., Uttamani, J. R., Kulkarni, V. & Nares, S. MicroRNA: Dynamic regulators of macrophage polarization and plasticity. *Front. Immunol.* **8**, 1–18 (2017).
294. Hannedouche, S. *et al.* Oxysterols direct immune cell migration via EBI2. *Nature* **475**, 524–527 (2011).
295. Rutkowska, A. *et al.* The EBI2 signalling pathway plays a role in cellular crosstalk between astrocytes and macrophages. *Sci. Rep.* **6**, 1–7 (2016).
296. Bartlett, S. *et al.* GPR183 Regulates Interferons, Autophagy, and Bacterial Growth During Mycobacterium tuberculosis Infection and Is Associated With TB Disease Severity. *Front. Immunol.* **11**, 1 (2020).
297. Tang, J., Shi, Y., Zhan, L. & Qin, C. Downregulation of GPR183 on infection restricts the early

- infection and intracellular replication of mycobacterium tuberculosis in macrophage. *Microb. Pathog.* **145**, 104234 (2020).
298. Tyteca, D. *et al.* Regulation of macrophage motility by the water channel aquaporin-1: Crucial role of M0/M2 phenotype switch. *PLoS One* **10**, (2015).
299. Li, B. *et al.* Aquaporin-1 attenuates macrophage-mediated inflammatory responses by inhibiting p38 mitogen-activated protein kinase activation in lipopolysaccharide-induced acute kidney injury. *Inflamm. Res.* **68**, 1035–1047 (2019).
300. Sarafi, M. N., Garcia-Zepeda, E. A., MacLean, J. A., Charo, I. F. & Luster, A. D. Murine monocyte chemoattractant protein (MCP)-5: A novel CC chemokine that is a structural and functional homologue of human MCP-1. *J. Exp. Med.* **185**, 99–109 (1997).
301. Shang, X. Z. *et al.* Eosinophil recruitment in type-2 hypersensitivity pulmonary granulomas: Source and contribution of monocyte chemoattractant protein-3 (CCL7). *Am. J. Pathol.* **161**, 257–266 (2002).
302. Bardina, S. V. *et al.* Differential Roles of Chemokines CCL2 and CCL7 in Monocytosis and Leukocyte Migration during West Nile Virus Infection. *J. Immunol.* **195**, 4306–4318 (2015).
303. Xuan, W., Qu, Q., Zheng, B., Xiong, S. & Fan, G.-H. The chemotaxis of M1 and M2 macrophages is regulated by different chemokines. *J. Leukoc. Biol.* **97**, 61–69 (2015).
304. Ford, J. *et al.* CCL7 Is a Negative Regulator of Cutaneous Inflammation Following *Leishmania major* Infection. *Front. Immunol.* **9**, 3063 (2019).
305. Lee, S. H. *et al.* M2-like, dermal macrophages are maintained via IL-4/CCL24-mediated cooperative interaction with eosinophils in cutaneous leishmaniasis. *Sci. Immunol.* **5**, (2020).
306. DeLeon-Pennell, K. Y. *et al.* Periodontal-induced chronic inflammation triggers macrophage secretion of Ccl12 to inhibit fibroblast-mediated cardiac wound healing. *JCI insight* **2**, (2017).
307. Chiu, B. C. & Chensue, S. W. Chemokine responses in schistosomal antigen-elicited granuloma formation. in *Parasite Immunology* **24**, 285–294 (John Wiley & Sons, Ltd, 2002).
308. Anand, R. J. *et al.* A Role for Connexin43 in Macrophage Phagocytosis and Host Survival after Bacterial Peritoneal Infection. *J. Immunol.* **181**, 8534–8543 (2008).
309. Kimura, A. *et al.* Aryl hydrocarbon receptor protects against bacterial infection by promoting macrophage survival and reactive oxygen species production. *Int. Immunol.* **26**, 209–220 (2014).
310. Kimura, A. *et al.* Aryl hydrocarbon receptor in combination with Stat1 regulates LPS-induced inflammatory responses. *J. Exp. Med.* **206**, 2027–2035 (2009).
311. McCormick, S. M. & Heller, N. M. Regulation of macrophage, dendritic cell, and microglial phenotype and function by the SOCS proteins. *Frontiers in Immunology* **6**, (2015).
312. Duncan, S. A., Baganizi, D. R., Sahu, R., Singh, S. R. & Dennis, V. A. SOCS proteins as regulators of inflammatory responses induced by bacterial infections: A review. *Frontiers in Microbiology* **8**, 2431 (2017).

313. Echtermeyer, F. *et al.* Delayed wound repair and impaired angiogenesis in mice lacking syndecan-4. *J. Clin. Invest.* **107**, (2001).
314. Das, S., Majid, M. & Baker, A. B. Syndecan-4 enhances PDGF-BB activity in diabetic wound healing. *Acta Biomater.* **42**, 56–65 (2016).
315. Ichihara, S. *et al.* A role for the aryl hydrocarbon receptor in regulation of ischemia-induced angiogenesis. *Arterioscler. Thromb. Vasc. Biol.* **27**, 1297–1304 (2007).
316. Yi, T. *et al.* Aryl Hydrocarbon Receptor: A New Player of Pathogenesis and Therapy in Cardiovascular Diseases. *BioMed Research International* **2018**, (2018).
317. Czopek, A. *et al.* A novel role for myeloid endothelin-B receptors in hypertension. *Eur. Heart J.* **40**, 768–784 (2019).
318. Marasciulo, F., Montagnani, M. & Potenza, M. Endothelin-1: The Yin and Yang on Vascular Function. *Curr. Med. Chem.* **13**, 1655–1665 (2006).
319. Riabov, V. *et al.* Role of tumor associated macrophages in tumor angiogenesis and lymphangiogenesis. *Frontiers in Physiology* **5 MAR**, (2014).
320. Guo, C., Buranych, A., Sarkar, D., Fisher, P. B. & Wang, X. Y. The role of tumor-associated macrophages in tumor vascularization. *Vasc. Cell* **5**, 20 (2013).
321. Carmeliet, P. & Jain, R. K. Angiogenesis in cancer and other diseases. *Nature* **407**, 249–257 (2000).
322. Alkim, C., Alkim, H., Koksall, A. R., Boga, S. & Sen, I. Angiogenesis in inflammatory bowel disease. *International Journal of Inflammation* **2015**, (2015).
323. Park, S., Kim, J. W., Kim, J. H., Lim, C. W. & Kim, B. Differential roles of angiogenesis in the induction of fibrogenesis and the resolution of fibrosis in liver. *Biological and Pharmaceutical Bulletin* **38**, 980–985 (2015).
324. Elpek, G. Ö. Angiogenesis and liver fibrosis. *World J. Hepatol.* **7**, 377–391 (2015).
325. Zadorozhna, M., Di Gioia, S., Conese, M. & Mangieri, D. Neovascularization is a key feature of liver fibrosis progression: anti-angiogenesis as an innovative way of liver fibrosis treatment. *Molecular Biology Reports* **47**, 2279–2288 (2020).
326. Jönsson, F., Gurniak, C. B., Fleischer, B., Kirfel, G. & Witke, W. Immunological Responses and Actin Dynamics in Macrophages Are Controlled by N-Cofilin but Are Independent from ADF. *PLoS One* **7**, e36034 (2012).
327. McWhorter, F. Y., Wang, T., Nguyen, P., Chung, T. & Liu, W. F. Modulation of macrophage phenotype by cell shape. *Proc. Natl. Acad. Sci. U. S. A.* **110**, 17253–17258 (2013).
328. Pergola, C. *et al.* Modulation of actin dynamics as potential macrophage subtype-targeting anti-tumour strategy. *Sci. Rep.* **7**, 1–12 (2017).
329. Al-Fageeh, M. B. & Smales, C. M. Control and regulation of the cellular responses to cold shock: The responses in yeast and mammalian systems. *Biochemical Journal* **397**, 247–259 (2006).

330. Kizaki, T. *et al.* Relationship between cold tolerance and generation of suppressor macrophages during acute cold stress. *J. Appl. Physiol.* **83**, 1116–1122 (1997).
331. Sesti-Costa, R., Ignacchiti, M. D. C., Chedraoui-Silva, S., Marchi, L. F. & Mantovani, B. Chronic cold stress in mice induces a regulatory phenotype in macrophages: Correlation with increased 11 β -hydroxysteroid dehydrogenase expression. *Brain. Behav. Immun.* **26**, 50–60 (2012).
332. Elliott, J. A. & Winn, W. C. Treatment of alveolar macrophages with cytochalasin D inhibits uptake and subsequent growth of *Legionella pneumophila*. *Infect. Immun.* **51**, 31–36 (1986).
333. Mimura, N. & Asano, A. Synergistic effect of colchicine and cytochalasin D on phagocytosis by peritoneal macrophages. *Nature* **261**, 319–321 (1976).
334. Shinji, H., Akagawa, K. S. & Yoshida, T. Cytochalasin D inhibits lipopolysaccharide-induced tumor necrosis factor production in macrophages. *J. Leukoc. Biol.* **54**, 336–342 (1993).
335. Zhang, Y., Hoppe, A. D. & Swanson, J. A. Coordination of Fc receptor signaling regulates cellular commitment to phagocytosis. *Proc. Natl. Acad. Sci. U. S. A.* **107**, 19332–19337 (2010).
336. Medina, C. B. *et al.* Metabolites released from apoptotic cells act as tissue messengers. *Nature* **580**, 130–135 (2020).
337. Sarang, Z. *et al.* Macrophages Engulfing Apoptotic Cells Produce Nonclassical Retinoids To Enhance Their Phagocytic Capacity. *J. Immunol.* **192**, 5730–5738 (2014).
338. Champion, J. A. & Mitragotri, S. Role of target geometry in phagocytosis. *Proc. Natl. Acad. Sci. U. S. A.* **103**, 4930–4934 (2006).
339. Pacheco, P., White, D. & Sulchek, T. Effects of Microparticle Size and Fc Density on Macrophage Phagocytosis. *PLoS One* **8**, e60989 (2013).
340. Liebold, I. The interplay between apoptotic cells and macrophages: impact on macrophage phenotype and function. (2021).
341. Chassaing, B., Aitken, J. D., Malleshappa, M. & Vijay-Kumar, M. Dextran sulfate sodium (DSS)-induced colitis in mice. *Curr. Protoc. Immunol.* **104**, Unit (2014).
342. Spalinger, M. R. *et al.* Loss of PTPN22 abrogates the beneficial effect of cohousing-mediated fecal microbiota transfer in murine colitis. *Mucosal Immunol.* **12**, 1336–1347 (2019).
343. Brinkman, B. M. *et al.* Gut Microbiota Affects Sensitivity to Acute DSS-induced Colitis Independently of Host Genotype. *Inflamm. Bowel Dis.* **19**, 2560–2567 (2013).
344. Sutherland, T. E. *et al.* Ym1 induces RELM α and rescues IL-4R α deficiency in lung repair during nematode infection. *PLoS Pathog.* **14**, (2018).
345. Cai, Y., Kumar, R. K., Zhou, J., Foster, P. S. & Webb, D. C. Ym1/2 Promotes Th2 Cytokine Expression by Inhibiting 12/15(S)-Lipoxygenase: Identification of a Novel Pathway for Regulating Allergic Inflammation. *J. Immunol.* **182**, 5393–5399 (2009).
346. Zhang, W. *et al.* Arginase activity mediates retinal inflammation in endotoxin-induced uveitis. *Am. J. Pathol.* **175**, 891–902 (2009).

-
347. Kavalukas, S. L., Uzgare, A. R., Bivalacqua, T. J. & Barbul, A. Arginase inhibition promotes wound healing in mice. *Surgery* **151**, 287–295 (2012).
348. Scott, C. L., Wright, P. B., Milling, S. W. F. & Mowat, A. M. Isolation and identification of conventional dendritic cell subsets from the intestine of mice and men. *Methods Mol. Biol.* **1423**, 101–118 (2016).
349. Webster, H. C., Andrusaite, A. T., Shergold, A. L., Milling, S. W. F. & Perona-Wright, G. Isolation and functional characterisation of lamina propria leukocytes from helminth-infected, murine small intestine. *J. Immunol. Methods* **477**, 112702 (2020).
350. Ferrer-Font, L. *et al.* High-dimensional analysis of intestinal immune cells during helminth infection. *Elife* **9**, (2020).
351. Nascimento, M. *et al.* Ly6Chi Monocyte Recruitment Is Responsible for Th2 Associated Host-Protective Macrophage Accumulation in Liver Inflammation due to Schistosomiasis. *PLoS Pathog.* **10**, (2014).
352. Byram, J. E. & Von Lichtenberg, F. Altered schistosome granuloma formation in nude mice. *Am. J. Trop. Med. Hyg.* **26**, 944–956 (1977).
353. De Oliveira Fraga, L. A., Torrero, M. N., Tocheva, A. S., Mitre, E. & Davies, S. J. Induction of type 2 responses by schistosome worms during prepatent infection. *J. Infect. Dis.* **201**, 464–472 (2010).
354. Davies, S. J. *et al.* Modulation of blood fluke development in the liver by hepatic CD4+ lymphocytes. *Science (80-.)*. **294**, 1358–1361 (2001).
355. Fabre, V. *et al.* Tissue Inhibitor of Matrix-Metalloprotease–1 Predicts Risk of Hepatic Fibrosis in Human *Schistosoma japonicum* Infection. *J. Infect. Dis.* **203**, 707–714 (2011).
356. Vaillant, B., Chiamonte, M. G., Cheever, A. W., Soloway, P. D. & Wynn, T. A. Regulation of Hepatic Fibrosis and Extracellular Matrix Genes by the Th Response: New Insight into the Role of Tissue Inhibitors of Matrix Metalloproteinases. *J. Immunol.* **167**, 7017–7026 (2001).
357. Schwartz, C. & Fallon, P. G. *Schistosoma* ‘Eggs-iting’ the Host: Granuloma Formation and Egg Excretion. *Front. Immunol.* **9**, 2492 (2018).
358. Cosin-Roger, J., Ortiz-Masià, M. D. & Barrachina, M. D. Macrophages as an emerging source of wnt ligands: Relevance in mucosal integrity. *Frontiers in Immunology* **10**, 2297 (2019).
359. Wang, Q. *et al.* Enhanced Wnt signalling in hepatocytes is associated with *Schistosoma japonicum* infection and contributes to liver fibrosis. *Sci. Rep.* **7**, 1–14 (2017).
360. Fernandes, J. S. *et al.* Monocyte Subsets in Schistosomiasis Patients with Periportal Fibrosis. (2014). doi:10.1155/2014/703653
361. Souza, C. O. S., Gardinassi, L. G., Rodrigues, V. & Faccioli, L. H. Monocyte and Macrophage-Mediated Pathology and Protective Immunity During Schistosomiasis. *Front. Microbiol.* **11**, 9 (2020).

-
362. Morais, S. B. *et al.* Schistosoma mansoni SmKI-1 serine protease inhibitor binds to elastase and impairs neutrophil function and inflammation. *PLoS Pathog.* **14**, (2018).
363. Smith, P. *et al.* Schistosoma mansoni secretes a chemokine binding protein with antiinflammatory activity. *J. Exp. Med.* **202**, 1319–1325 (2005).
364. Hirata, M., Hara, T., Kage, M., Fukuma, T. & Sendo, F. Neutropenia augments experimentally induced Schistosoma japonicum egg granuloma formation in CBA mice, but not in C57BL/6 mice. *Parasite Immunol.* **24**, 479–488 (2002).
365. Chuah, C. *et al.* Defining a pro-inflammatory neutrophil phenotype in response to schistosome eggs. *Cell. Microbiol.* **16**, 1666–1677 (2014).
366. Campos, N. *et al.* Macrophages from IBD patients exhibit defective tumour necrosis factor- α secretion but otherwise normal or augmented pro-inflammatory responses to infection. *Immunobiology* **216**, 961–970 (2011).
367. Vos, A. C. W. *et al.* Regulatory macrophages induced by infliximab are involved in healing in vivo and in vitro. *Inflamm. Bowel Dis.* **18**, 401–408 (2012).
368. Na, Y. R., Stakenborg, M., Seok, S. H. & Matteoli, G. Macrophages in intestinal inflammation and resolution: a potential therapeutic target in IBD. *Nature Reviews Gastroenterology and Hepatology* **16**, 531–543 (2019).
369. Justus, C. R., Leffler, N., Ruiz-Echevarria, M. & Yang, L. V. In vitro cell migration and invasion assays. *J. Vis. Exp.* **88**, 51046 (2014).
370. Green, T. D. *et al.* Directed migration of mouse macrophages in vitro involves myristoylated alanine-rich C-kinase substrate (MARCKS) protein. *J. Leukoc. Biol.* **92**, 633–639 (2012).
371. Cui, K., Ardell, C. L., Podolnikova, N. P. & Yakubenko, V. P. Distinct Migratory Properties of M1, M2, and Resident Macrophages Are Regulated by α D β 2 and α M β 2 Integrin-Mediated Adhesion. *Front. Immunol.* **9**, 2650 (2018).
372. Aziz, M. H. *et al.* The Upregulation of Integrin α D β 2 (CD11d/CD18) on Inflammatory Macrophages Promotes Macrophage Retention in Vascular Lesions and Development of Atherosclerosis . *J. Immunol.* **198**, 4855–4867 (2017).
373. Guet, R. *et al.* The Process of Macrophage Migration Promotes Matrix Metalloproteinase-Independent Invasion by Tumor Cells. *J. Immunol.* **187**, 3806–3814 (2011).
374. Vailhé, B., Vittet, D. & Feige, J. J. In vitro models of vasculogenesis and angiogenesis. *Laboratory Investigation* **81**, 439–452 (2001).
375. Staton, C. A. *et al.* Current methods for assaying angiogenesis in vitro and in vivo. *International Journal of Experimental Pathology* **85**, 233–248 (2004).
376. Goodwin, A. M. In vitro assays of angiogenesis for assessment of angiogenic and anti-angiogenic agents. *Microvascular Research* **74**, 172–183 (2007).
377. Gangadaran, P. *et al.* Extracellular vesicles derived from macrophage promote angiogenesis In

- vitro and accelerate new vasculature formation In vivo. *Exp. Cell Res.* **394**, 112146 (2020).
378. Gurevich, D. B. *et al.* Live imaging of wound angiogenesis reveals macrophage orchestrated vessel sprouting and regression. *EMBO J.* **37**, e97786 (2018).
379. Johnson, J. S. *et al.* Evaluation of 16S rRNA gene sequencing for species and strain-level microbiome analysis. *Nat. Commun.* **10**, 1–11 (2019).
380. Osman, M.-A., Neoh, H., Ab Mutalib, N.-S., Chin, S.-F. & Jamal, R. 16S rRNA Gene Sequencing for Deciphering the Colorectal Cancer Gut Microbiome: Current Protocols and Workflows. *Front. Microbiol.* **9**, 767 (2018).
381. Stackowicz, J., Jönsson, F. & Reber, L. L. Mouse Models and Tools for the in vivo Study of Neutrophils. *Frontiers in Immunology* **10**, 3130 (2020).
382. Auwerx, J. The human leukemia cell line, THP-1: A multifaceted model for the study of monocyte-macrophage differentiation. *Experientia* **47**, 22–31 (1991).
383. Chanput, W., Peters, V. & Wichers, H. THP-1 and U937 cells. in *The Impact of Food Bioactives on Health: In Vitro and Ex Vivo Models* 147–159 (Springer International Publishing, 2015). doi:10.1007/978-3-319-16104-4_14
384. Larrick, J. W., Fischer, D. G., Anderson, S. J. & Koren, H. S. Characterization of a human macrophage-like cell line stimulated in vitro: a model of macrophage functions. *J. Immunol.* **125**, (1980).
385. Driehuis, E. & Clevers, H. CRISPR/Cas 9 genome editing and its applications in organoids. *American Journal of Physiology - Gastrointestinal and Liver Physiology* **312**, G257–G265 (2017).
386. Matano, M. *et al.* Modeling colorectal cancer using CRISPR-Cas9-mediated engineering of human intestinal organoids. *Nat. Med.* **21**, 256–262 (2015).

9. Acknowledgements

A doctoral thesis is a presentation of an individual's work. But people do not function well in isolation, and in the sciences in particular, no individual person can get far without the help of others.

I would like to thank PD Dr. Thomas Jacobs and Prof. Dr. Christian Lohr for supervising my doctoral project and evaluating this thesis.

Very special thanks go to my group leader and supervisor Dr. Lidia Bosurgi not only for her continual scientific and moral support during this project, but also for providing this incredible opportunity. Thank you for all the advice, within and without the scope of this thesis, for your tireless efforts in promoting our work, and for motivating myself and the whole group to not only dive deep into our own research topics, but also cooperate and communicate with others to put our work into a wider context.

Special thanks also to Dr. Imke Liebold as the "senior" PhD student of the Bosurgi group, for introducing me to the lab and most of the methods I needed to complete this thesis, for her patience in answering my intermittent questions posed at the least convenient times, and for all the entertaining hours spent within and without the lab. Thanks also to my fellow Bosurgi PhD students, Amirah Al jawazneh, Stephanie Leyk, Clarissa Lanzloth, and Simon Meyer for your daily support – both scientifically and socially – as well as the engaging conversations and collaborations.

I would also like the DFG for funding this project through the SFB 841, and would particularly like to thank Dr. Lidia Bosurgi, PD Dr. Thomas Jacobs, and Prof. Dr. med. Samuel Huber for supervising my project as part of the SFB841 graduate school.

Many thanks to group leaders PD Dr. Thomas Jacobs, Prof. Dr. med. Samuel Huber, Prof. Dr. med. Nicola Gagliani, and PD Dr. Minka Breloer for their advice, support, and feedback during this project, and to the members of their groups for their feedback and support. In particular, thank you to Christian Casar, Leonie Konczalla, Jana Meiners, Mikolaj Nawrocki, Penelope Pelzcar, and Nicola Schaltenberg for providing me with methods, materials, information, and time. I would also especially like to thank Ulrike Richardt for imparting her limitless knowledge of the lab's inner workings to teach me the methods or provide materials I needed to perform experiments, and for always being ready to lend an ear to her co-workers. Many thanks also to the staff of the BNITM animal facility, especially Yvonne Richter and Constantin Pretnar, for maintaining and caring for our mice.

In addition to thanks for help with the scientific side of this project, I would like to thank my fellow Master students, PhD students, and post-doctoral researchers in the Jacobs and Breloer groups for all the conversations, jokes, commiserations, celebrations, and occasional faux pas that made day-to-day life in the lab an enjoyable experience, rather than a tedious one.

Lastly, I would like to thank my friends in the Schwarzmeterik acapella group – Corona will be over some day, guys! – my family, and my husband Greg for their constant moral support, for putting up with me during the bad times, and lifting me even higher during the good times.

Thank you all.